PARAMAGNETIC RESONANCE ABSORPTION SPECTRA OF SOME ADSORBED TRANSITION METAL IONS

By

Roger Jack Faber

A THESIS

Submitted to the School of Advanced Graduate Studies of
Michigan State University of Agriculture and Applied Science
in partial fulfillment of the requirements
for the degree of

DOCTOR OF PHILOSOPHY

Department of Chemistry

1957

ACKNOWLEDGMENTS

The author wishes to express his sincere appreciation to Professor M. T. Rogers for his guidance and assistance throughout the course of this work, to Dr. H. B. Thompson, who designed and constructed much of the electronic circuitry used in these experiments, to Mr. F. Betts and Mr. R. Brigham, who assisted in the construction of the electromagnet and its fittings, and to the Atomic Energy Commission and the Union Carbide Corporation for grants subsidizing this research.

****

VITA

Roger Jack Faber

candidate for the degree of

Doctor of Philosophy

Final examination, December 16, 1957, 2:00 P.M., Room 128, Kedzie Chemical Laboratory

Dissertation: Paramagnetic Resonance Absorption Spectra of Some Adsorbed Transition Metal Ions

Outline of Studies:

Major subject -- Physical Chemistry
Minor subjects -- Physics, Mathematics

Biographical Items:

Born, October 4, 1931, Grand Rapids, Michigan

Undergraduate Studies, Calvin College, 1949-53

Graduate Studies, Michigan State University, 1953-57

Experience: Graduate Assistant, Michigan State University, 1953-54
Special Graduate Research Assistant, Michigan State University, 1954-56
Graduate Fellow, Michigan State University, 1956-57

Member of American Chemical Society, Society of the Sigma Xi

PARAMAGNETIC RESONANCE ABSORPTION SPECTRA OF SOME ADSORBED TRANSITION METAL IONS

By

Roger Jack Faber

AN ABSTRACT

Submitted to the School of Advanced Graduate Studies of
Michigan State University of Agriculture and Applied Science
in partial fulfillment of the requirements
for the degree of

DOCTOR OF PHILOSOPHY

Department of Chemistry

Year 1957

Approved 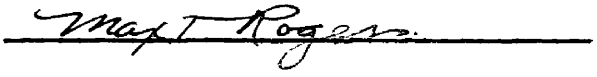

ABSTRACT

Paramagnetic resonance absorption spectra were obtained for samples containing manganous, cupric, and vanadyl ions adsorbed on various adsorbents. The adsorbents included two forms of commercial sulfonic-acid-type cation exchange resins, a carboxylic-acid-type cation exchange resin, an anion exchange resin, silica gel, commercial zeolite, and sugar charcoal activated at 400° centigrade.

The spectra were obtained by means of a paramagnetic resonance spectrometer employing a transmission cavity which resonated at 9,240 megacycles. The microwave radiation was generated by a klystron, detected by a silicon diode crystal, and the resulting signal was analyzed by a lock-in amplifier and displayed on a strip-chart recorder. Magnetic field strengths were measured by means of the magnetic resonance frequency of the proton. The g values and hyperfine structure intervals were computed on the basis of measured line positions.

A study of the spectra of manganese adsorbed on various resins enables a number of conclusions to be drawn concerning the properties of the adsorbed ions. All the spectra of the manganese samples had g values of 2.00. All but the spectra obtained from the anion exchange resin showed nuclear hyperfine structure with intervals of 96 gauss between the various lines. The presence of a weak fine structure in the charcoal and cation exchange resin spectra indicated electrostatic fields of less than cubic symmetry, probably tetragonal. A lower

symmetry, which left the hyperfine structure barely detectable, was present in the zeolite samples. The electrostatic field symmetry about the manganous ions bound to the anion exchange resin was even lower; no hyperfine structure was resolved. The hyperfine structure interval indicated essentially ionic bonding about the manganous ion in all the spectra where resolution was obtained. The line width of the unresolved spectrum of manganese on an anion exchange resin suggested approximately fifty percent covalent bonding between the manganese and the resin.

The most useful information was obtained from the study of adsorbed cupric ion because variations in the g values and hyperfine structure constants were observed in the copper samples. These quantities depended upon both the nature of the adsorbent and upon the coordinated ligands about the cupric ion. Higher g values and smaller hyperfine structure intervals were present in the spectra of hydrated cupric ions on the sulfonic-acid-type cation exchangers. The g values decreased and the hyperfine structure intervals increased as the amount of covalent character in the bond to the adsorbent increased. For a given adsorbent, the g values were substantially reduced and the hyperfine structure interval increased when the coordinated water molecules attached to the cupric ion were replaced with ammonia molecules. The spectra of the samples containing cupric ions adsorbed on the anion exchanger suggest the formation of bonds to four nitrogen atoms on the adsorbent. Some evidence was found for an unresolved hyperfine structure due to interaction of the electron spin with the nitrogen nuclei in both the anion

exchanger and the ammoniated samples. The results with the copper samples seem to support the molecular orbital theory proposed by Stevens and Owen.

Very narrow lines and g values very close to 2.00 indicate a strongl non-cubic, axially symmetrical electrostatic field about the vanadyl ion. Hyperfine structure interaction constants with absolute magnitudes of 0.0182 and 0.00745 cm^{-1} for A and B, respectively, were found for vanadyl ion adsorbed on the sulfonic-acid-type cation exchangers. These constants were reduced by covalent bonding in the case of vanadyl ion adsorbed on the anion exchanger to 0.0158 and 0.00612 cm^{-1}, respectively. Assuming that the decrease was due principally to a decrease in an isotropic contribution to the hyperfine structure, it was shown that the constants A and B must have the same relative sign.

In general, the spectra obtained from the adsorbed ions were similar to the spectra of these ions when in solution or in crystals of known symmetry. Consequently, it was possible to draw a number of conclusions concerning the nature of the bonding between the ions and the adsorbents, and the nature of the adsorbed phase.

TABLE OF CONTENTS

TABLE OF CONTENTS - Continued

LIST OF TABLES

LIST OF FIGURES

LIST OF FIGURES - Continued

FIGURE Page

INTRODUCTION

Despite the work which has been done by means of various physical methods on the nature and state of adsorbed substances, some points remain unsettled; for example, the actual way in which ions are bound to adsorbents is not completely clear. Since paramagnetic resonance absorption provides a new tool for studying paramagnetic ions, it was thought that this technique might provide additional information about the environment of the adsorbed ions. Hence, a group of paramagnetic ions were selected for study, the spectra of which are obtainable at room temperatures and show nuclear hyperfine structure. Spectra were obtained for these ions adsorbed on a number of typical adsorbents.

HISTORICAL SUMMARY

Introduction

When a substance containing unpaired electron spins is placed in a magnetic field, the magnetic moments associated with the spinning electronic charges assume quantized orientations with respect to the direction of the applied magnetic field. The energies associated with the possible orientations are different, being greater for those orientations which oppose the applied field. These energy levels are the Zeeman levels, and the differences between them appear as a fine structure in the optical spectra of paramagnetic substances. Paramagnetic resonance absorption is a means of observing directly transitions between the various spin states. The experimental procedure involves varying the strength of an applied magnetic field until the energy separation between the Zeeman levels is equal to the fixed energy of quanta of radiation incident upon the sample. A plot of energy transmitted by the sample against magnetic field strength shows a peak or peaks corresponding to these transitions. Investigation of paramagnetic ions is usually performed with the electromagnetic radiation in the microwave region and field strengths in the neighborhood of 3000 gauss.

The paramagnetic resonance absorption phenomenon was first observed by Zavoisky (1) in Russia in 1945 and slightly later by Cummerow and Halliday (2) in the United States and by Bagguley and Griffiths (3) in England. Since then a large number of publications have appeared, mainly from British and American workers, reporting both theoretical

and experimental investigations. Wertz (4), Ingram (5), and Gordy, Smith, and Trambarulo (6) have produced brief general reviews of the field. Detailed summaries of the theoretical and experimental work on crystals have been made by Bleaney and Stevens (7) and Bowers and Owen (8).

General Theoretical Principles

Characteristic Parameters of the Spectra

The energy separation between successive spin states of a paramagnetic substance is given by

$$\triangle E = g \beta H \qquad (1)$$

where H is the applied external magnetic field; β is the Bohr magneton, and g is the spectroscopic splitting factor. The g factor is one of the important parameters of paramagnetic resonance absorption spectra, for the position of any line in such spectra can be specified by expressing the g factor associated with it. $\triangle$ E and H are variables depending upon the experimental conditions; g is characteristic of a given line.

The number of different spin levels in a paramagnetic ion is equal to the spin multiplicity, $2S + 1$. Each level corresponds to a different value of the spin quantum number, M, which in the vector model is the component of the spin vector, S, in the direction of the axis of quantization, as shown in Figure 1. Transitions between these levels are allowed, with the selection rule $\triangle M = \pm 1$. Depending on the symmetry of the crystalline electrostatic field in which the ion is located, these 2S allowed transitions will occur at different values

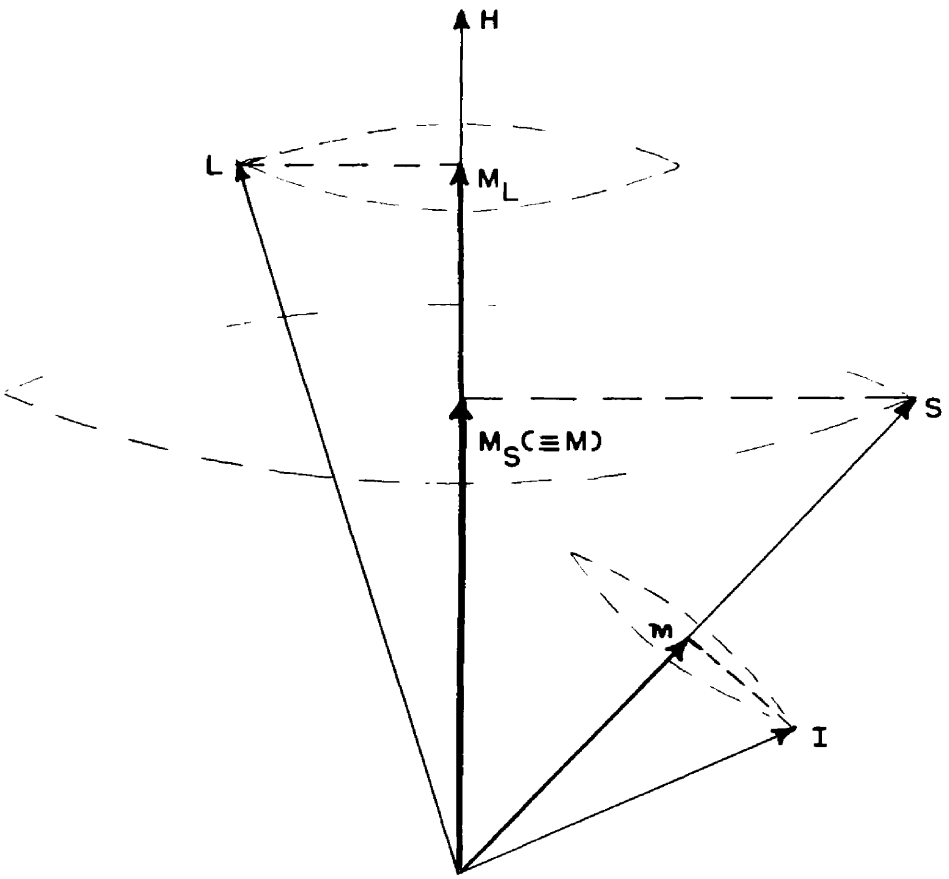

Figure 1. Diagram of L, S, I, and H based on the vector model of the atom. At the field strengths used in paramagnetic resonance experiments, the orbital magnetic moment vector, L, and the electron spin magnetic moment vector, S, precess independently about the direction of the applied magnetic field, H. The nuclear spin magnetic moment vector, I, precesses about the direction of S. M_L, M_S (= M), and m are the projections of L, S, and I, respectively, on the appropriate axes of quantization.

of the applied magnetic field. This multiplicity of lines in the paramagnetic resonance absorption spectrum is termed fine structure.

The line corresponding to a given spin transition in the paramagnetic resonance absorption spectrum may be further split if the nucleus of the paramagnetic ion possesses a spin, I, and an associated magnetic moment. Interaction between the nuclear and electronic spins splits each electronic level into a number of components corresponding to the various nuclear spin levels. There are $2I + 1$ such levels, one for each of the values taken by the nuclear spin quantum number, m. The latter is the component of the nuclear spin vector, I, on the axis of quantization which in this case is the direction of the magnetic field produced by the unpaired electrons. The selection rule in the presence of nuclear spin is $\Delta m = 0$; that is, the nuclear orientation does not change during an electronic spin transition. A splitting of the spectral lines still occurs, however, for the order of the $2I + 1$ component levels is inverted for spin states of opposite sign, with the result that each electronic transition is split into $2I + 1$ lines.[1] This splitting of lines in the paramagnetic resonance absorption spectrum due to interaction with the nuclear spin magnetic moment is termed hyperfine structure.

For a free ion (in the absence of any fields) there is one orbital energy level which is $(2L + 1)$ - fold degenerate. In the presence of an electrostatic field produced by ions and dipoles in the vicinity of the paramagnetic ion, some or all of this degeneracy may be lifted,

---

[1]This effect is illustrated by the behavior of the energy levels of the cupric ion as shown in Figure 2.

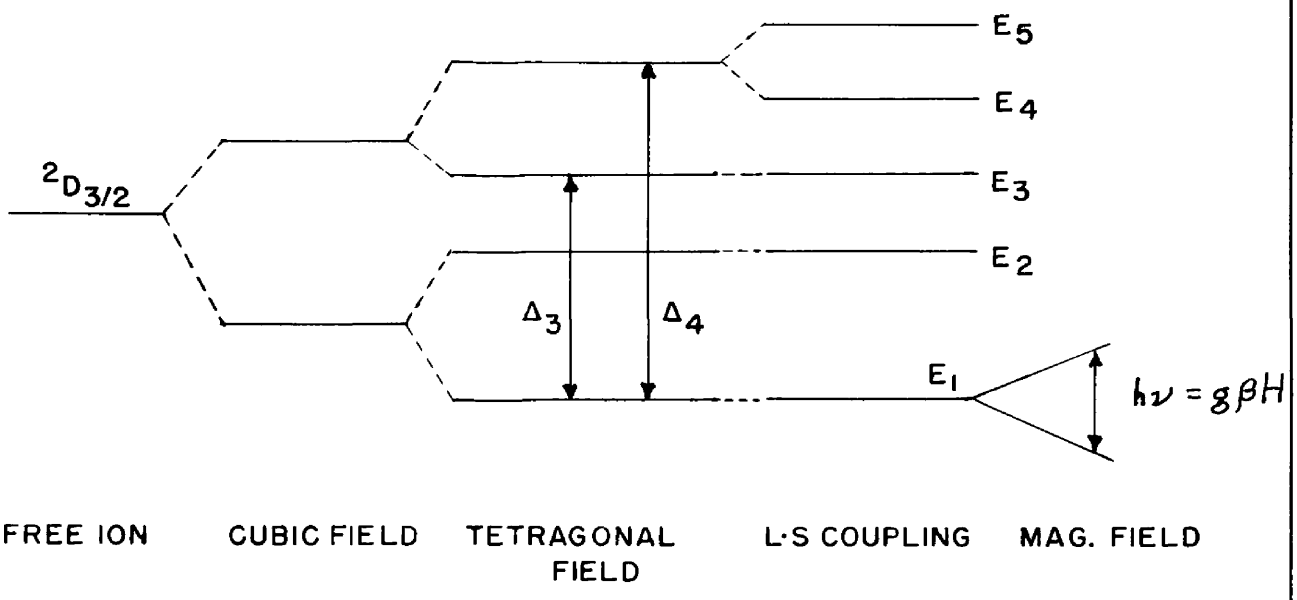

A. ELECTRONIC SPLITTING

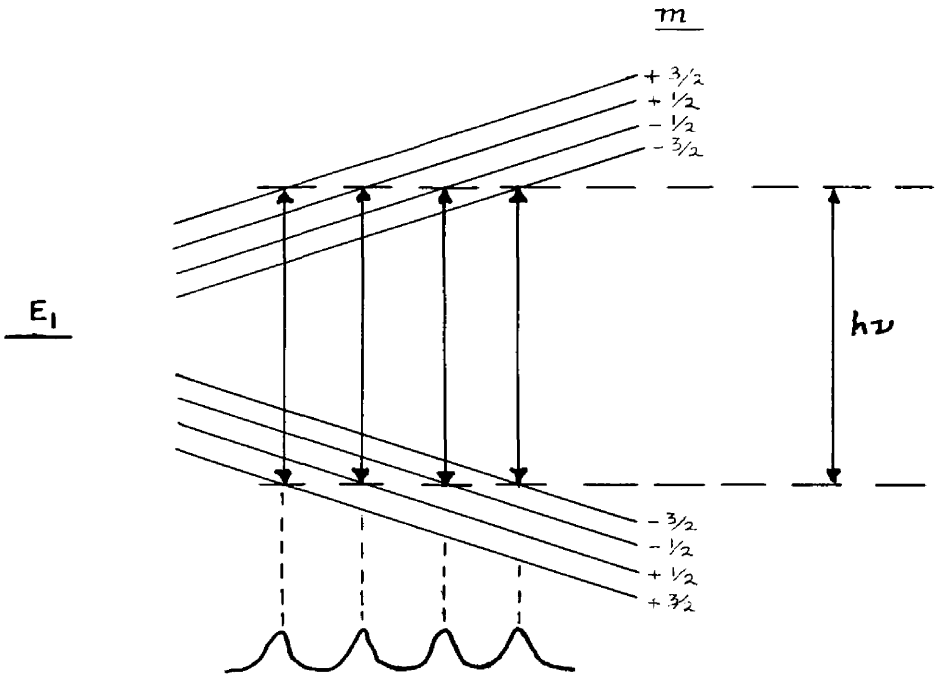

B. NUCLEAR SPLITTING

FIGURE 2. ENERGY LEVELS OF Cu^{++}

depending on the strength and symmetry of the field. Each of the orbital levels is (2S + 1)- fold degenerate in spin. This spin degeneracy may also be partially or completely lifted by second order effects in which the electrostatic field interacts with the electron spins by means of the spin- orbit coupling, which even in strong fields is not completely absent. The spin levels may then be further separated by the external magnetic field. The influence of these two interactions with the crystalline field will become evident later when particular paramagnetic ions will be discussed in more detail.

Line Positions

The totality of the interactions of a paramagnetic ion has been expressed by Abragam and Pryce (9) thus:

$$W = W_F + V + W_{LS} + W_{SS} + \beta \underline{H}\cdot(\underline{L} + 2\underline{S}) + W_N - \gamma\beta_N \underline{H}\cdot\underline{I} \qquad (2)$$

In this equation, the various symbols have the following meanings:

W is the total energy of the ion.

W_F is that part of the energy which depends only on the configurational variables of the electrons and not on their spin.

V is the electrostatic energy due to the crystalline field.

W_{LS} is the energy due to coupling of the spin and orbital motions, commonly called spin-orbit coupling.

W_{SS} is the spin-spin coupling energy.

$\beta\underline{H}\cdot(\underline{L} + 2\underline{S})$ describes the interaction of the external magnetic field with the orbital and spin magnetic moments.

W_N includes two interactions involving the nuclear spin, I; namely the interaction of the nuclear moment with the orbital and spin magnetic moments and, if $I \geq 1$, the interaction of the nuclear quadrupole moment with the gradient of the crystalline electric field.

$\gamma\beta_N \underline{H}\cdot\underline{I}$ is the energy of interaction of the external magnetic field with the nuclear spin magnetic moment.

β is the Bohr magneton

β_N is the nuclear magneton

On the basis of this analysis of the interaction energies, a general Hamiltonian expression for an ion in a crystalline field of axial (tetragonal or trigonal) symmetry was constructed.

$$\mathcal{H} = \beta\,[g_{\parallel} H_Z S_Z + g_{\perp}(H_X S_X + H_Y S_Y)] + D[S_Z^2 - 1/3\, S(S+1)] + A S_Z I_Z + B(S_X I_X + S_Y I_Y) \quad Q[I_Z^2 - 1/3\, I(I+1)] - \gamma\beta_N \underline{H}\cdot\underline{I} \qquad (3)$$

In this equation the various symbols have the following meanings:

H_X, H_Y, and H_Z are the components of the magnetic field vector along the coordinate axes.

S_X, S_Y, and S_Z are the corresponding components of the electron spin vector.

I_X, I_Y, and I_Z are the corresponding components of the nuclear spin vector.

$g_{\parallel}$ and $g_{\perp}$ are the two principal values assumed by a tensor, g, when directed respectively parallel and perpendicular to the symmetry axis.

D is a constant associated with the fine structure separation in the spectrum.

A and B are similar constants associated with the hyperfine structure intervals.

Q is related to the degree of interaction of the nuclear quadrupole moment with the gradient of the electrostatic field.

S is defined by setting the multiplicity of the electrostatic energy levels equal to 2S + I.

Bleaney (10) has used this Hamiltonian to derive an expression for the allowed transitions in strong magnetic fields, using perturbation theory carried to the second order. His calculations were carried out

with two limitations imposed on the problem, namely that the electrostatic field must have axial symmetry and that Q must be much less than A and B. He obtained equations describing the separation, $h\nu$, between energy levels, as a function of the angle, θ , between the external magnetic field and the symmetry axis. The selection rules were $\Delta M = \pm 1$, $\Delta m = 0$. Since paramagnetic resonance absorption experiments are commonly performed at constant frequency and variable field, it is more convenient to adopt the custom of defining H_0 as $h\nu / g\beta$, and dividing through by $g\beta$ to obtain equations for the values of the magnetic field strength, H, at which allowed transitions occur. When this is done, Bleaney's equations assume the following forms.

For fine structure only, ignoring nuclear spin interactions,

$$H = H_0 - \frac{D}{g\beta}(M - 1/2)\left[3\left\{g_{\parallel}^2(\cos^2\theta)/g^2\right\} - 1\right] + \left(\frac{D}{g\beta}\right)^2 \frac{1}{2H_0}\left(\frac{g_{\parallel} g_{\perp}\cos\theta\sin\theta}{g^2}\right)^2 \cdot [4S(S+1)-24M(M-1)-9] - \left(\frac{D}{g\beta}\right)^2 \frac{1}{8H_0}\left(\frac{g_{\perp}\sin\theta}{g}\right)^4 [2S(S+1)-6M(M-1)-3] \quad (4)$$

In the presence of hyperfine structure, the following terms must be added to the right hand side of equation 4.

$$Km \quad \frac{B^2}{4H_0}\left(\frac{A^2+K^2}{K^2}\right)[I(I+1)-m^2] \quad \frac{B^2}{2H_0}\cdot\frac{A}{K}[m(2M-1)] - \frac{1}{2H_0}\left(\frac{A^2-B^2}{K}\right)^2\cdot\left(\frac{g_{\parallel} g_{\perp}}{g^2}\right)^2 m^2\sin^2\theta\cos^2\theta - \frac{Q^2}{2KM(M-1)}\cdot\left(\frac{ABg_{\parallel}g_{\perp}}{K^2g^2}\right)^2\cdot[4I(I+1)-8m^2-1]\, m\sin^2\theta\cos^2\theta \quad \frac{Q^2}{8KM(M-1)}\cdot\left(\frac{B g_{\perp}}{Kg}\right)^4\cdot[2I(I+1)-2m^2-1]\, m\sin^4\theta \quad (5)$$

In these equations, $g^2 = g_{\parallel}^2 \cos^2 \theta + g_{\perp}^2 \sin^2 \theta$, $K^2g^2 = A^2g_{\parallel}^2 \cos^2 \theta + B^2g_{\perp}^2 \sin^2 \theta$ and the other symbols have the same meanings as before. M is the higher quantum number in the transition $M \longrightarrow M-1$.

The various parameters, $g_{\parallel}$, $g_{\perp}$, H_0, A, B, D, and Q may be determined empirically from measurements of the positions of the spectral lines, provided that the interactions associated with them contribute noticeably to the spectrum. It is the aim of theoretical studies in electron spin paramagnetism to account for and predict the observed values.

Line Widths

The widths of paramagnetic resonance absorption lines are important, both theoretically and practically. Practically, observation of very broad lines is difficult or impossible; narrow lines are more easily detectable and permit more precise measurement of the spectral parameters. The theoretical implications of line width may be indicated by a brief survey of the factors influencing line width.

A given paramagnetic ion experiences not only the steady magnetic field produced by the external magnet, but also a small, random field produced by neighboring magnetic dipoles. The result is that resonance occurs throughout a range of field strengths and the absorption line is broadened. This effect involves a direct interaction between electron spins (spin-spin interaction) and the resulting broadening of the absorption line is called dipolar broadening. Since the spin-spin interaction decreases as the inverse cube of the distance between

interacting dipoles, only near neighbours contribute to the line width. Consequently, line widths may be greatly reduced by diluting a paramagnetic substance with a diamagnetic one, thereby increasing the separation between paramagnetic centers. This technique, which has been widely used, is known as magnetic dilution.

According to the uncertainty principle, the uncertainty in the energy of an excited state increases as the lifetime in that state decreases. Hence, any relaxation process, which provides a mechanism for the unpaired electron spins to return from a higher spin level to a lower one, reduces the lifetime in the higher state and broadens the absorption line corresponding to that transition. The process which provides this mechanism is the indirect interaction between the electron spin and the thermal vibrations of the crystalline lattice by means of the spin-orbit coupling and spin-spin coupling. The lattice vibrations affect the orientation of the orbital magnetic moment because of electrical interactions with the non-spherical electron cloud. The orbital magnetic moment is, in turn, magnetically coupled to the electron spin. Likewise, the lattice vibrations produce periodic variations in the distance between neighboring magnetic spin dipoles. Both of these effects provide means whereby the excess energy of the electron spin in an excited state may be transferred to the lattice and the spin may return to alignment with the magnetic field. The lifetime of the excited spin state is directly proportional to the amount of splitting of the orbital levels by the crystalline electrostatic field and inversely proportional to the spin-orbit coupling constant, λ ,

and to the temperature. As a result, when spin-lattice interaction contributes significantly to the line width, the width may be decreased by reducing the temperature.

The third major factor influencing line width is electron exchange interaction between neighboring paramagnetic centers. The effect is analogous to the valence bond treatment of the single bond, in which the two bonding electrons resonate between orbitals associated with each of the nuclei because of the indistinguishability of electrons. When a pair of paramagnetic ions between which exchange occurs are oriented identically with respect to the magnetic field and therefore have identical resonance frequencies, the effect of exchange is to smooth out the random magnetic fields experienced by the two and sharpen the absorption lines. Van Vleck (11) has calculated the effect of exchange interaction on the various moments of the absorption line and finds that no contribution to the second moment occurs, but that the fourth moment is greatly increased. The effect on line shape is that the line is much more sharply peaked at the center than is the typical Gaussian curve. When the two ions between which exchange occurs are differently oriented in the magnetic field and therefore tend to resonate at different field strengths, the effect of exchange is to produce a single resonance line at the arithmetic mean of the two individual lines, and line broadening occurs. This contribution to line width also depends on the distance between paramagnetic centers and may be reduced by magnetic dilution.

Specific Transition-metal Ions

It is now possible to consider the application of the general principles outlined above to the special cases of the three iron-group transition elements which were the subject of this investigation.

Manganese

The doubly charged manganous ion occupies the middle position in the series of iron-group transition elements, because here the 3d shell is exactly half filled ($S = 5/2$) and there is no orbital degeneracy of energy levels ($L = 0$). Under the proper conditions, a fine structure consisting of five lines may be expected in the paramagnetic resonance absorption pattern and, since the Mn^{55} nucleus possesses a spin of 5/2, each of the spin levels is resolved into six components and a six-line hyperfine structure pattern is also to be expected. Hence, with all the degeneracy removed, the absorption pattern of manganous ion should consist of thirty lines.[1] An energy level diagram is shown in Figure 3.

Resonance absorption has been detected at room temperature for most of the compounds involving manganous ion, since, with $L = 0$ for the ground state, there is almost no spin-orbit coupling and the spin-lattice relaxation time is very long. However, narrow lines have been obtained only at high dilution, for the large value of the spin makes dipolar broadening an important factor at higher magnetic concentrations.

In cubic fields, the hyperfine structure only is observed; the fine structure becomes evident in fields of lower symmetry. The effect of

---

[1]Under certain conditions more have been observed (12).

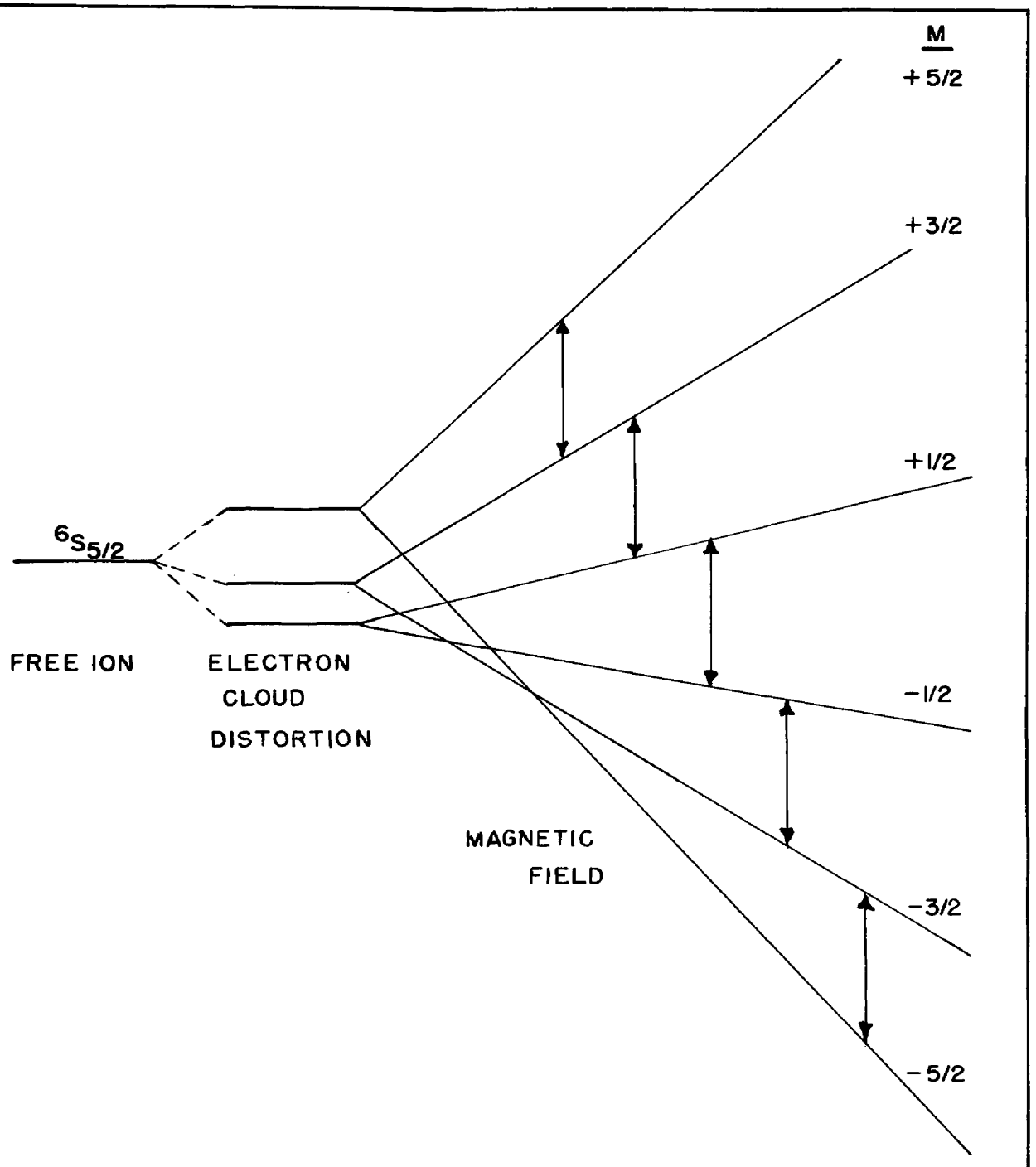

FIGURE 3.

ELECTRON SPIN LEVELS OF Mn^{++}

(FROM INGRAM[5])

crystalline field symmetry upon the paramagnetic resonance absorption pattern is illustrated by the results of Hershberger and Leifer (13), who investigated various phosphor crystals containing small amounts of manganese. These workers found a simple six line spectrum due to hyperfine structure in three crystals possessing cubic symmetry, a thirty line spectrum in hexagonal zinc sulfide, and a single, broad resonance 750 to 1000 gauss wide in seven crystals of tetragonal, rhombohedral and rhombic symmetry.

The observed value of the hyperfine structure constant, A, is anomalously high (ca. 0.01 cm^{-1}) if the only electron configuration contributing to the ground state is $3s^2\ 3d^5$, ^6S. Abragam and Pryce (9) postulated the promotion of inner electrons in order to explain this large interaction with the nuclear spin. Although the energy involved in promoting 3s electrons is very large, their contribution to the hyperfine structure is also very large, because of the large value of the s-type wave function at the nucleus. Consequently, a small admixture of the configuration $3s\ 3d^5\ 4s$, ^6S was postulated, so that the actual state of the ion could be represented by $^6S + \alpha\ ^6S'$, where ^6S stands for the main term and $^6S'$ for some normalized linear combination of these two terms, and α is a small coefficient. With this treatment, A is proportional to α and to the values of the 3s and 4s wave functions at the origin.

Van Wieringen (14) investigated paramagnetic resonance absorption in powdered samples containing manganous ion diluted in various diamagnetic compounds of cubic symmetry. The observed six line spectra

conformed to the equation

$$H = H_0 - A'm - A'^2/2H_0 \left[I (I + 1) - m^2 \right] \qquad (6)$$

This equation is derived from equations 4 and 5 by setting D = 0, A = B, and taking only the first two terms of equation 5. Here, for convenience, A' is defined as

$$A' = A/g \beta, \qquad (7)$$

where A has dimensions of energy and A' of field strength. A progressive decrease in the magnitude of A' was observed as the extent of covalent bonding between the manganous ion and its neighbors increased.

On the basis of the promoted s-electron hypothesis of Abragam and Pryce, Van Wieringen concluded that the contribution to the hyperfine splitting from the covalent bond is less by a factor of ten than the contribution from the ionic bond. In the first approximation the covalent contribution can be neglected. Thus, the amount of hyperfine splitting is directly proportional to the amount of ionic bonding. With the further assumption that the bonding is completely ionic when the neighbors are fluoride ions or water dipoles, it is possible to state the percent of covalent bonding on the basis of measured values of A'. The results for a few phosphors are collected in Table I.

The effect of exchange interactions on the manganous ion spectrum has been observed in powered zinc sulfide phosphor containing varying amounts of manganous ion (14), and in aqueous solutions of manganous ion (15). In both cases, as the magnetic concentration increases the hyperfine structure first disappears because of dipolar broadening, and exchange interaction then narrows this single broad resonance.

TABLE I

COVALENT BONDING IN MANGANESE-CONTAINING PHOSPHORS
(From Van Wieringen (14))

Neighbour	H_2O	F^-	CO_3^{-2}	O^{-2}	S^{-2}	Se^{-2}	Te^{-2}
Approx. A'	98	98	94	80 - 90	69	65	59
Percent covalent bonding	0	0	5	10 - 20	30	35	40

A disappearance of the paramagnetic resonance absorption spectrum was observed in aqueous solution by Cohn and Townsend (16) when a complexing agent was added. This effect was attributed to line broadening due to decreasing symmetry about the ion. The dissociation constants of several biochemically important complexes involving manganese were measured using the fact that only the uncomplexed ion contributed to the resonance absorption.

McGarvey (17) investigated aqueous solutions of a number of iron group ions, including manganous, cupric, and vanadyl. The observed widths were accounted for by assuming that the ion is present in a small micro-crystal formed from solvent molecules or complexing groups and that this micro-crystal possesses a spin Hamiltonian similar to that observed in solid crystals. The widths depended on the symmetry of the electric field created by the complexing groups.

Copper

The ground state of the cupric ion is $^2D_{3/2}$. The free ion has fivefold orbital degeneracy which is lifted in cubic and tetragonal crystalline fields in the manner shown in Figure 2. In the hydrated salts the separation between the two lowest orbital levels is so great that only the lowest level is inhabited at room temperature. Since the 3d shell lacks one electron of being completely filled, the net spin is S = 1/2. The behaviour in paramagnetic resonance absorption experiments is similar to that of an ion having only one electron in the 3d shell. No fine structure is to be expected for S = 1/2. In most compounds owing to the wide separation of the orbital levels, the spin-lattice relaxation time of the cupric ion is sufficiently long to allow room temperature observation of absorption. Both copper isotopes, Cu^{63} and Cu^{65}, possess nuclear spins of I = 3/2. The resulting four-line hyperfine structure in the spectrum is due mainly to the Cu^{63} isotope, which is much more abundant.

In tetragonal fields, when the line widths are too great for nuclear quadrupole interactions to be observed, the angular variation of the spectrum is described by the following equation:

$$H = H_0 - Km - \frac{B^2}{4 H_0} \left(\frac{A^2 + K^2}{K^2} \right) [\, I (I + 1) - m^2 \,]$$

$$- \frac{1}{2 H_0} \left(\frac{A^2 - B^2}{K} \right)^2 \cdot \frac{(g_{\parallel} g_{\perp})^2}{(g^2)} \cdot m \sin^2 \theta \cos^2 \theta \quad (8)$$

This equation is obtained from equations 4 and 5 by setting D and Q equal to zero.

The positions of the lines in the copper spectrum change considerably as the angle θ between the symmetry axis and the magnetic field is varied. Typical values for the various parameters are as follows: $g_{\parallel} = 2.4$; $g_{\perp} = 2.1$; $A = 0.010\ cm^{-1}$; $B = 0.003\ cm^{-1}$.

On the assumption that the only electronic configuration contributing to the ^2D ground state of the hydrated cupric ion is $3s^2\ 3p^6\ 3d^9$, Polder (18) calculated g values as follows:

$$g_{\parallel} = 2(1 - 4\lambda / \Delta_3) \qquad (8)$$

$$g_{\perp} = 2(1 - \lambda / \Delta_4) \qquad (9)$$

In these equations, λ is the spin-orbit coupling constant in the crystal, and Δ_3, and Δ_4, are the orbital energy separations indicated in Figure 2. Because the 3d shell is more than half filled, λ is negative and the g values are greater than 2.00. A simplified presentation of Polder's treatment and its application to cupric sulfate has been made by Kikuchi and Spence (19). More recent experimental values for cupric sulfate than those quoted in the latter paper were reported by Bagguley and Griffiths (20).

Although Polder's theory accounts fairly well for observed g values, it fails to explain the hyperfine structure. Specifically, this theory predicts that B should be greater than A, whereas the reverse is invariably true. Abragam and Pryce (21,22) have invoked the promoted s electron hypothesis which was used to explain the hyperfine structure of the manganese spectrum, to account for this anomaly, too. Polder's theory, with no s electron promotion, leads to the following relations between the hyperfine structure parameters and the g values:

$$A = [(g_{\parallel} - 2) \quad 3/7 \ (g_{\perp} - 2) \ - 4/7] \ P \tag{10}$$

$$B = [(g_{\perp} - 2) \quad 3/14 \ (g_{\perp} - 2) \quad 2/7] \ P \tag{11}$$

P is estimated by comparison with the optical hyperfine spectrum of the free copper atom in the configuration $3d^9 4s^2$, or by calculating the mean value of $1/r^3$ from known Hartree wave functions for the configuration $3d^{10}$ of the cuprous ion. Both methods lead to approximately the same result:

$$P \simeq 0.035 \text{ cm}^{-1} \tag{12}$$

The assumption of a promoted s electron leads to an isotropic correction, k, on the hyperfine structure parameters so that with typical values of 2.4 and 2.1 inserted for $g_{\parallel}$ and $g_{\perp}$, A and B become,

$$A = (-k - 0.13) \ P \tag{13}$$

$$B = (-k + 0.365) \ P \tag{14}$$

If k is arbitrarily taken to be 0.25, A and B become -0.013 cm^{-1} and 0.004 cm^{-1}, respectively, in good agreement with observation. Here, k is proportional to the degree of admixture of excited configurations and to the values of the 3s and 4s wave functions at the origin.

Sands (23) reported the application of this theory to the cupric ion resonance spectrum in glass. The observed quantities were $g_{\parallel} = 2.32$; $g_{\perp} = 2.06$; $A = -0.0157 \text{ cm}^{-1}$; $B = 0.00228 \text{ cm}^{-1}$. By means of equations 13 and 14 a value of $k = 0.26$ was obtained.

The question of the formation of covalent bonds involving the paramagnetic cupric ion is a difficult one. The coordination number of copper is four, and the ligands are commonly arranged in a square about the central ion. These facts lead naturally to the supposition that

dsp^2 hybridization of the orbitals belonging to the cupric ion occurs. This possibility has been considered by Abragam and Pryce (9,21) and repeated by Abragam (22), who reported that, although a satisfactory anisotropy can be obtained for the hyperfine structure, the presence of the unpaired electron in the state $4p_z$ leads to $g_{\parallel} = 2$. Moreover, this covalent structure has different symmetry properties from Polder's ionic structure, and no resonance can exist between them.

Stevens (24) and Owen (25,26) have proposed a molecular orbital theory of covalent bonding in octahedral cupric complexes which does not involve the change in electron configuration. The complex is treated by the method of molecular orbitals with the assumption that the unpaired spin is partly in the central d orbits and partly in P_π orbits around the outer nuclei. This leads to a reduction in the orbital g factor and to the possibility of observing hyperfine structure from the outer nuclei. The resulting equations for the g values are:

$$g_{\parallel} = 2 - 8(\lambda'/\Delta_3)a^2 b^2 \qquad (15)$$

$$g_{\perp} = 2 - (\lambda'/\Delta_4)a^2 (1 + b^2) \qquad (16)$$

where λ' is nearly equal to the spin-orbit coupling factor in the free ion. The parameters a and b may assume values between zero and one.

Howard (27) proposed an explanation of the magnetic properties of the covalent ferricyanide complex based on the assumption of a strong electrostatic field which removes the coupling of spin to orbit and of spin to spin. Here, the results were the same as if the molecular orbital or the Slater-Pauling theory had been applied. The theory of Howard was later used by Kotani (28) to calculate the magnetic moment of the

ferricyanide complex. Again the results were qualitatively the same as Pauling's covalent theory.

Orgel (29) has given a simple electrostatic interpretation of the extra stability of the non-octahedral complexes of the cupric ion. If the four ligands in one plane move closer and the other two move away from the central ion, a plane of higher electron density is formed. Then, the copper orbital containing the unpaired electron moves into this plane, giving stabilization.

The predictions concerning the g values and hyperfine structure intervals made by the various theories may be compared with some experimental results in a number of cupric compounds possessing tetragonal symmetry. Polder's theory predicts $g_{\parallel} = 2.4$, $g_{\perp} = 2.1$ for ionic bonds between the central cupric ion and its neighbour. The promoted s electron hypothesis of Abragam and Pryce further predicts $A = 0.013\ cm^{-1}$ and $B = 0.004\ cm^{-1}$. Bagguley and Griffiths (20) found $g_{\parallel} = 2.47$, $g_{\perp} = 2.08$ for cupric sulfate pentahydrate. Bleaney, Bowers and Ingram (30) found $g_{\parallel} = 2.45$, $g_{\perp} = 2.14$, $A = 0.0103\ cm^{-1}$, and $B = 0.0035\ cm^{-1}$ for cupric potassium sulfate.

Spence and Carlson (31) reported $g_{\parallel} = 2.22$, $g_{\perp} = 2.05$ in copper tetrammine sulfate. These workers discussed the covalent bonding in this crystal in terms of the ratio, λ/λ_0, of the spin-orbit coupling constant in the crystal to that of the free ion. In the hydrated complexes this ratio is 0.8, whereas in the tetrammine complex it is 0.55.

McGarvey (32) found $g_{\parallel} = 2.254$, $g_{\perp} = 2.075$ in single crystals of cupric acetylacetonate. A nuclear hyperfine structure was observed in solutions of cupric acetylacetonate in mixtures of various solvents. Because of the averaging effect of the random motion in liquids, the observed splitting should be due only to the isotropic term, kP, in equations 13 and 14. Also observed was a solvation effect amounting to a ten percent variation in the splitting as the composition of the solvent was changed. The magnitude of the splitting decreased as the complexing action of the solvent increased.

Perhaps the smallest g values were observed by Bennett and Ingram (33) in cupric phthalocyanine. They found $g_{\parallel} = 2.165$, $g_{\perp} = 2.045$. In a crystal in which the copper ions were diluted with zinc, a hyperfine structure appeared with $A = 0.021$ cm^{-1} and $B = 0.003$ cm^{-1}.

When the orientation of the various cupric ions in a bulk sample is completely random, and the local field about each ion has axial symmetry, it is also possible to measure the spectral parameters. The absorption spectrum, which is the sum of the absorptions over all possible orientations of the symmetry axis, possesses sharp upper and lower boundaries. Sands (23) has calculated the shape of this absorption. In the absence of nuclear hyperfine structure, the absorption intensity is related to the magnetic field thus:

$$I = \frac{N\,(H_0^2 / H^3)}{\left((g_{\parallel}^2 - g_{\perp}^2)\,[(H_0/H)^2 - g_{\perp}^2] \right)^{1/2}} \qquad (17)$$

Here, I is the intensity of absorption; N is a proportionality factor related to the number of paramagnetic centers in the sample; $H_0 = h\nu/\beta$.

The shape of this curve is shown in Figure 4. In the presence of hyperfine structure, there would be 2I + 1 such absorption curves, corresponding to the various orientations of the nuclear spin, I. In this case the positions of the upper and lower edges of the spectrum are given by the following equations:

$$H_U = H_0/g_\perp - m B'/\beta g_\perp \qquad (18)$$

$$H_L = H_0/g_\parallel - m A'/\beta g_\parallel \qquad (19)$$

where H_U and H_L are, respectively, the upper and lower boundaries of the absorption curve corresponding to the nuclear spin quantum number, m.

Additional hyperfine structure arising from interaction of the unpaired electron spin with nuclear spins in the ligands has been reported by Ingram, Bennett, George, and Goldstein (34). These authors investigated the paramagnetic resonance absorption spectra of cupric complexes of tetraphenylporphyrin and its parachloro derivative. In the unchlorinated compounds the hyperfine structure consisted of four lines, with spacing about the same as in cupric phthalocyanine. In the chloro derivative a further splitting of about 100 gauss occurred, indicating that the unpaired electron was associated with the chlorine nuclei for an appreciable time. The estimated copper-chlorine distance was nine to ten angstroms.

Paramagnetic resonance absorption of supercooled non-aqueous solutions of cupric salts at 90°K was investigated by Garifyanow, as quoted by Kozyrev (35). The spectrum consisted of an "exchange peak," with a g factor of 2.091, and four hyperfine structure peaks centered at g = 2.369 separated by intervals of 130 gauss.

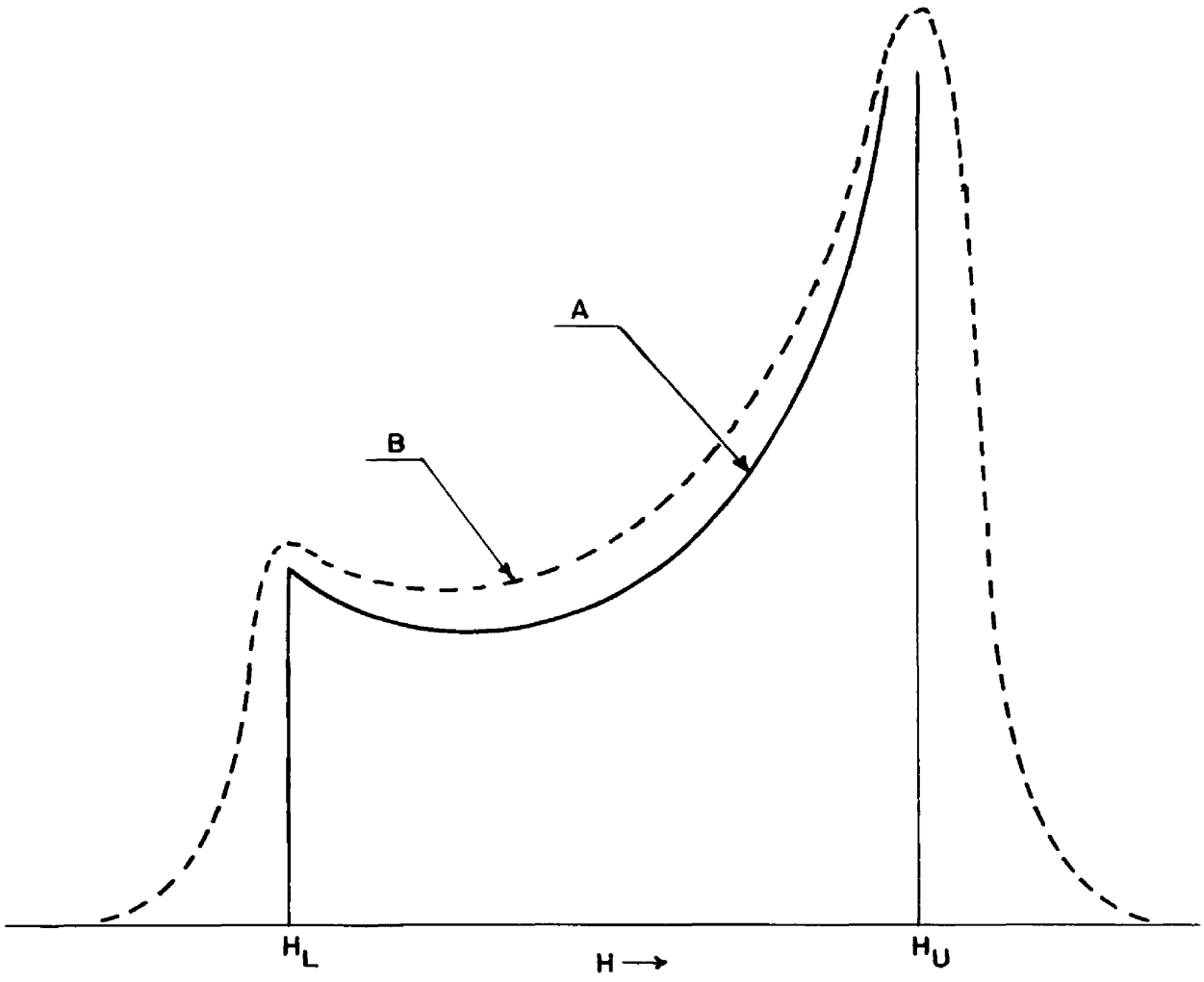

A dN/dH, THEORETICAL ABSORPTION CURVE

B OBSERVED CURVE, FINITE LINE WIDTH

FIGURE 4. Cu^{++} ABSORPTION LINE FOR RANDOM ORIENTATION OF SYMMETRY AXES (FROM SANDS[23])

Vanadium

The V^{+4} ion, with one electron in the 3d shell, has a $^2D_{5/2}$ ground state. The spin Hamiltonian has the same form as that for the cupric ion. The order of the orbital levels is reversed, however, as shown in Figure 5. When the symmetry of the crystalline field is cubic or nearly cubic, the separation of orbital levels is small. Consequently, the spin-lattice relaxation time is short and no room temperature resonance is observed. In the vanadyl ion (VO^{+2}), however, the departure from cubic symmetry is extreme. As a result the spin-lattice relaxation time is long and very narrow absorption lines are observed at room temperature.

Because of the weak spin-orbit interaction, g factors very close to 2.00 have been observed (36). Interaction of the electron spin with the abundant V^{51} nucleus (I = 7/2) to produce an eight-line hyperfine structure in aqueous solution was observed by Pake and Sands (37). The hyperfine structure interval was 120 gauss. Kozyrev (35) also reported a paramagnetic resonance absorption spectrum of vanadyl salts in organic solvents at 90°K. Thirteen lines were observed, of which eight central lines centered at g = 1.960 were much more intense; the separation between these central lines was 76 gauss. The other five lines were part of a second group of eight, partially obscured by the first group. The second group were centered at g = 1.92 and were separated by intervals of approximately 200 gauss.

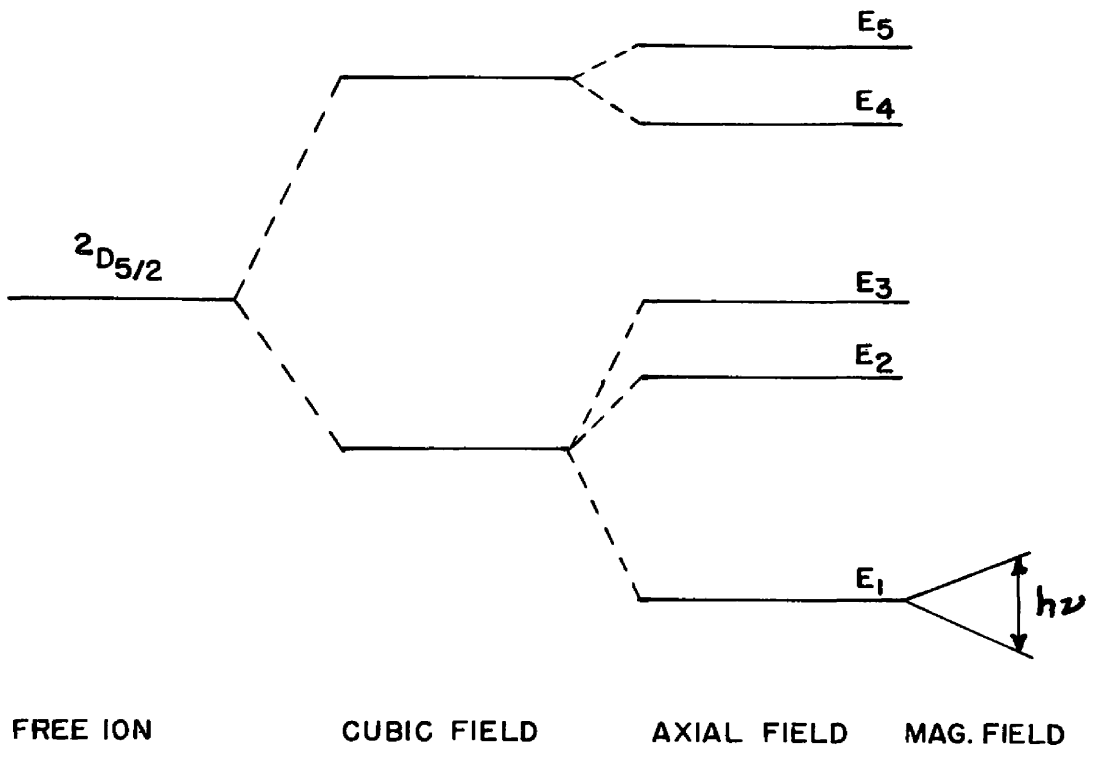

FIGURE 5. ORBITAL LEVELS OF V^{+4} (NOT TO SCALE)

PARAMAGNETIC RESONANCE SPECTROMETER

Introduction

The apparatus required in order to observe the paramagnetic resonance absorption phenomenon consists of three rather distinct systems. First, there is required a magnetic field, which is homogeneous throughout the volume of the sample, steady over a period of time up to one-half hour long and capable of variation between zero and several thousand gauss. This magnetic field removes the degeneracy between the various magnetic spin states of the paramagnetic material. Second, there must be a source of radiation to provide the energy needed to effect transitions between these spin states. The energy of the quanta absorbed and therefore the wavelength of the absorbed radiation at resonance depends upon the strength of the magnetic field which separates the magnetic energy levels. With field strengths of about 3000 gauss the wavelength of absorbed radiation is about three cm. corresponding to a frequency of about 9300 megacycles. Third, since the power absorbed in paramagnetic resonance absorption is frequently only a minute fraction of the total power incident on the sample, devious means must be employed to detect the absorption, to increase the signal-to-noise ratio, and to display the resulting signal as a function of the magnetic field strength.

Apparatus

The Magnetic Field

The Electromagnet.[1] The magnet was designed for a high voltage power supply since electronic regulation of high voltage supplies is somewhat simpler than the regulation of low voltage supplies. A rectangular yoke was used to provide the necessary mechanical strength and improve uniformity of field. Pole pieces 7 1/2 inches in diameter provide a uniform field over a relatively large area. Water cooling was employed to minimize change of the resistance of the coils through heating. A mechanical means of varying the pole gap was considered desirable since it is occasionally necessary to accommodate larger apparatus. Since pole caps of different materials are useful under various circumstances a means should be provided for replacing these. The yoke must have a large enough cross section to provide a low reluctance magnetic path and also mechanical strength. With these considerations in mind the design outlined below was adopted.

The dimensions and method of assembly of yoke and pole pieces are shown in Figure 6 and the mechanical means of varying the pole gap is indicated. These parts were constructed from cold-rolled steel and were machined to close tolerances in the Mechanical Engineering Department. The yoke was assembled first, using 1/2" x 13" cap screws, and the holes for the pole pieces bored together in one operation.

---

[1]Many of the details of the construction of the magnet and some of its associated electronic circuitry have been previously described by Rogers, Thompson, and Faber (38).

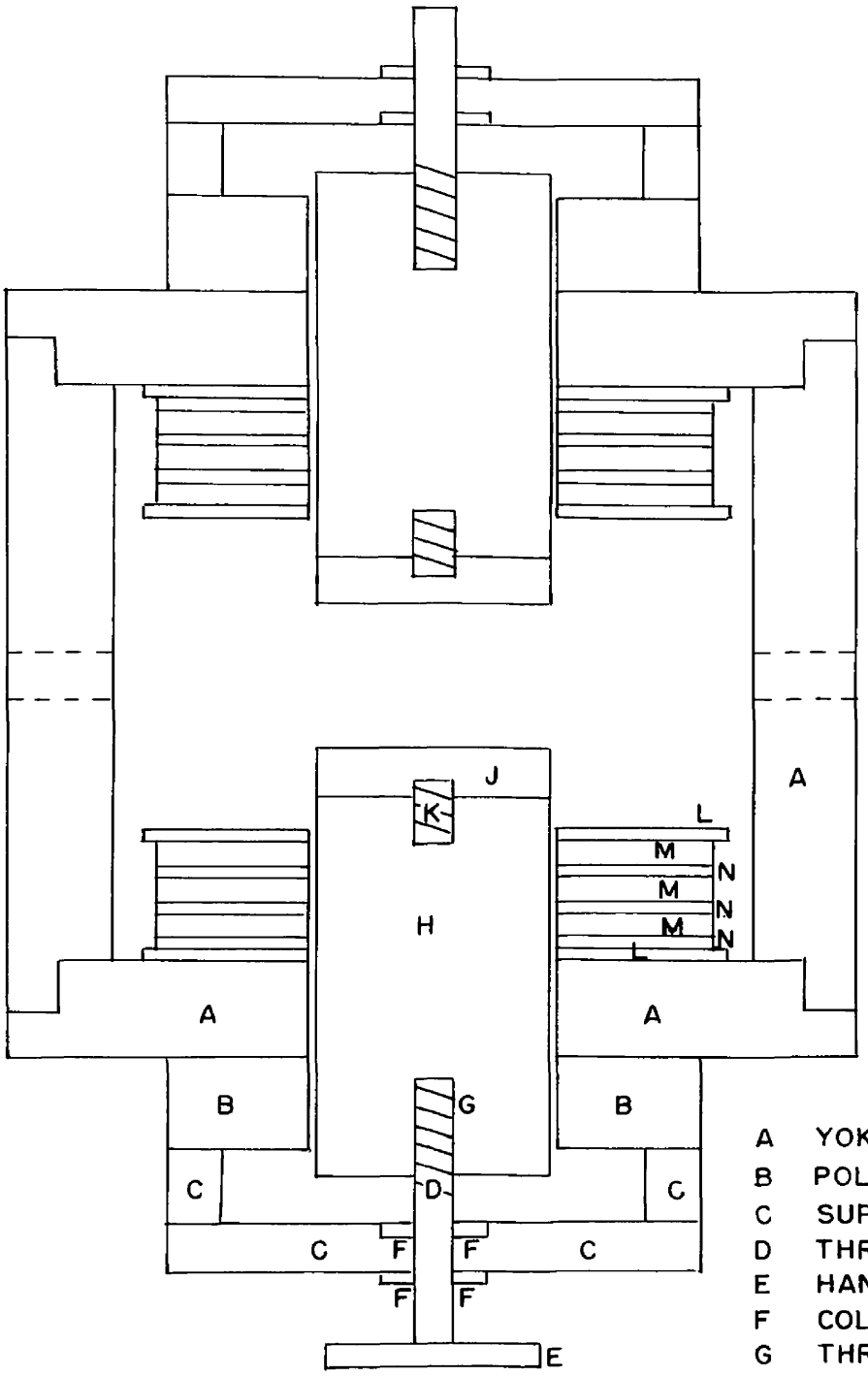

A YOKE
B POLE PIECE SUPPORT
C SUPPORT FOR BOLT D
D THREADED 1" STEEL ROD
E HANDWHEEL
F COLLARS LOCKED TO BOLT
G THREADED 1" HOLE
H POLE PIECE, 7 1/2" DIA.
J POLE CAP
K STUD TO HOLD CAP
L ALUMINUM END PLATES
M MAGNET COILS
N COOLING COILS

FIGURE 6. THE ELECTROMAGNET

The pole pieces were then inserted and hand-lapped for a smooth sliding fit. The parts for moving the pole pieces in and out were added and the entire assembly placed on a welded angle-iron base.

The energizing coils are wound in six sections. Each section is wound on a copper spool as shown in Figure 6. The copper spool was built from sheet copper cut to size and soldered. The cooling coils consist of one turn of 1/4" o.d. copper tubing soldered to each side of the spool and shaped so that adjacent spools fit together with the copper coils of one spool contacting the sheet copper side of the next. In this way heat transfer is maximized and, since the coils are all in parallel, resistance to flow of cooling water is minimized. About 1200 turns of Formvar-insulated No. 14 copper magnet wire are wound on each spool in 60 layers of 20 turns each. The inner lead is brought out through a hole in the side of the coil and is protected by a fluorothene sleeve. Three coils are placed on each pole piece with a piece of 1/4" aluminum sheet on each side and the whole sandwich bolted together by bolts through the aluminum. This is done to bring the cooling coils into close contact with the spools. The electrical leads are carried out to a terminal board and the copper tubing leads were connected to water inlet and outlet manifolds.

The six coils taken together have about 7200 turns of No. 14 wire with a length of about 23,000 feet and resistance of about 50 ohms. With a maximum current of 9 amperes from the power supply the maximum number of ampere-turns is about 63,000.

The uniformity of the magnetic field at the sample depends upon the homogeneity of the metal in the pole caps and the smoothness of their surfaces. The faces of the machined pole caps were first made reasonably flat by grinding on a centerless grinder. Next they were annealed to remove internal strain. Finally the faces were ground by hand lapping with Pyrex discs and Carborundum powder in a vehicle of turpentine and polished with jewellers' rouge suspended in turpentine on a cloth lap. The technique employed was the standard three-disc method of making optical flats as described by Ingalls (39). The polished pole faces were compared with a quartz optical flat by observing the interference fringes formed between the two surfaces in the monochromatic light of a sodium lamp. Grinding and polishing were stopped when both pole faces were within two or three fringes of true optical flatness. The surfaces thus formed were washed with turpentine, then with acetone and wiped free of dust with lens tissue. The entire face and sides of both caps were then covered with several coats of a clear plastic spray of the sort used to protect automobile chrome against corrosion.

The Magnet Power Supply. Power for the magnet is produced from the local 220 volt three-phase supply, which is converted to direct current by selenium rectifiers in a three-phase bridge as shown in Figure 7. This bridge is capable of delivering 250-300 volts at up to 25 amperes. The rectifiers are forced-air cooled by means of a fan which is automatically turned on with the input to the rectifiers. The rectifiers may also be connected to a 440 volt supply; as yet the current control circuitry for the magnet is not adapted for this voltage although the necessary changes are minor.

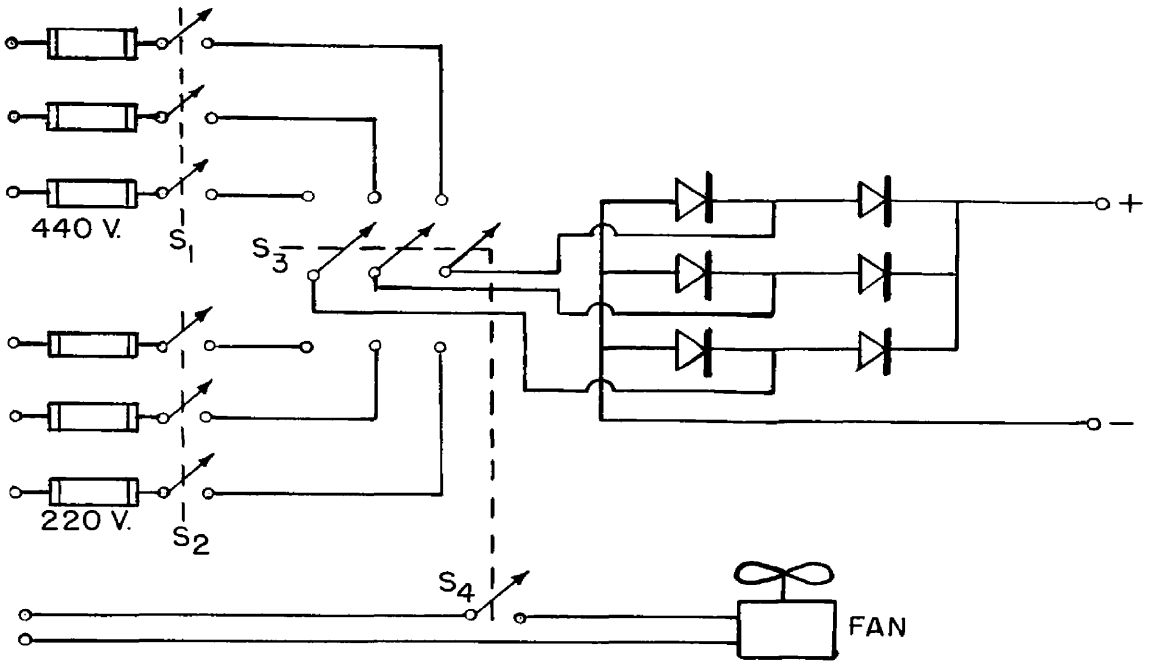

FIGURE 7. 3-PHASE BRIDGE RECTIFIER FOR MAGNET POWER SUPPLY

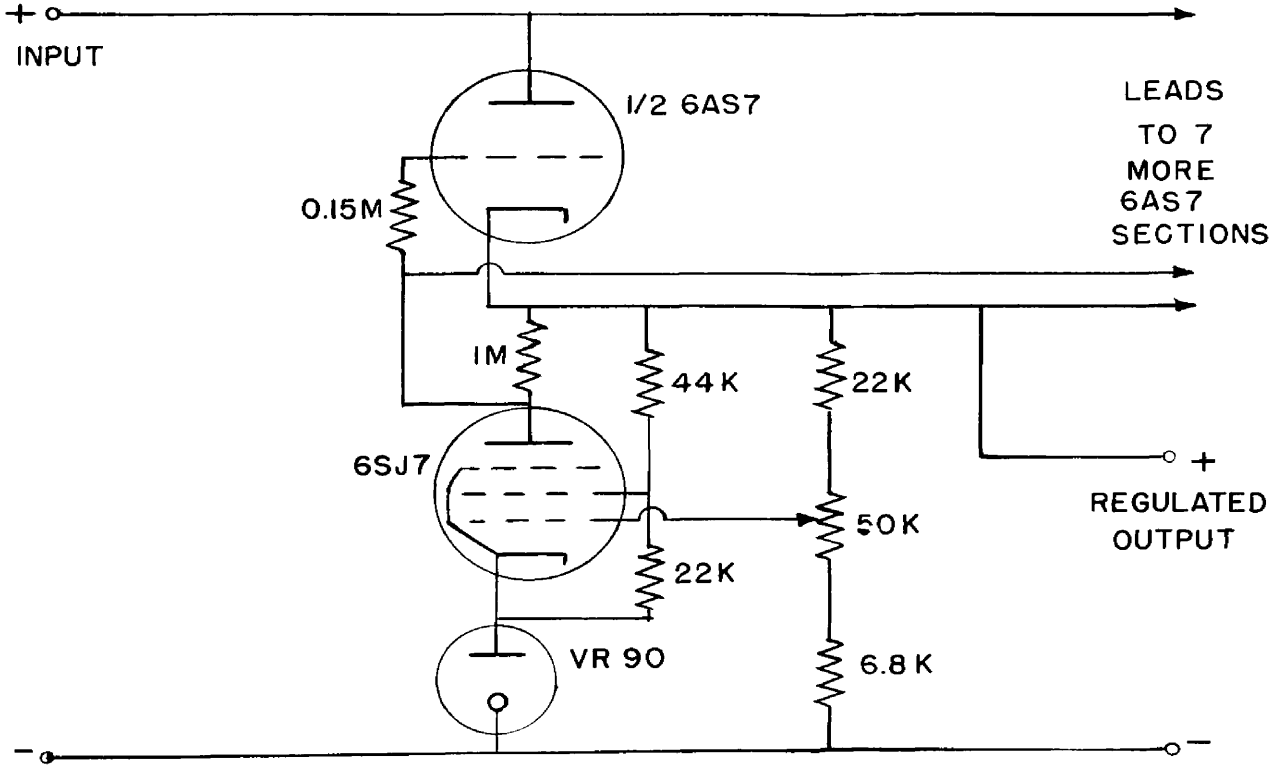

FIGURE 8. SCREEN-VOLTAGE REGULATOR FOR MAGNET POWER SUPPLY

The rectified, pulsed direct current is next smoothed by a series of inductance-capacitance filters to produce 300 volts of direct current with a low percentage of ripple. At this point, however, the ripple voltage is still too great to produce the steady magnetic field required for the observation of narrow resonance lines; there is also a random fluctuation of the line voltage with a period of about a second. These remaining sources of instability in the magnet current are minimized by a voltage regulator circuit which also provides a means of varying the magnet current through a wide range. The schematic diagram is shown in Figure 9.

The magnet coils are placed between ground potential and the cathodes of a large number of 6L6 power tetrode vacuum tubes. The 6L6's are arranged in parallel on five chassis containing eighteen tubes each. Hence the magnet current depends upon the grid potential of the 6L6 tubes; in fact the voltage across the magnet coils will differ from this grid potential only by the small negative grid bias at which the 6L6 operates. The grid potential in turn is obtained from the one megohm dropping resistor connecting the grids to the positive supply and will vary with the current through this resistor, which also acts as the plate resistor of the 6AU6 tube. This tube provides essentially complete negative feedback of any variations in the voltage across the magnet, since its control grid is a.c. connected directly to the positive terminal of the magnet coils by means of a capacitor, and its d.c. grid bias, obtained via the fixed and variable resistors which connect it to the positive terminal, is compared with the fixed cathode

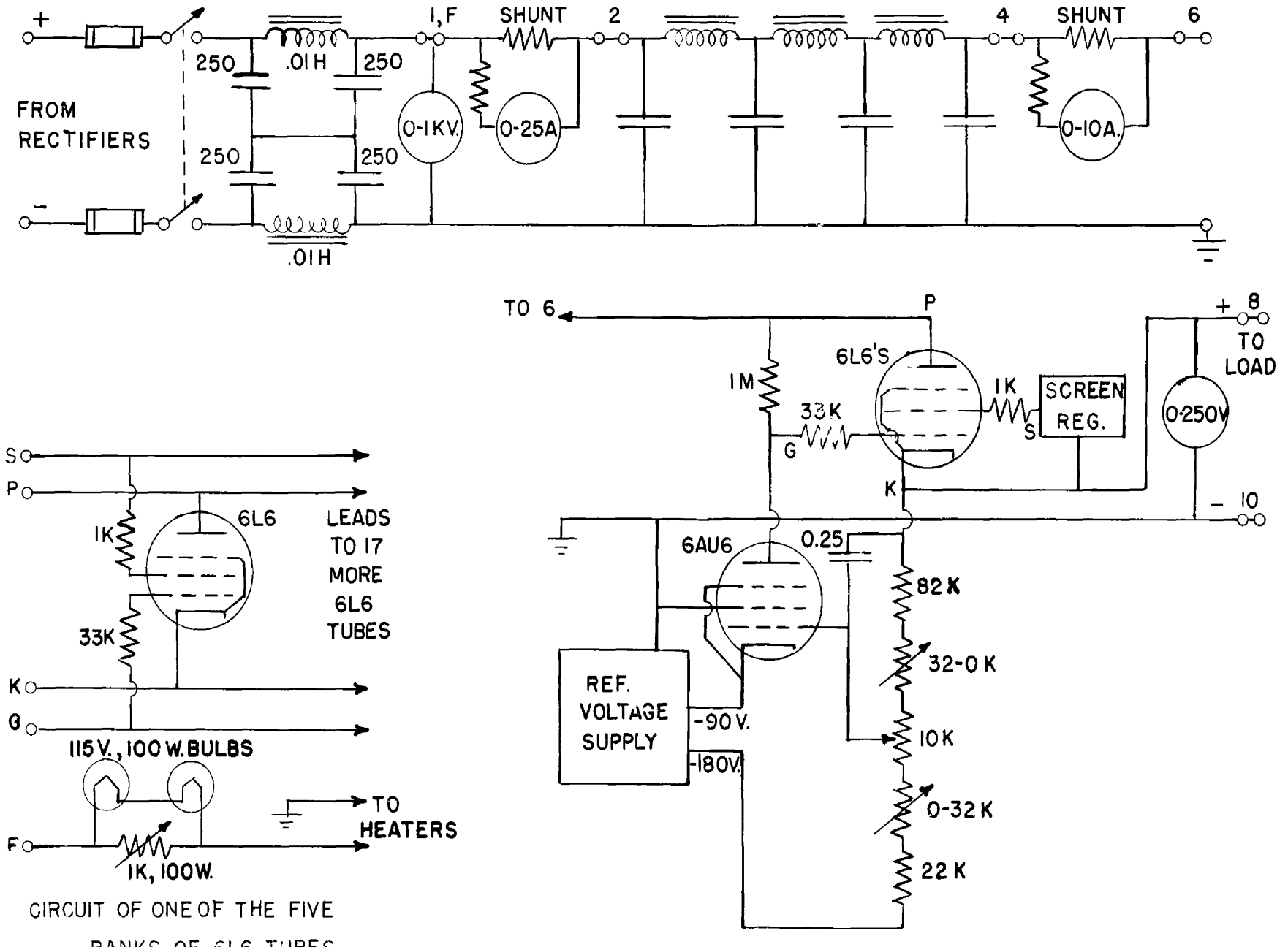

CIRCUIT OF ONE OF THE FIVE
BANKS OF 6L6 TUBES

FIGURE 9. MAGNET CURRENT CONTROL CIRCUIT

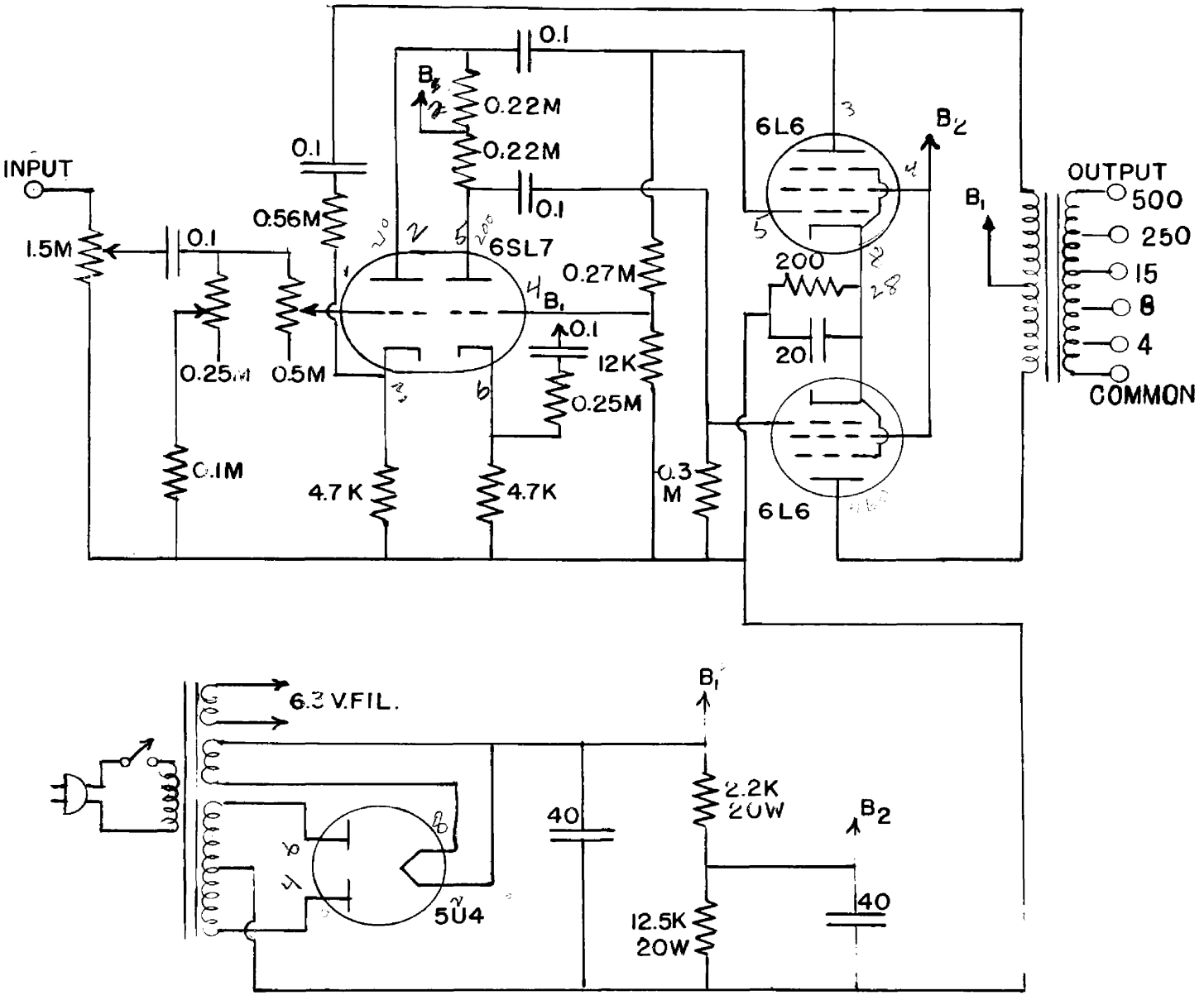

FIGURE 10. 25 WATT AUDIO AMPLIFIER

potential provided by an independent voltage supply and the two OB3 voltage regulator tubes. Thus, any positive excursion of the positive terminal of the magnet coils produces a positive excursion of the 6AU6 grid bias which increases the current through the one megohm dropping resistor, resulting in a negative excursion of the 6L6 grids and a decrease in the magnet current which cancels the original fluctuation.

Although this type of circuit would operate satisfactorily with the 6L6 screen grid voltage obtained from the positive supply via another dropping resistor, it was found convenient to obtain this grid voltage from the separate fixed voltage regulator circuit shown in Figure 8 which had been installed in a previous modification of the power supply unit.

The output current of the voltage regulator is determined by the grid potential of the 6AU6. Hence coarse control of the magnet current is provided by the two ganged 32K potentiometers and fine control by the fifteen-turn 10K Model B Helipot potentiometer. The latter is driven by an a.c. motor and gear train for automatic sweeping through an absorption signal. Control of the sweep rate is obtained by varying the voltage across the motor coils by means of a Variac autotransformer.

Magnetic Field Modulation. Modulation of the magnetic field is obtained with an auxiliary pair of "wobbling" coils which are wound on two separate forms and mounted coaxially with the main coils, one on each pole piece as shown in Figure 6. Rings of felt separate them from the aluminum retaining plates of the main coils, and they are held in place by four aluminum rods which bridge the gap between them.

The coils are connected in series, with their external leads connected to the same terminal board as the main coils. From here a connection is made by means of the overhead conduit to the output terminals of the twenty-five watt audio amplifier shown in Figure 10. Thus a voltage signal of any desired shape may be impressed across the input terminals of the audio amplifier and be converted into a fairly large current through the wobbling coils. At 100 cycles/second the impedance of the coils is about eight ohms and a current of about three amperes can be obtained from the amplifier. This gives a modulation of the magnetic field whose amplitude is about ten gauss.

Because the modulation signal obtained from the multivibrator is very strong and no voltage amplification is necessary, the audio amplifier consists only of power supply, volume, treble and bass attenuators and a power stage involving a 6SL7 twin triode which divides the signal between two 6L6 tetrodes arranged for push-pull operation.

The circuit of the multivibrator and its power supply is shown in Figure 11. Such a circuit acts essentially as a non-sinusoidal oscillator. Although the two halves of the 6SN7 twin triode are nearly equivalent, the condition of equal plate currents is unstable; i.e. the tendency is for the grid of one triode section (say the one on the left) to be driven below cutoff and the other to full conduction. Any random tendency in this direction is supported by positive feedback: a negative excursion of the left-hand grid produces an increase in the left-hand plate voltage and, since the voltage across the capacitor C cannot change suddenly, a positive excursion of the right-hand grid occurs, producing

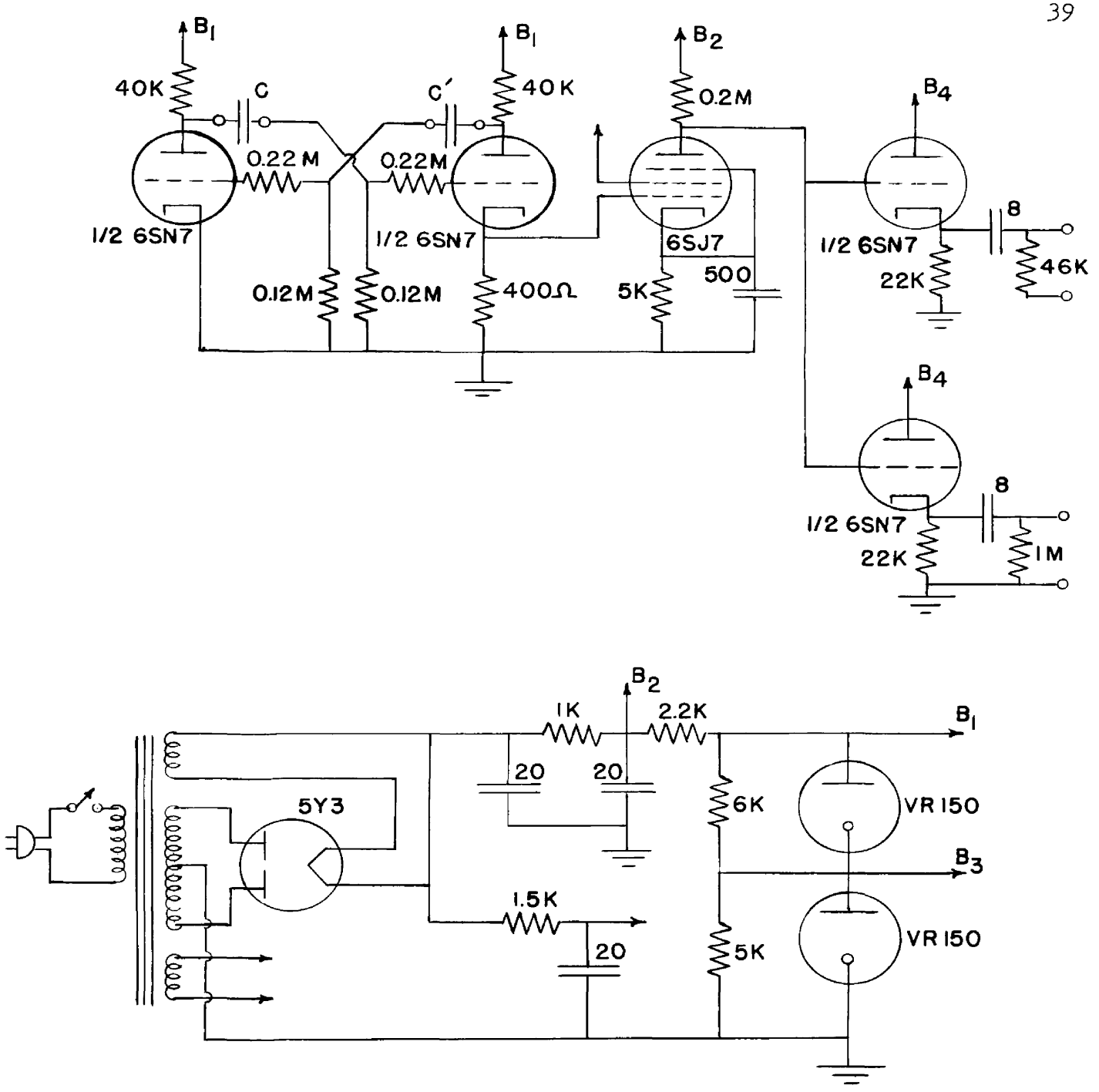

FIGURE 11. MULTIVIBRATOR AND POWER SUPPLY

a decrease in the plate potential which sends the left-hand grid further toward cutoff. With complete cutoff attained the charges on the capacitors C, C' slowly leak off through the 0.12M resistors at a rate determined by the time constants of the resistance-capacitance circuits. The left-hand grid potential rises above cutoff causing current to flow in that section and the right-hand grid potential falls, reducing the current in that section. When the currents reach equality, the circuit again triggers and the right-hand triode becomes non-conducting. This oscillation continues at a rate determined by the values of the capacitors C and C'.

A pentode amplifying stage employing a 6SJ7 is direct-coupled to a cathode in the multivibrator and the output of the amplifier is in turn direct-coupled to two cathode follower output stages. Since capacitative coupling is avoided, the amplifier and output stages operate at any frequency at which the multivibrator will oscillate. The capacitors in the first stage are plugged into a receptacle on the front panel and the frequency is changed by plug-in units. The output of the modulator is an approximately square wave of about 130 volts height.

Magnetic Field Measurement. The nuclear magnetic resonance frequency of the proton as a function of magnetic field strength is well known and is given by the formula:

$$\nu_p = 4.2577 \text{ H} \times 10^3 \text{ cm.}^{-1} \qquad (20)$$

Consequently, a measurement of ν_p by a conventional nuclear magnetic resonance technique is a simple, convenient and highly accurate method of measuring the field strength.

A sample containing a dilute solution of manganous sulfate in distilled water is placed within the probe coil of a Pound-Knight marginal oscillator and the coil is placed as closely as possible to the waveguide absorption cavity with its axis perpendicular to the direction of the steady magnetic field, as shown in Figure 13. The oscillator output is impressed across the vertical plates of an oscilloscope whose horizontal sweep is synchronized with the modulation frequency. Then as the magnetic field is swept back and forth through the proton resonance frequency which the oscillator is tuned to receive, a peak will appear on the oscilloscope trace which represents the proton resonance line shape. The frequency to which the oscillator is tuned may be measured accurately to five significant figures by means of a type BC-221-O United States Army Signal Corps frequency meter.

In the marginal oscillator, whose circuit diagram is shown in Figure 12, the sample coil and the two variable capacitors form a parallel tuned combination in the grid circuit of a cathode-coupled oscillator employing a 12AT7 twin triode. This oscillator is simply an amplifier with sufficient positive feedback between the right-hand plate and the tuned grid to supply its own input and thus to maintain continuous oscillation. Both the oscillation amplitude and the amount of radio-frequency current in the sample coil can be controlled by the two 2000-ohm potentiometers in the cathode and second grid circuits. When the nuclear magnetic resonance condition is reached, an absorption of energy occurs in the sample coil causing a decrease in the oscillation amplitude. The radio frequency voltage developed by the 12AT7 is

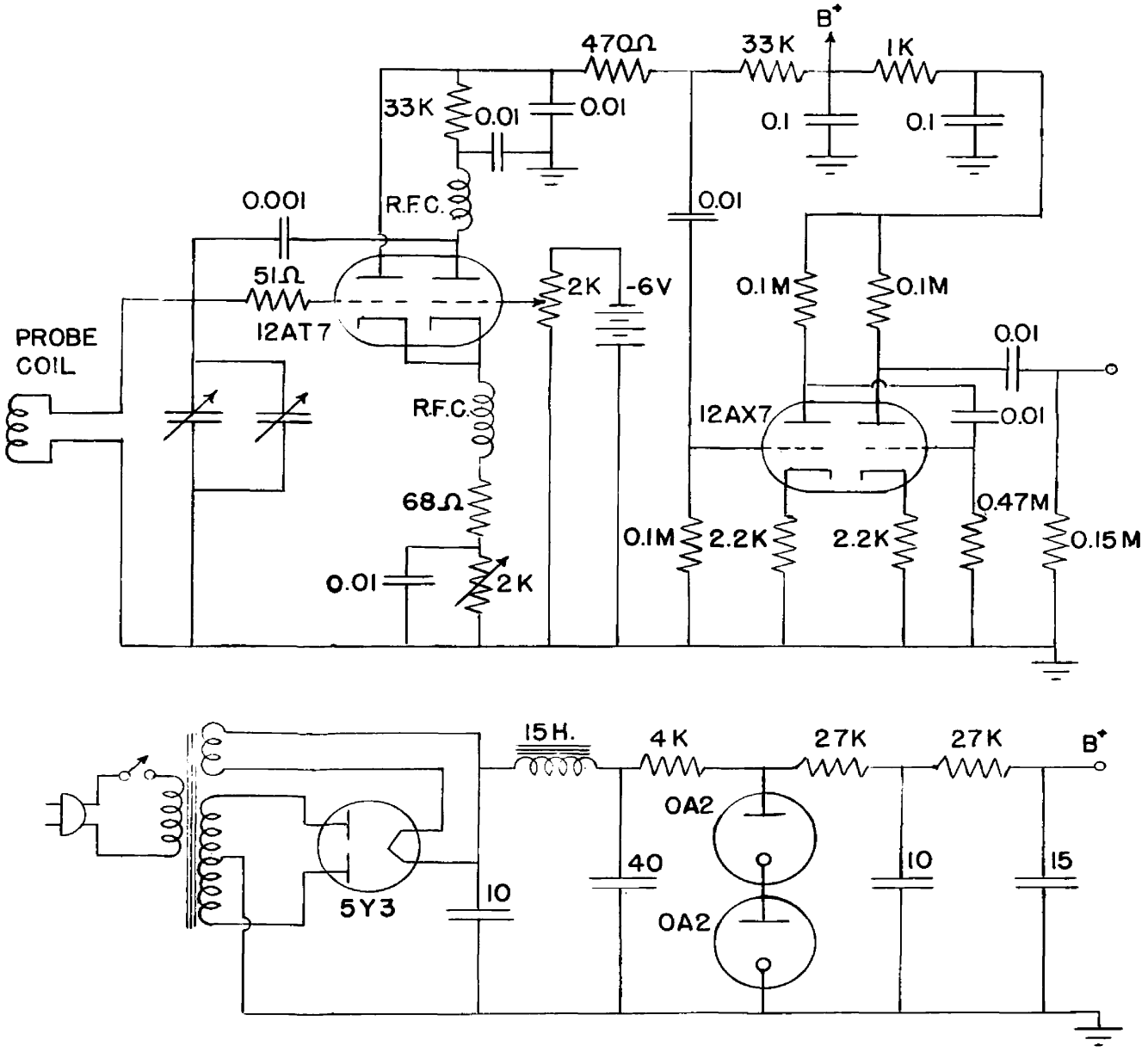

FIGURE 12. PROTON RESONANCE MAGNETIC FIELD STRENGTH METER

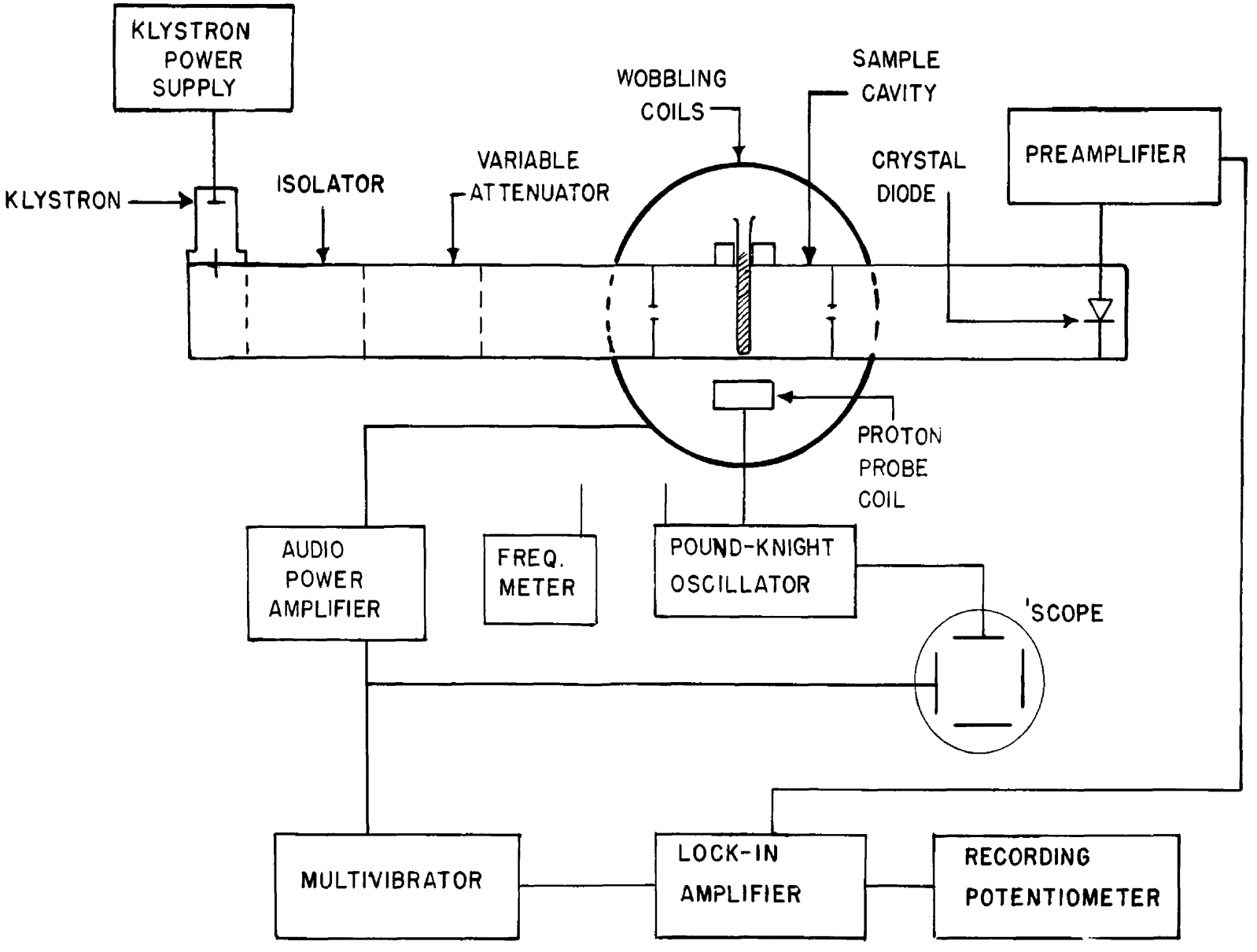

FIGURE 13. SCHEMATIC DIAGRAM OF MICROWAVE AND SIGNAL DETECTION SYSTEMS

filtered by the choke and resistance-capacitance filter network in the plate circuit so that only the audio-frequency modulation produced by the absorption signal passes. This audio-frequency signal is then amplified by a conventional two-stage audio amplifier consisting of a 12AX7 twin triode.

The power supply for this circuit, shown in Figure 12, is mounted, along with the dry cells used to provide the grid bias, on a panel rack attached to the angle-iron frame of the magnet. A power cable leads from the power supply chassis and terminates in a plug which fits a four-hole socket in the chassis of the oscillator. The output of the oscillator is brought via a shielded cable to a phono jack in the magnet terminal box and thence through the overhead conduit to the oscilloscope.

The Microwave System

The microwave system has but few components. In the order of their appearance there is a type 2K25 reflex klystron which generates the microwave radiation, a directional attenuator, a variable attenuator which controls the amount of microwave power incident on the sample, followed by a length of hollow rectangular waveguide which confines the radiation and conducts it to the absorption cavity. From the cavity the radiation is conducted through another length of waveguide to a 1N24E silicon crystal diode which detects the incident radiation.

A stable variable-voltage power supply is required to operate the klystron; the schematic diagram of this circuit is shown in Figure 14. It was constructed from a model PS-3 Heathkit to which a regulated auxiliary supply for the repeller was added. The unit is mounted in

the central control panel and the cathode, repeller, and filament voltages are brought out to an octal socket on the front of the panel. Connection is made to the terminal box mounted on the side of the magnet by means of a power cable which passes through the overhead conduit shown in Figure 15, and ends in another octal socket in the terminal box. The principles governing the operation of voltage-regulated power supplies have been discussed in connection with the magnet power supply and are applicable also to this circuit. The shell of the klystron is commonly operated at ground potential, the cathode at -300 volts, and the repeller at about 180 volts negative with respect to the cathode.

The klystron is mounted in a socket which forms one end of the waveguide train and is enclosed in a metal box. Because the reflector potential must always be negative with respect to the cathode to prevent drawing reflector current and burning out the tube, a 6H6 diode is mounted in the box with its plate connected to the klystron repeller and its cathode connected to the klystron cathode. The 6H6 acts as a safety valve to prevent positive excursions of the repeller with respect to the cathode. The power for the klystron and the filament voltages for klystron and diode are obtained via a power cable which terminates in a plug which fits the above mentioned octal socket in the magnet terminal box.

In order to isolate the klystron from the rest of the system a unidirectional transmission line[1] is placed next in line. This isolator

---

[1]Uniline Microwave Gyrator Model 88-96B, Cascade Research Corp., Los Gatos, Calif.

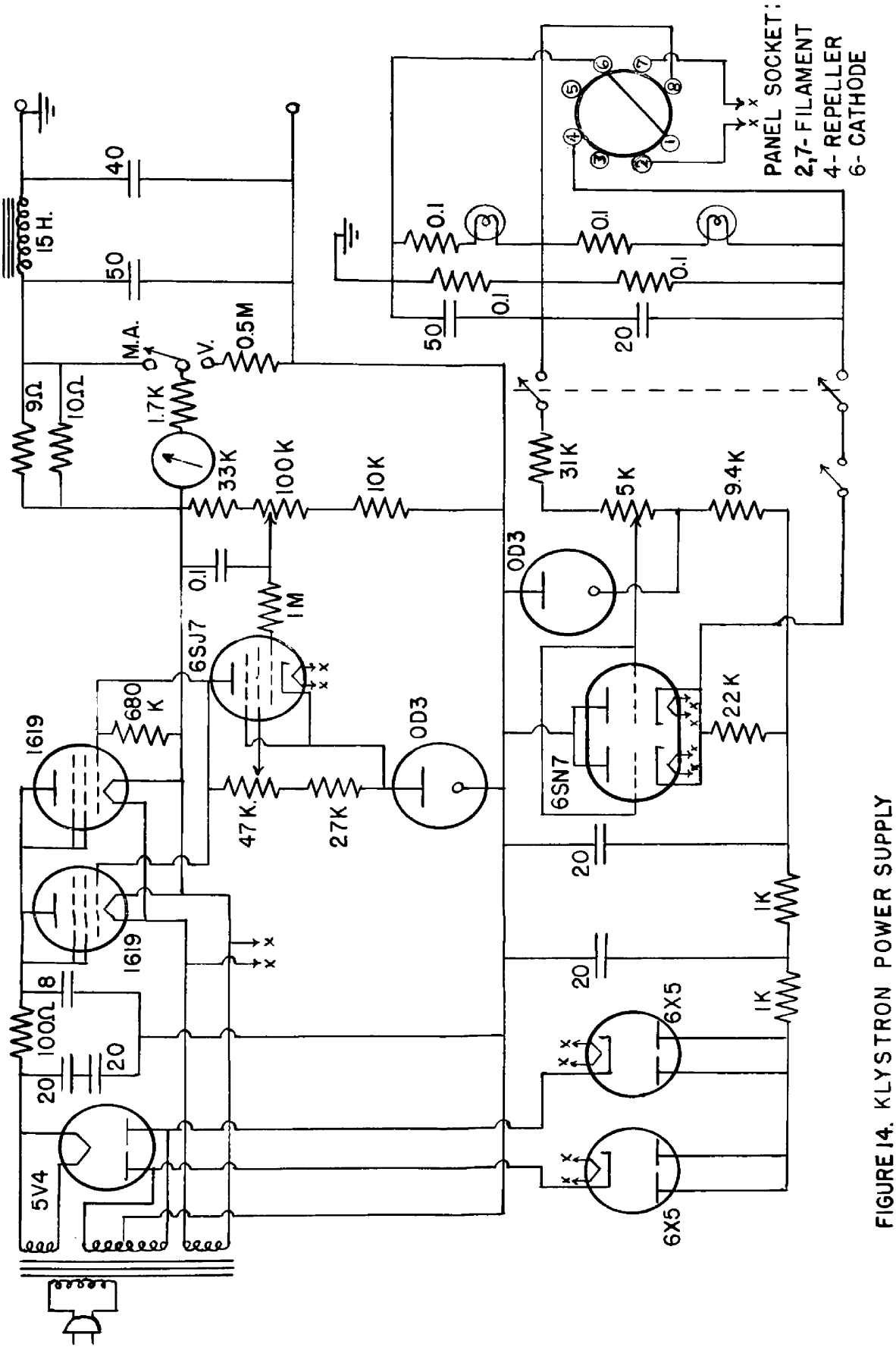

FIGURE 14. KLYSTRON POWER SUPPLY

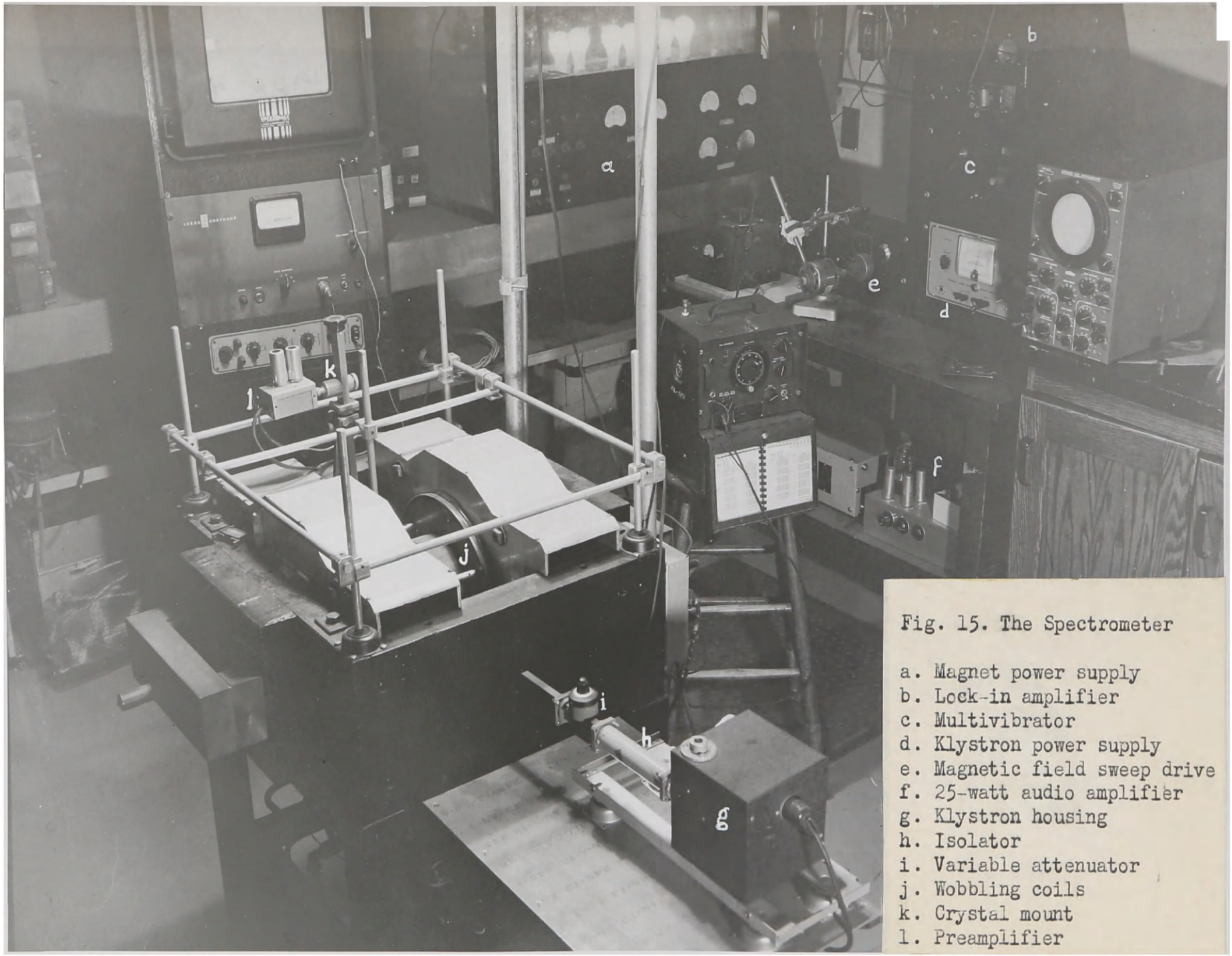

Fig. 15. The Spectrometer

a. Magnet power supply
b. Lock-in amplifier
c. Multivibrator
d. Klystron power supply
e. Magnetic field sweep drive
f. 25-watt audio amplifier
g. Klystron housing
h. Isolator
i. Variable attenuator
j. Wobbling coils
k. Crystal mount
l. Preamplifier

allows radiation to pass in the forward direction virtually undiminished but attenuates reflected radiation passing in the reverse direction. This component is necessary to prevent "pulling" of the klystron frequency by the reflected waves.

The sample cavity shown schematically in Figure 13 is a rectangular box with 0.25 inch holes coupling it to the waveguide line at both ends. Its dimensions are such that it will resonate at 9250 megacycles. It is a full-wavelength cavity 1.88 inches long, the other two outside dimensions being those of the one by one-half inch waveguide. With this type of coupling and these cavity dimensions the cavity resonates in the TE_{102} mode as shown in Figure 16. There is a node in the plane a-a, the magnetic lines of force being most intense there. A hole 5/16 inches in diameter was made in the top of the cavity at the plane a-a and was used for insertion of the samples into the cavity. The electric node at this plane allows insertion of samples with a minimum of dielectric loss in a region of maximum magnetic field intensity. This node of oscillation is important in paramagnetic resonance absorption experiments, since it is the magnetic component of the radiation which will induce the necessary magnetic dipole transitions in the inserted samples, and such a cavity produces polarization of the radio-frequency field normal to the external magnetic field when the sample is placed on the axis of the cavity. The "Q" of a resonant cavity is defined as the ratio of the power stored in the cavity to the power dissipated in the cavity per cycle. When the sample absorbs energy from the cavity, the Q decreases and, as a result, the power transmitted through the cavity decreases.

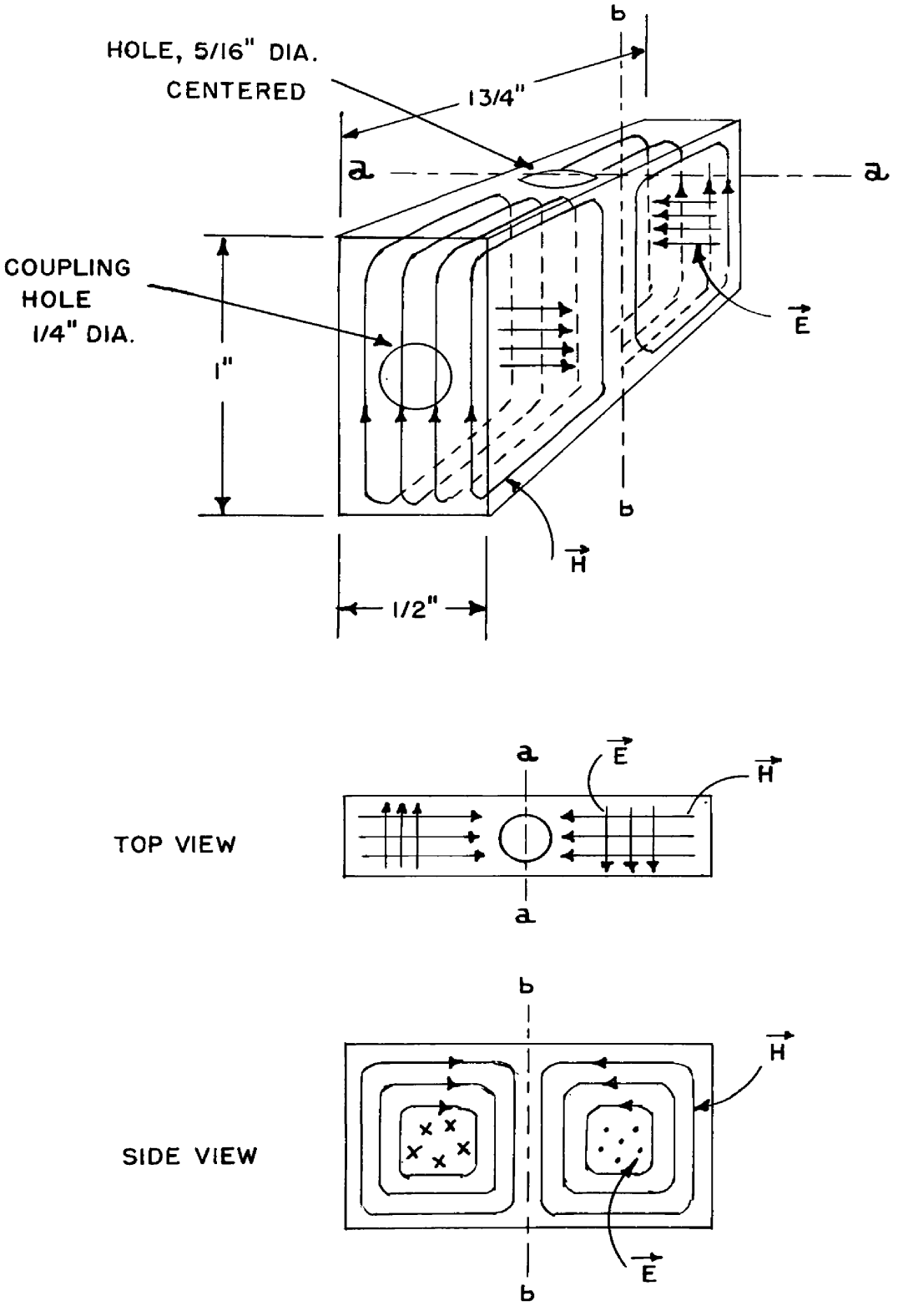

FIGURE 16. STANDING WAVE PATTERN FOR RECTANGULAR CAVITY OSCILLATING IN THE TE_{102} MODE (AFTER HUTCHISON[47])

The transmission line consists of type RG-52/U waveguide. The various sections are coupled by flanges, type UG-39/U, and chokes, type UG-40/U, soldered to each section. The attenuator is a Waveline type 611 variable attenuator. The tunable crystal mount which forms the end of the line is a Hewlett-Packard Model X-485B.

The entire system, including the klystron housing, is supported by rubber shock absorbers fastened to the magnet frame. Pickup of vibrations transmitted by the floor of the building and the vibrations caused by the wobbling coils is thereby reduced.

The Signal Detection and Display System

The Preamplifier. Alternating current variations in the voltage across the crystal detector are amplified by a wide-band preamplifier mounted in a small box on the end of the waveguide train, as shown in Figure 15, to minimize signal attenuation and noise introduced by the transmission cable. The circuit diagram for this preamplifier is shown in Figure 17. The only special feature of this circuit is a cathode feedback loop between the 12AU7 and the first half of the 12AX7 tube. This connection furnishes noise reduction and gain stability.

Power for this unit is obtained from the supply for the lock-in amplifier, which is mounted in the panel rack as shown in Figure 15. The power cable terminates in a Magnal four-prong plug which fits a four-hole socket in the magnet terminal box. This socket, in turn, is connected to the power supply by means of a cable which is passed through the overhead conduit.

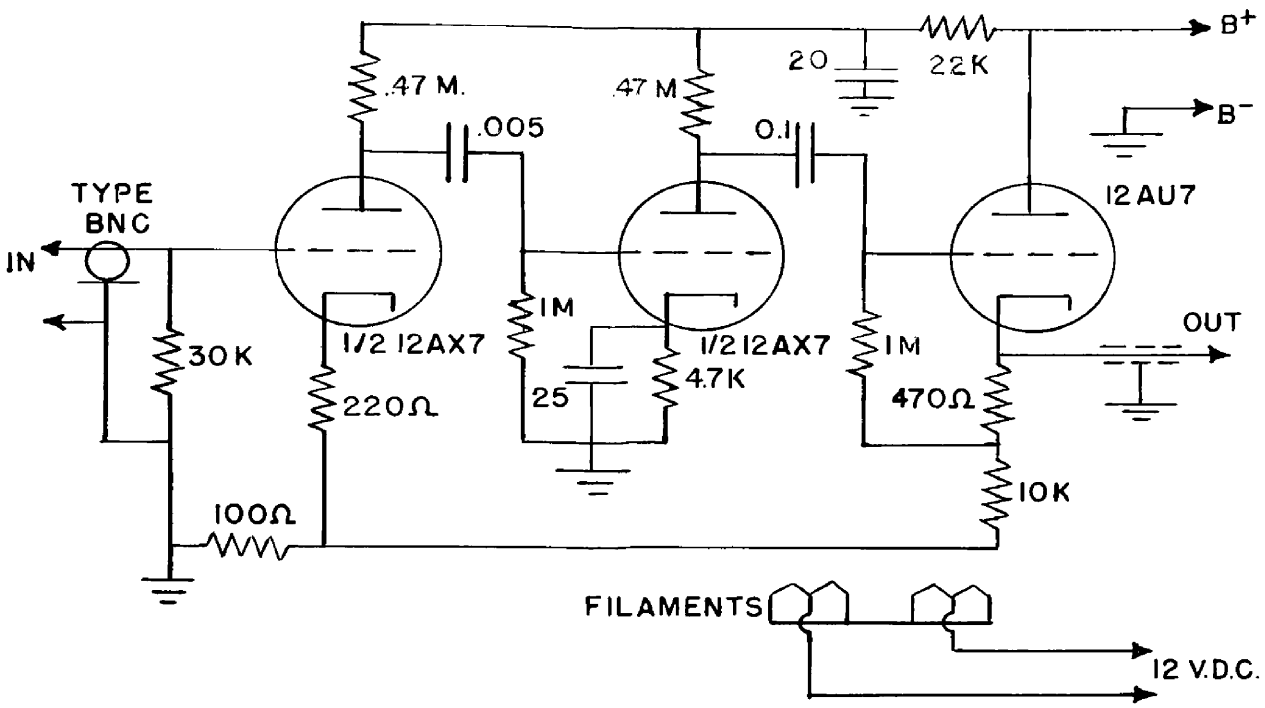

FIGURE 17. PREAMPLIFIER

$$2\pi F = \frac{1}{RC}$$

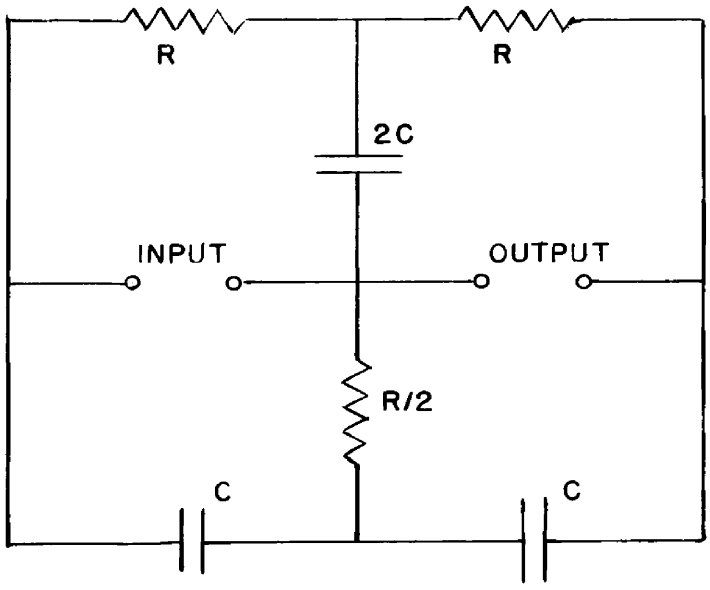

FIGURE 18. TWIN-TEE FILTER FOR LOCK-IN AMPLIFIER

The voltage gain of this amplifier was determined as a function of frequency by connecting the input to a variable-frequency signal generator and comparing the output and input voltages by displaying them on the calibrated screen of an oscilloscope. At 20 cycles/second the gain was found to be 320; at 20,000 cycles/second it was 620. The gain was fairly constant between 820 and 850 in the frequency range 200 to 6000 cycles/second. At 100 cycles/second, the modulation frequency used in all the experimental work here described, the gain was 710.

The Lock-in Amplifier. The output of the preamplifier is connected via a shielded cable, the magnet terminal board, and the overhead conduit to the lock-in amplifier circuit shown in Figure 19.

In order to appreciate the operation of this circuit one must first consider the nature of the signal which it receives. The amplitude of the modulation of the magnetic field is chosen so that only a fraction of the total width of the paramagnetic resonance absorption line is swept through. Under these conditions, the power incident on the crystal detector and therefore the voltage output of the preamplifier will be modulated at a frequency equal to the modulation frequency of the magnetic field; in this case 100 cycles/second. The magnitude and phase of this voltage modulation are determined by the magnitude and sign, respectively, of the first derivative of the absorption line. How this occurs can readily be seen in Figure 20.

The input to the lock-in amplifier then, consists of random voltage fluctuations (noise) of a wide range of frequencies, superimposed on

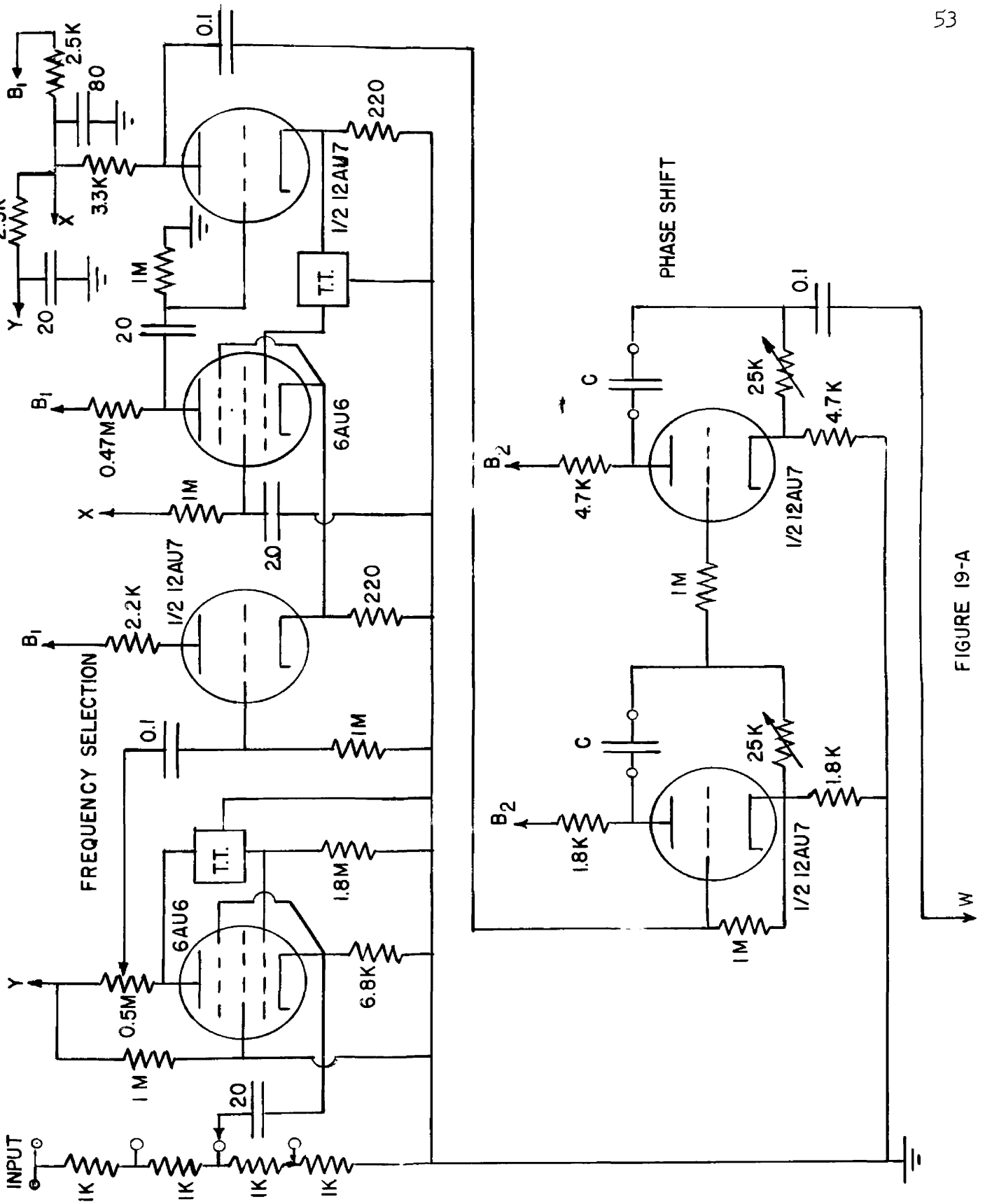
INPUT
1K
1K
1K
1K
20
1 M
0.5M
Y
FREQUENCY SELECTION
6AU6
6.8K
1.8M
T.T.
1M
0.1
B1
2.2K
1/2 12AU7
220
20
X
1M
0.47M
B1
6AU6
20
1M
T.T.
1/2 12AU7
220
0.1
2.5K
80
B1
3.3K
2.5K
X
Y
20
PHASE SHIFT
C
B2
4.7K
25K
4.7K
1/2 12AU7
1M
C
B2
1.8K
25K
1.8K
1/2 12AU7
1M
0.1
W

FIGURE 19-A

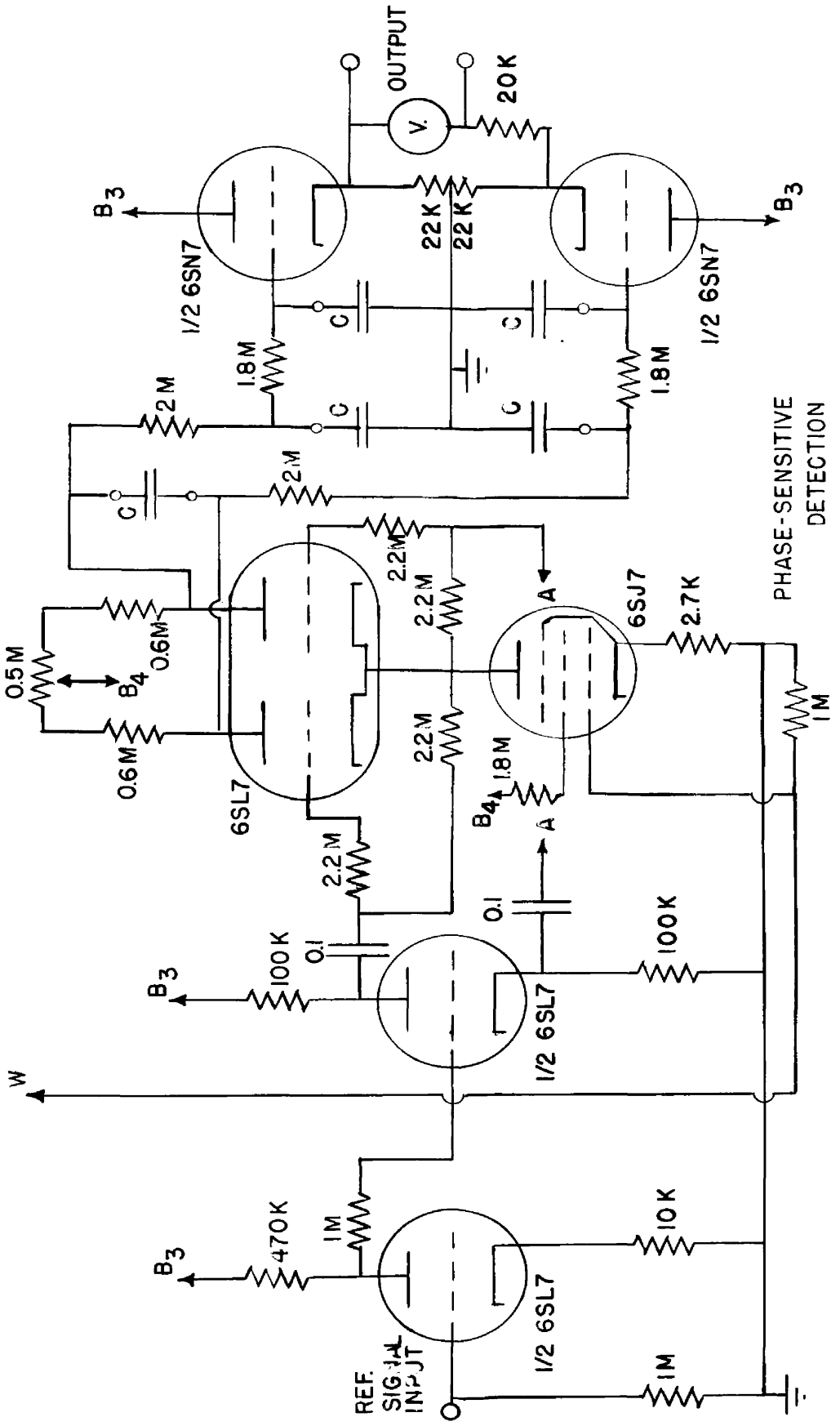

FIGURE 19-B LOCK-IN AMPLIFIER

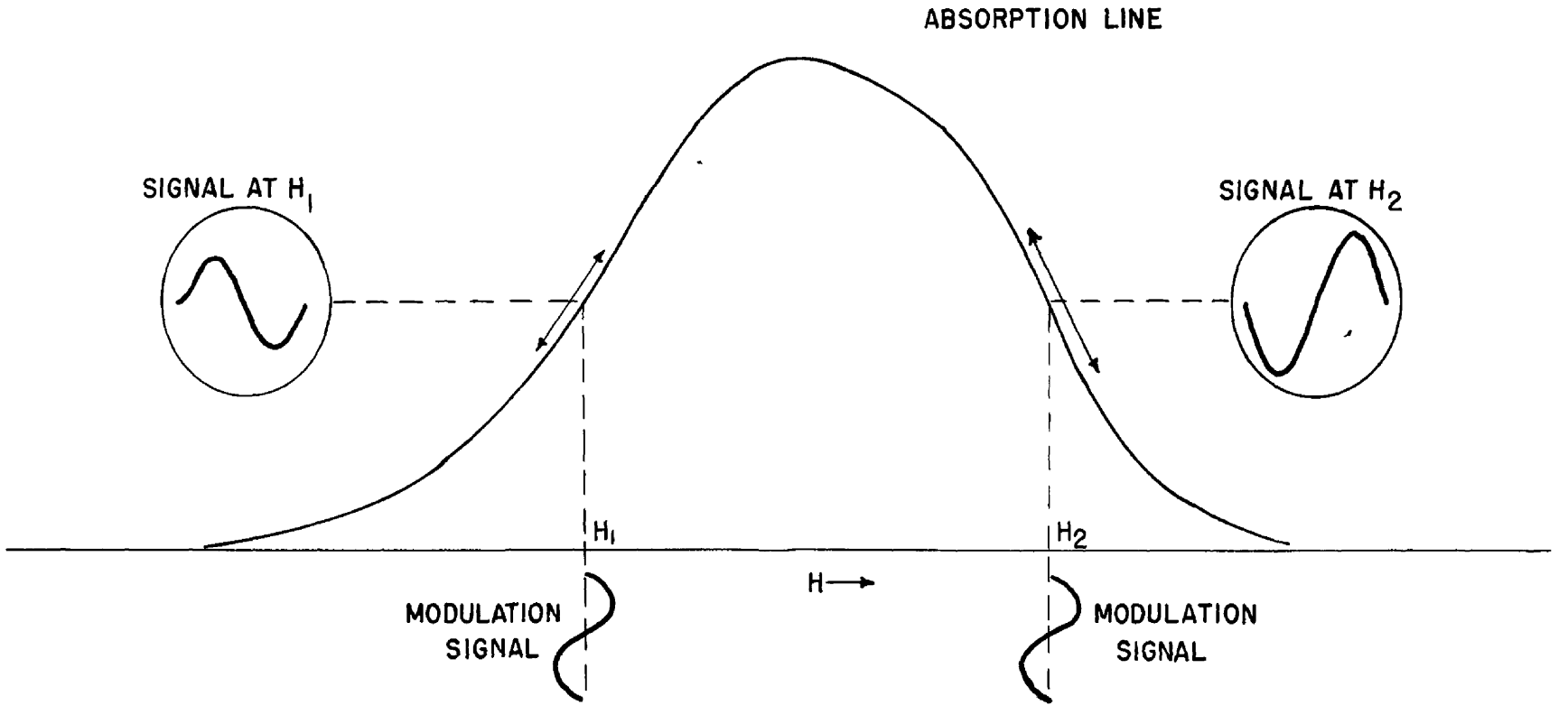

Figure 20. Audio signal derived from paramagnetic resonance line by field modulation. The amplitude of the audio signal obtained at constant modulation amplitude is proportional to the magnitude of the slope of the absorption line. The phase of the audio signal is determined by the sign of the slope.

which is the signal, at 100 cycles/second. The function of the lock-in amplifier is to separate the signal from as much noise as possible and measure both the amplitude and phase of the signal.

The first section of this circuit is a frequency-selective amplifier which is tuned to amplify the signal frequency at the expense of all other frequencies, thereby increasing the signal-to-noise ratio. Frequency selection is accomplished by employing two twin-T bridge circuits (see Figure 18). The impedance of a twin-T bridge varies with frequency in such a way that it has a low impedance at all frequencies except one, at which the plot of impedance versus frequency has a sharp peak.

The first tube, a 6AU6, provides additional amplification of the signal, and a certain amount of frequency selection, since the signal is negatively fed back to its grid via a twin-T bridge. The amount of gain in this stage is varied by the potentiometer tap on its plate resistor. The signal is then impressed on the grid of the first half of a 12AU7, which simply serves as an impedance matching device to couple the signal into the twin-T amplifier, consisting of the second 6AU6 and the second half of the 12AU7. Here a positive excursion of the 6AU6 cathode results in an amplified positive excursion of its plate. This plate is connected through a capacitor to the grid of the 12AU7. Thus, a positive excursion of the 12AU7 grid occurs, producing two results. An amplified negative excursion of its plate is produced, and this signal is sent to the next stage of the circuit. Also resulting, however, is a positive excursion of the 12AU7 cathode as it "follows"

the grid, and this signal is fed back through the twin-T bridge to the 6AU6 grid, cancelling the original signal except at the selected frequency (100 cycles/second), where the impedance of the twin-T bridge is high. Consequently, the only strong signal passing through this stage is found in a narrow band of frequencies centered upon 100 cycles/second.

The next stage consists of the two halves of a 12AU7 twin triode arranged to provide two stages of variable phase-shift in series. In each stage, the output signal is taken from the junction of the capacitor and resistor which connect the plate and cathode. The phase of the output signal, relative to the input signal at the grid, is determined by the values of the resistor and capacitor. Coarse, step-wise control of phase-shift is accomplished by switching capacitors of various values into the circuit, and fine control is furnished by the variable 25K resistors.

The third stage is a phase-selective detector. Here the signal is compared with a reference signal derived from the multivibrator which drives the magnetic field modulation coils. Hence, the reference signal and the absorption signal have identical frequency and the phase angle between them is made to be zero or an integral multiple of pi by the phase-shift stage. The reference signal is a square wave whose fundamental frequency is 100 cycles/second. It is first amplified and then divided into two parts of equal magnitude but opposite phase by the successive action of the two halves of a 6SL7 twin triode. The two equal and opposite signals thus produced are applied to the grids of

another 6SL7 tube in such a way that one-half of this tube conducts only during the first half-cycle and the second half conducts only during the second half-cycle. The absorption signal, after leaving the phase-shift stage, is applied to the grid of a 6SJ7 whose plate is connected directly to the combined cathodes of the last-mentioned 6SL7. Under these conditions, with zero absorption signal, the two plates of the 6SL7 will be at the same potential. (Exact balance between the two halves is achieved by adjusting the 0.5M variable resistor in the plate circuit.) However, if an absorption signal is present which produces a positive excursion of the 6SJ7 grid during the first half of the reference cycle, there will result a negative excursion of the 6SL7 cathodes and, for the half-tube which conducts, a positive excursion of its plate relative to the zero-signal level. Hence a positive absorption signal during the first half cycle causes a potential difference between the plates of the 6SL7, with the half-tube which conducts during the first half cycle being positive with respect to the other. An absorption signal which is negative during the first half cycle, accordingly, produces a potential difference of opposite sign between the two plates.

The 6SL7 plates are connected via a resistance-capacitance filter network to a 6SN7 dual triode which acts as a vacuum-tube voltmeter to drive a meter and provide a signal for a recording potentiometer. The resistance-capacitance network filters out additional noise; the larger the time constant of this circuit, as determined by the values of the capacitors which are switched into the circuit, the lower the noise

level in the recorded signal. The penalty one must pay for a long time constant is a slow sweep rate through the absorption line. With broad lines this is not much of a problem but with the narrow lines found in free radicals, for example, one must exercise caution lest the recorded line shape be distorted by failure of this circuit to follow the change in the signal.

Power for the lock-in amplifier is obtained from the separate power supply chassis which is mounted on the same panel rack. The circuit diagram of this power supply, which also serves the preamplifier, is shown in Figure 21.

Operating Procedure

The resonance frequency of the sample cavity may be determined by placing a tuned cavity wavemeter in the microwave line, separated from the sample cavity by a directional coupler, and measuring the frequency at which maximum power is transmitted through the sample cavity. Although a calibrated wavemeter was available, a simpler, though indirect, procedure was adopted. The g value of solid diphenylpicryl-hydrazyl is known to be 2.0037. This is more precise by an order of magnitude than the most precisely known g value for the broad lines encountered in the spectra of paramagnetic ions. The Helipot dial reading in the magnet control circuit was noted at points where the proton resonance frequency was exactly equal to an harmonic of the 100 kc crystal oscillator in the frequency meter; namely at ν_p = 16,000, 15,000, 14,000 and 13,000 kc. These correspond to intervals of 235 gauss.

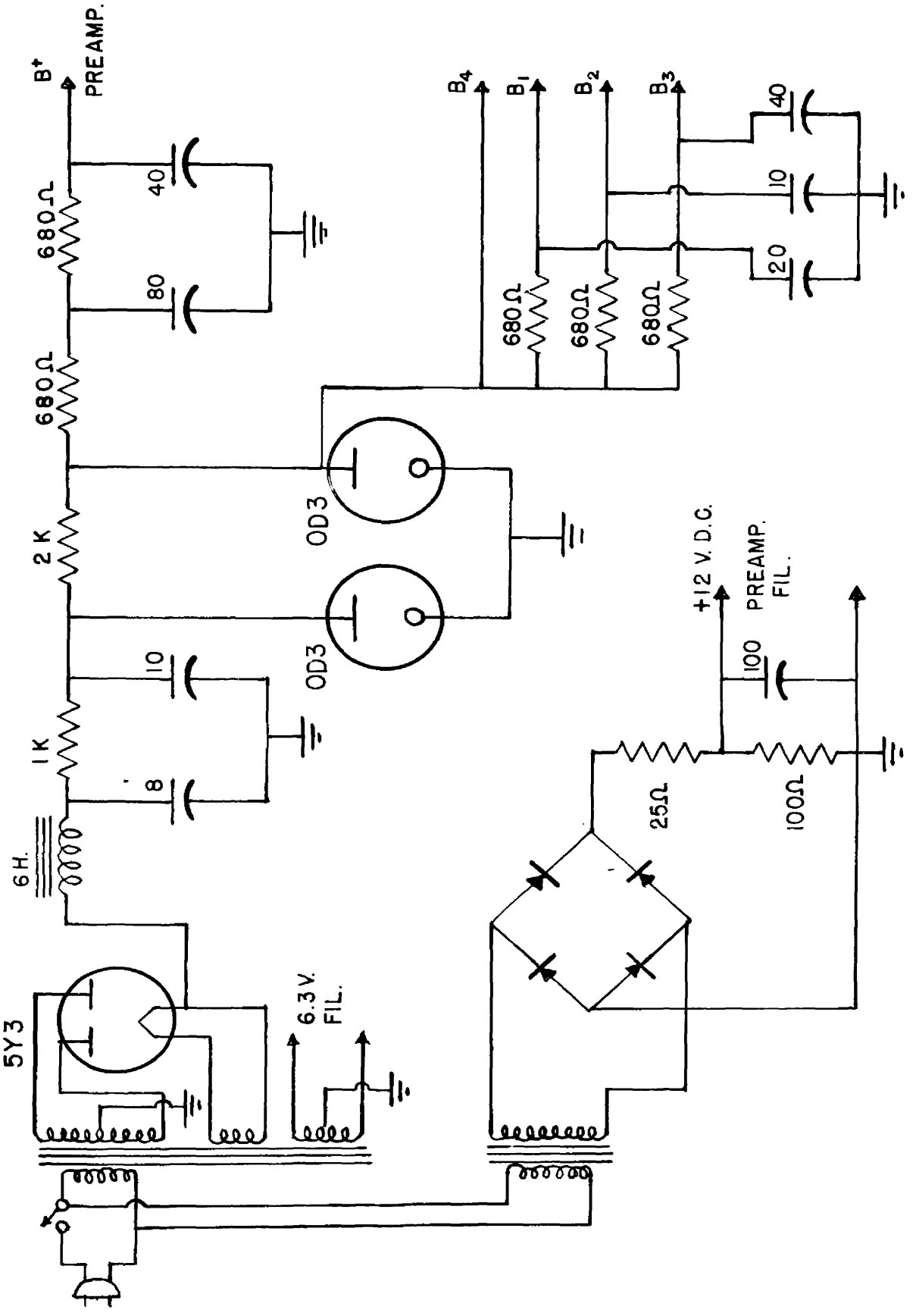

FIGURE 21. POWER SUPPLY FOR PREAMPLIFIER AND LOCK-IN AMPLIFIER

The Helipot dial reading was also noted at the point where the magnetic field strength was exactly equal to the resonance value for diphenylpicrylhydrazyl, as determined by displaying the output of the preamplifier directly on the oscilloscope screen, and centering the diphenylpicrylhydrazyl absorption line on the screen.

A change of 0.184 ± .002 gauss per division of the Helipot dial was obtained, and the diphenylpicrylhydrazyl resonance occurred only 25 divisions (4.6 gauss) above the 14,000 kc. check point. This check point corresponds to a value of the magnetic field strength of 3288.2 gauss; hence the value of H at the diphenylpicrylhydrazyl resonance point was determined as H = 3292.8 gauss. Consequently, the ratio $h\nu/\beta$, a constant characteristic of the sample cavity, can be found since

$$h\nu/\beta = gH = 6597.8 \text{ gauss.} \qquad (21)$$

This procedure was performed three times, at intervals separated by several days, and no variation in the fifth significant figure was observed.

The spectra were obtained by the following procedure: a warm-up period of at least two hours was allowed the klystron and its power supply, since even slight changes in the resistors of the power supply or in the internal cavity of the klystron tube might seriously change the output frequency. Provision was made for switching the input terminals of a Dumont type 304A oscilloscope to any one of four positions: the pre-amplifier output, position 2; the plate of one-half of the phase-sensing twin triode in the lock-in amplifier, position 3;

or the output of the Pound-Knight oscillator, position 4. Position one involved no connection. With the oscilloscope input selector switch on position 2, powdered cupric sulfate or any other concentrated paramagnetic material was placed in the sample cavity and the klystron frequency was adjusted by means of the repeller voltage until the resonant frequency of the cavity was reached. This point was determined by the fact that the 60 cycles/second ripple in the klystron power supply produces a 60 cycles/second modulation of the pre-amplifier output which is very large on either side of the cavity frequency and passes through zero with a phase reversal at that frequency.

With the klystron frequency adjusted to the cavity resonant frequency, the 25 watt amplifier was adjusted to send a current of about 3 amperes through the wobbling coils, and the magnetic field was brought to the proper value for absorption of microwave energy by the sample by manual adjustment of the potentiometer in the current control circuit. The oscilloscope input selector was then set to position 3, displaying the 100 cycles/second sine wave signal superimposed upon the 100 cycles/second square-wave reference signal. The phase difference between them was reduced to zero by adjusting the phase-shift capacitors and resistors in the lock-in amplifier circuit. The copper sulfate sample was then removed, and the sample whose spectrum was to be obtained was inserted. Dry powdered samples were placed in a fluorothene tube 2 1/2 inches long, with an outside diameter of about 3/16 inches and an inside diameter of about 1/8 inch. This tube rested on the bottom of the cavity and projected up out of the hole in the top.

Single crystal samples were fastened to the end of a fluorothene rod with Duco cement and positioned at the geometrical center of the cavity. Since the resonant frequency of the cavity changed slightly with each new sample in place, the oscilloscope input selector was again switched to position 2 and the klystron tuning procedure was repeated. With the oscilloscope connected to position 3, the magnet current was caused to pass through the absorption band and the gain and sensitivity controls of the lock-in amplifier were adjusted to give a signal of convenient strength at the output. When no signal was visible on the oscilloscope screen, these controls were simply set to give a maximum deflection of the output meter. The Pound-Knight oscillator was then tuned to receive a signal at 16,000 kc. by reducing to zero the beat frequency produced with an harmonic of the crystal oscillator, the magnet current was brought to a value well above that at which absorption occurred, and the automatic motor drive was connected to the control circuit Helipot. The Leeds and Northrup recorder was turned on and the oscilloscope input selector was switched to position 4. When the proton signal crossed the center of the oscilloscope screen, a pip was placed on the recorder trace by momentarily breaking the input connections to the recorder with a key in the circuit. The oscillator was then tuned to the next lower harmonic (15,000 kc.) and this procedure was repeated until the complete absorption pattern had been traced out by the recorder.

PREPARATION OF SAMPLES AND EXPERIMENTAL RESULTS

General Procedure

The general procedure for the production of samples of paramagnetic ions adsorbed on various substrates was as follows. The adsorbent materials were dried at 110°C for four hours, and approximately three-gram samples were weighed accurately into separate flasks. Various known quantities of standardized 0.1 molar solutions of the paramagnetic salts were added and the flasks stoppered. The solutions were allowed to equilibrate with the adsorbents at room temperature with occasional shaking of the flasks. No attempt was made to ensure complete equilibration or to standardize the length of time of contact between adsorbent and solution, since the amount of paramagnetic material adsorbed was to be determined later. After standing in contact with the solutions, the adsorbent was removed on a paper filter and washed several times. The filtrate and washings were collected and analyzed for the cation they contained. The quantity of paramagnetic cation adsorbed was calculated as the difference between the amount present in the filtrate and the amount added originally. The adsorbents used in the experiments were as follows: Dowex -50, an extremely fine-mesh sulfonic acid-type cation ion exchange resin; Amberlite IR-100, the prototype of sulfonic acid-type cation exchange resins; and Amberlite IR-4B which holds a similar position with respect to the anion exchange resins. Amberlite IRC-50H is a weakly acidic, carboxylic acid-type exchange resin. Also used were a commercial form of powdered zeolite,[1] activated silica

[1]E. H. Sargent and Co., Chicago, Ill.

gel,[1] and activated charcoal.[2]

Attempts were made to observe the spectrum of manganese adsorbed by single crystals of the natural zeolites, natrolite and analcite, which were obtained from the Geology department collection.

Manganese

Preparation of Samples

The method of analysis used was that developed by Lingane and Karplus (40). To the manganese sample to be analyzed was added 200 ml. of saturated sodium pyrophosphate buffer solution. Bromthymol blue indicator was added and enough hydrochloric acid to give a pH of six, as matched against a standard buffer solution containing the same concentration of indicator. This solution was then titrated with standard potassium permanganate solution. The equivalence point was detected with the Fisher Titrimeter.

The standard permanganate solution was prepared and analyzed according to the procedure of Pierce and Haenisch(41). Weighed samples of analytical grade arsenious oxide were dissolved in sodium hydroxide solution and aliquot portions of the diluted solutions were titrated with potassium permanganate solution, which proved to be 0.01206 ± 0.00006 normal.

---

[1]Commercial grade, mesh-size 60-200; sold by Davison Chemical Co., Baltimore, Md.

[2]Acid washed, prepared by R. E. VanderVennen

Five-ml. samples of 0.1 M manganese (II) sulfate solution were titrated with the standard permanganate solution according to the procedure outlined above. Five ml. of manganese (II) sulfate solution was equivalent to 50.42 ± .08 ml. of permanganate solution, indicating a molarity of 0.1316 for the manganese (II) sulfate solution.

Samples of manganese sulfate adsorbed on charcoal, Dowex -50, Amberlites IR-100 and IR-4B, zeolite, and silica gel were prepared. The charcoal sample was one previously prepared by R. E. Vander Vennen (42). Table II contains the pertinent data for the others. Column three of this table lists the number of ml. of 0.1316 M manganese (II) sulfate solution added to the dried sample of adsorbent, and column four lists the number of ml. of 0.01306 normal potassium permanganate solution required to titrate the combined filtrate and washings.

An approximately 0.1 M solution of hexacyanomanganate (II) complex anion was prepared by adding sodium cyanide to the standard manganese (II) sulfate solution until further addition did not deepen the yellow color of the solution. Ten ml. of this solution and approximately three grams of Amberlite IR-4B were placed in a stoppered flask and allowed to remain in contact, with occasional shaking, for four hours. The resin was then treated in the usual manner, but subsequent examination revealed no detectable paramagnetic resonance absorption. No absorption could be detected in a sample of the solution either.

The spectra obtained from the samples of Table II are shown in Figures 22-27. Some of the spectra are not reproduced in order to avoid unnecessary repetition. The complete series of five samples containing

TABLE II

ADSORPTION OF MANGANESE SULFATE BY VARIOUS ADSORBENTS

Sample		Wt. in g. of Adsorbent	Ml. $MnSO_4$	Ml. $KMnO_4$	Moles Mn^{++} Adsorbed x 10^3	Moles $Mn^{++}/g.$ x 10^3
Mn – Dowex-50	I	3.5499	10.00	1.00	1.303	0.367
	II	3.8364	5.000	0.56	0.651	0.170
	III	2.0695	1.000	0.40	0.126	0.061
	IV	2.8591	0.500	< 0.5	0.065	0.023
	V	3.4697	0.200	< 0.5	0.036	0.010
Mn – IR-100	I	2.9481	20.00	34.48	2.182	0.740
	II	3.4526	10.00	2.10	1.289	0.373
	III	3.2801	5.000	1.35	0.640	0.195
	IV	3.0870	1.000	< 0.5	0.065	0.031
	V	3.2803	0.500	< 0.5	0.036	0.011
Mn – Zeolite	I	2.2924	20.00	-	-	-
	II	2.1444	10.00	0.22	1.313	0.612
	III	2.0969	5.000	1.18	0.643	0.306
Mn – IR-4B	I	3.1036	10.00	8.85	1.200	0.387
	II	2.8818	5.000	12.66	0.493	0.171
	III	2.7353	1.000	7.19	0.038	0.014
	IV	3.0294	2.000	-	-	-
Mn – Silica gel	I	2.3926	5.000	48.27	0.028	0.012
	II	2.3885	1.000	10.10	0.00	0.000
	III	2.6100	0.500	4.5	0.007	0.003

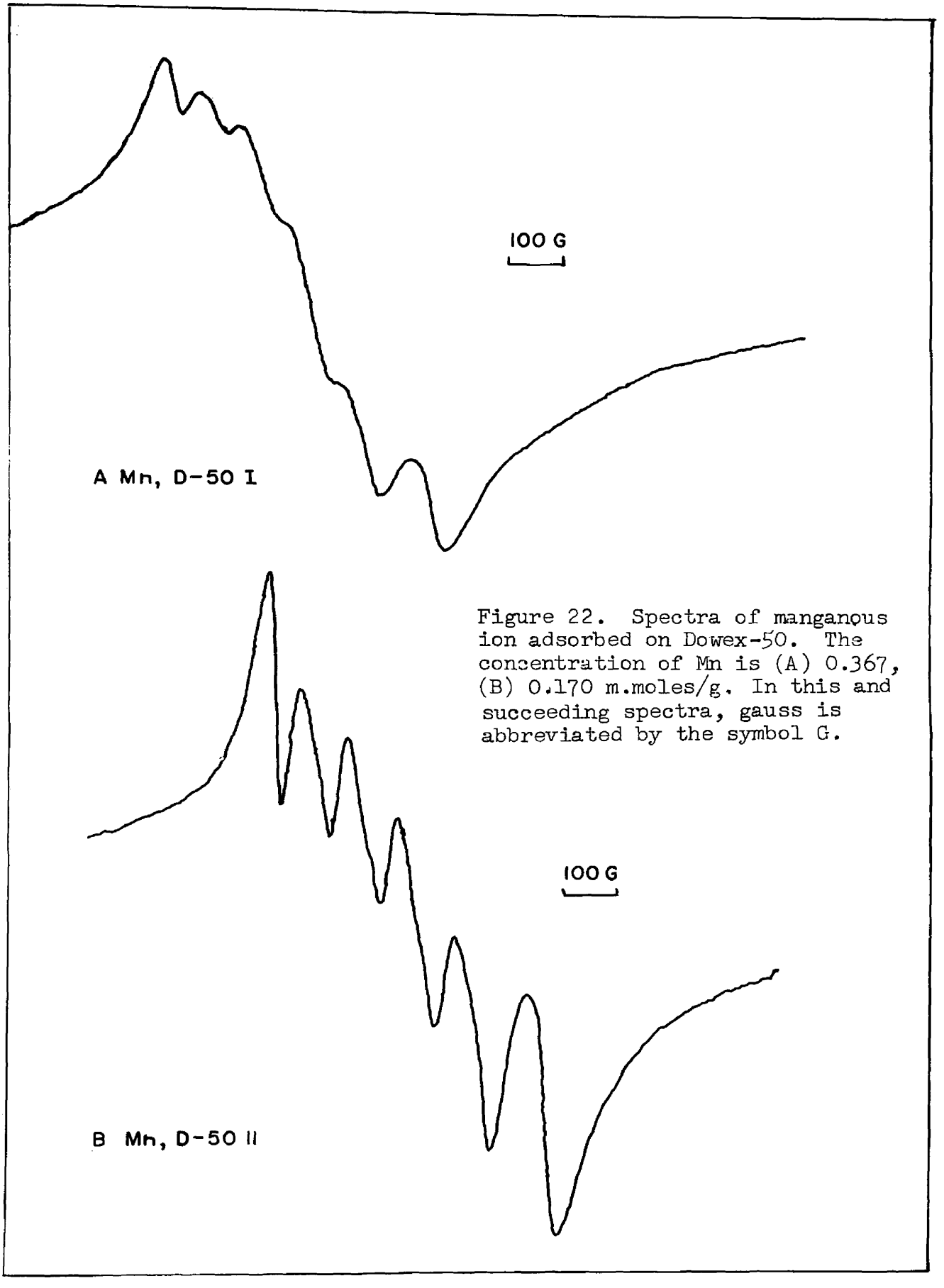

Figure 22. Spectra of manganous ion adsorbed on Dowex-50. The concentration of Mn is (A) 0.367, (B) 0.170 m.moles/g. In this and succeeding spectra, gauss is abbreviated by the symbol G.

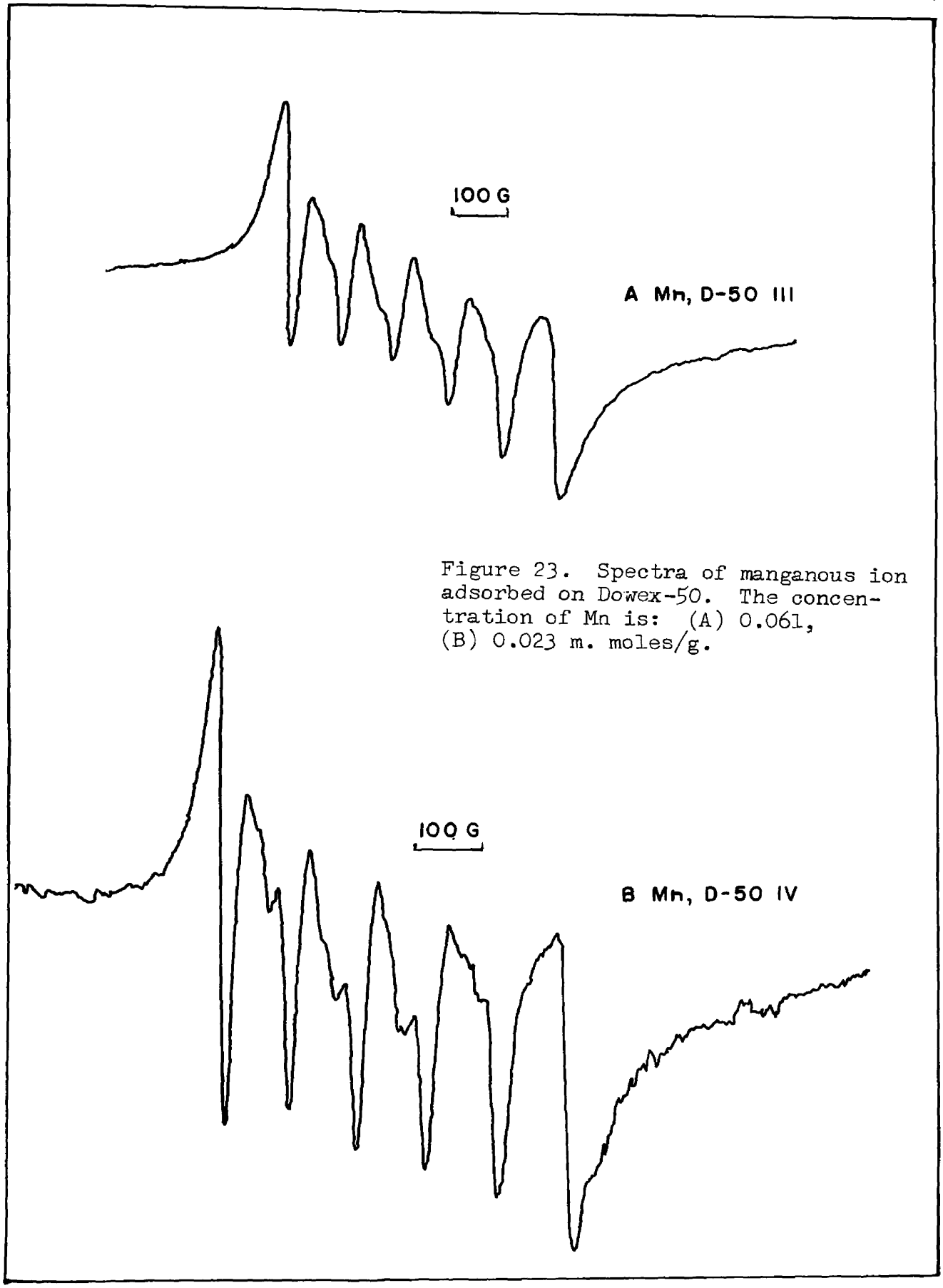

Figure 23. Spectra of manganous ion adsorbed on Dowex-50. The concentration of Mn is: (A) 0.061, (B) 0.023 m. moles/g.

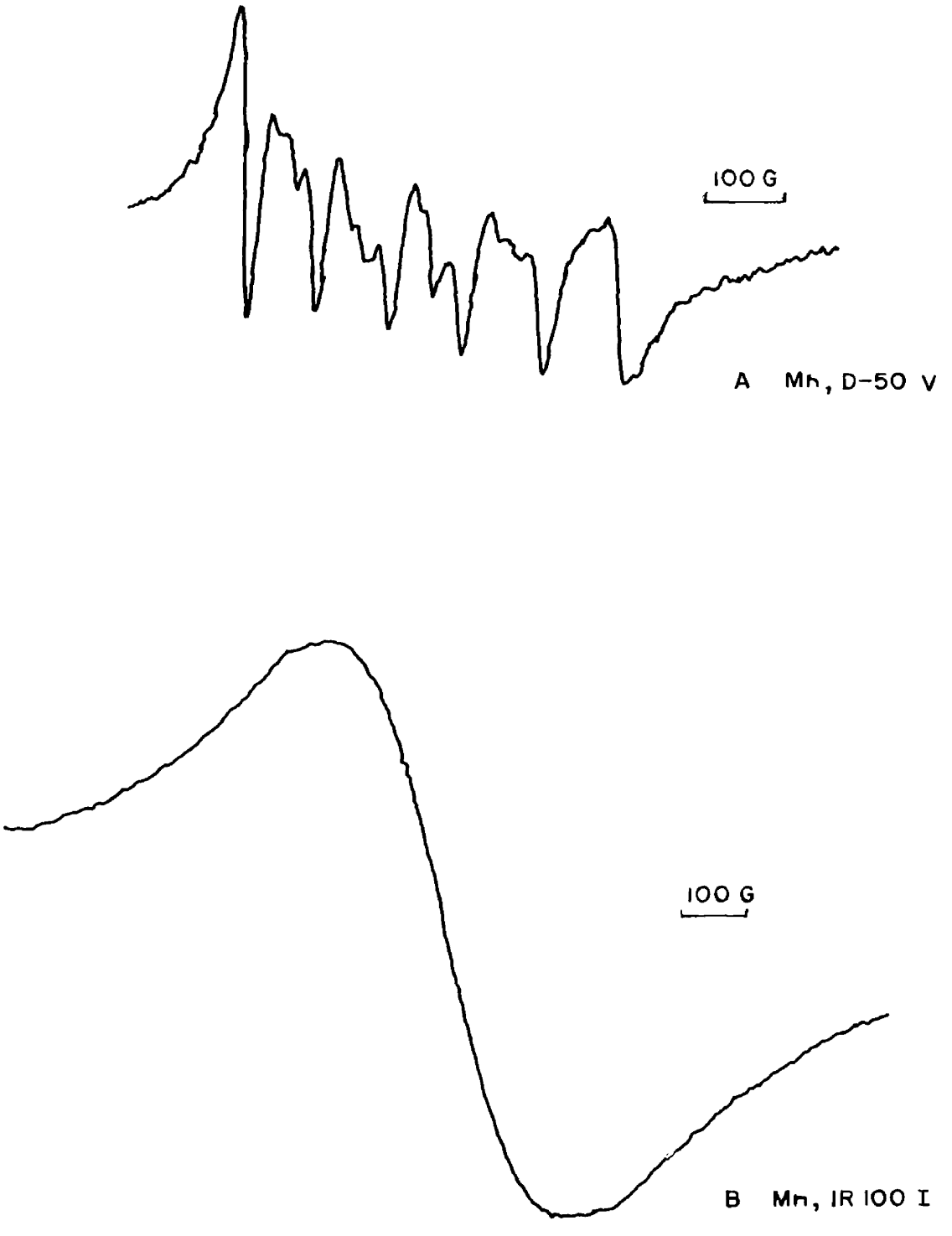

Figure 24. Spectra of manganous ion adsorbed on Dowex-50 and on Amberlite IR-100. The concentration of M_n is: (A) 0.010, (B) 0.740 m. moles/g.

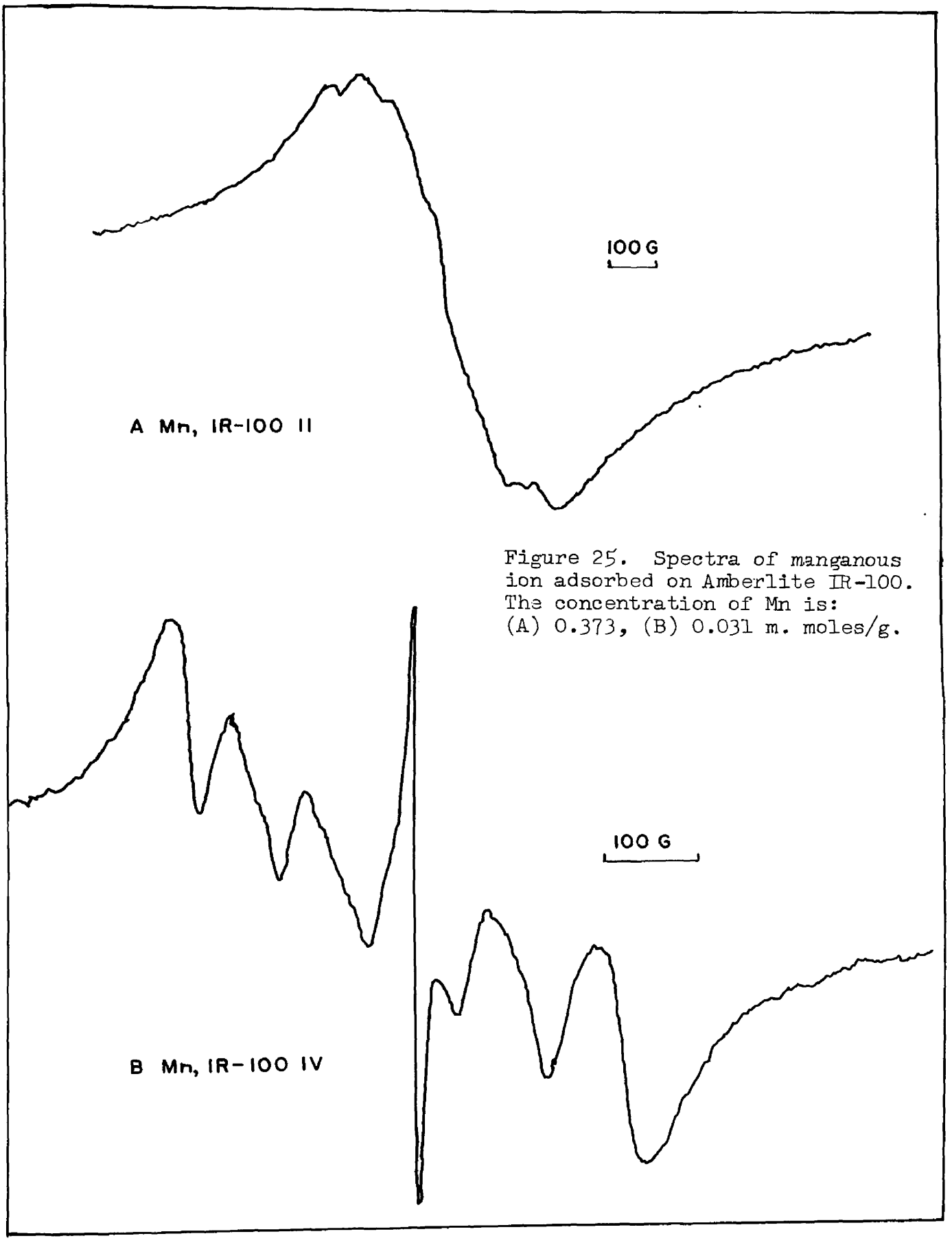

Figure 25. Spectra of manganous ion adsorbed on Amberlite IR-100. The concentration of Mn is: (A) 0.373, (B) 0.031 m. moles/g.

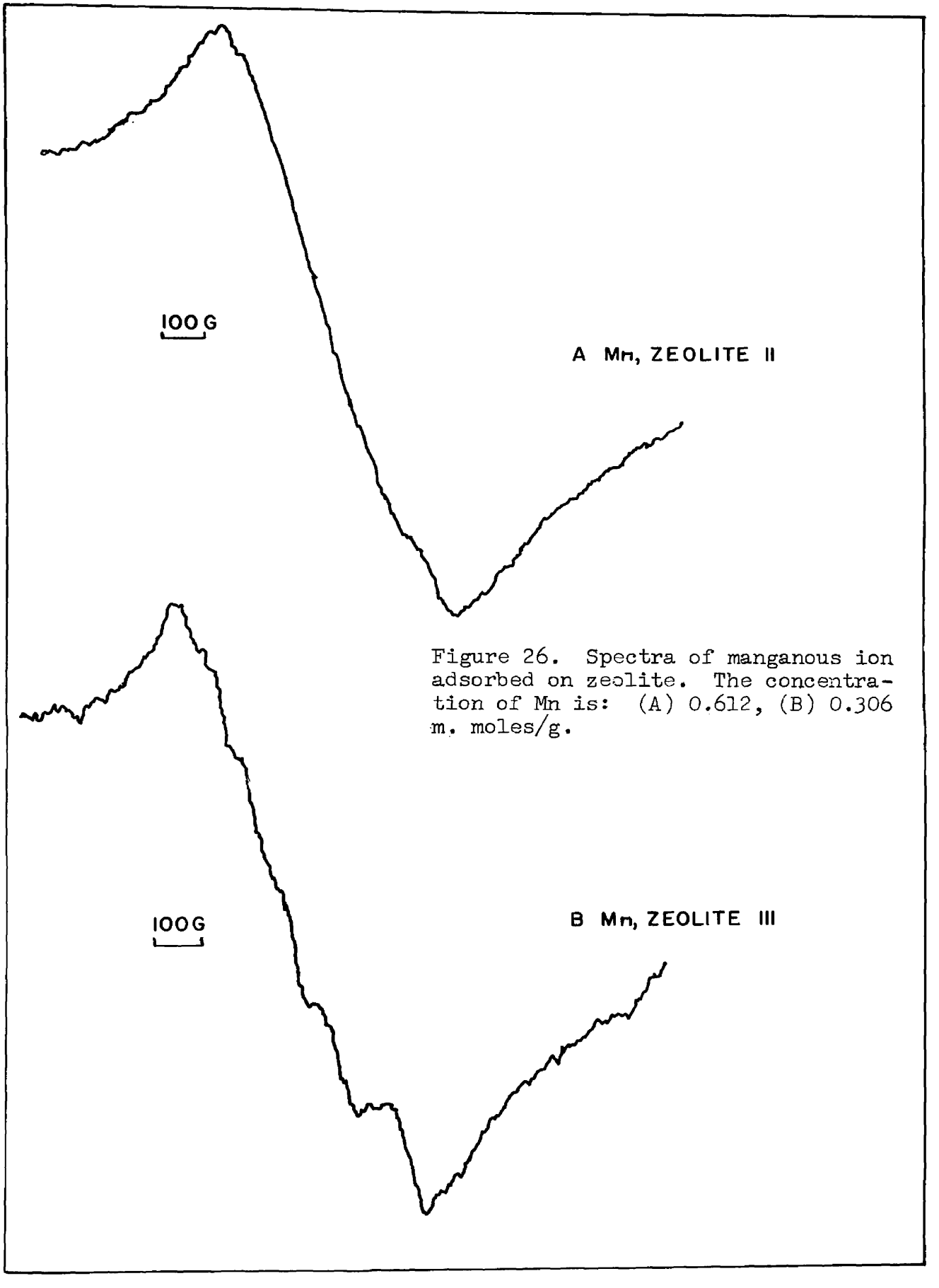

Figure 26. Spectra of manganous ion adsorbed on zeolite. The concentration of Mn is: (A) 0.612, (B) 0.306 m. moles/g.

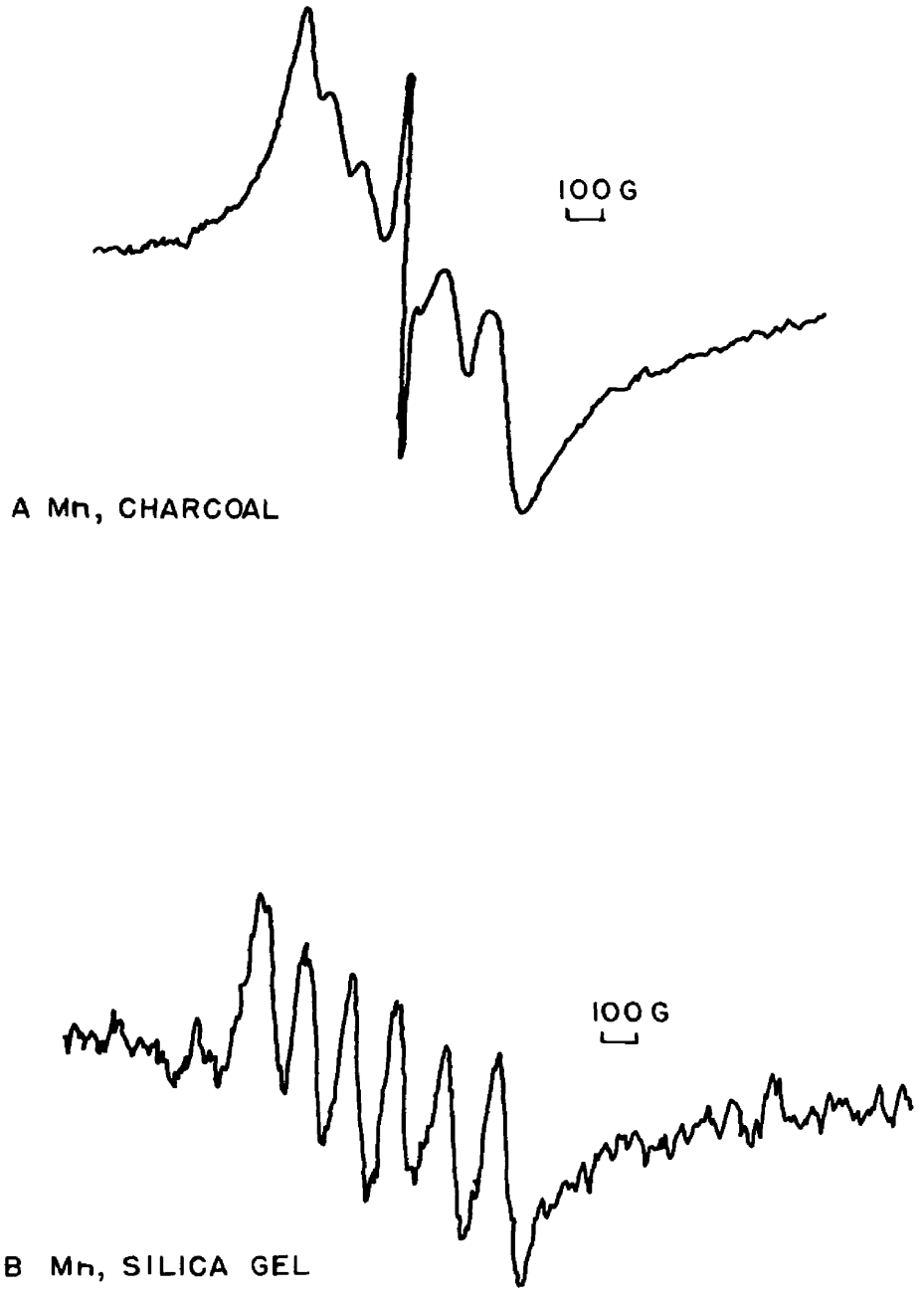

Figure 27. Spectra of manganous ion adsorbed on charcoal and silica gel. The concentration of Mn on silica gel is 0.012 m. moles/g.

manganese on Dowex-50 illustrate the effect of dipolar broadening on the paramagnetic resonance absorption. As the quantity of manganese adsorbed decreases, the line width decreases and the resolution of the pattern improves. As samples IV and V clearly show, the asymmetry in the pattern, which is noticeable in all the spectra, is due to the presence of fine structure. The series of spectra obtained from IR-100 is identical to that from Dowex-50, except that for equal quantities of manganese adsorbed per gram, the IR-100 spectrum is less completely resolved than the Dowex-50 spectrum. Samples I and II are reproduced here, because they provide an extension of the Dowex-50 series in the direction of less complete resolution, and sample IV is included for later reference. The spectrum of manganese-Zeolite I was completely unresolved and resolution was only incipient in samples II and III. The spectra of manganese-charcoal and manganese-silica gel I both represent the maximum amount of manganese able to be adsorbed on these substances. No resolution at all was visible in any manganese-IR-4B samples, which therefore are not reproduced here. Single broad line widths of 236, 242, and 277 gauss, respectively, were observed in samples I, II and IV. The resonance from sample III was too weak to be useful.

Samples containing paramagnetic ion adsorbed on charcoal, silica gel, and ion exchange resins are of necessity powder samples, with completely random orientation of the symmetry axes of the ions. Single crystals of various natural zeolite minerals do occur, however, and attempts were made to substitute manganous and cupric ions for part of

the cations naturally present in the minerals. Single crystals of analcite were placed in thick-walled combustion tubes in contact with saturated aqueous solutions of cupric sulfate and manganese sulfate and enough excess paramagnetic salt was added to maintain saturation even at elevated temperatures and pressures. The tubes were sealed at room temperature and maintained at a temperature of 240°C in a tube oven for three days. When the tubes were opened, the crystal of analcite which had been in contact with the cupric sulfate solution had disintegrated, but the crystal in contact with the manganese solution appeared slightly pink and showed a paramagnetic resonance absorption spectrum characteristic of manganese; the spectrum was nearly identical with that obtained from the powder sample manganese-zeolite III.

When a small amount of the surface of the crystal had been removed by scraping with the point of a knife, it was found that most of the manganese was contained in the powder thus produced. The intensity of the absorption signal from the powder was greater than the intensity of the signal due to the manganese left in the crystal.

In an attempt to determine the influence of water of hydration on the electrostatic field symmetry about the manganese atom, samples of manganese-Dowex-50 IV and manganese-IR-100 IV were placed in Teflon tubes similar to the standard fluorothene sample holders, and kept in a drying oven at 175°C for 18 hours. Upon removal from the oven the tubes were stoppered and the spectra were obtained. The Dowex-50 sample was noticeably blackened by charring at this temperature and a strong free radical resonance was added at the center of the manganese pattern.

No change was noticed in the latter. The manganese-IR-100 IV sample showed a considerable change, however. The spectrum obtained immediately after removal from the oven is reproduced in Figure 28-A. Besides an enhancement of the free radical resonance normally present in the resin, two changes were apparent in the manganese pattern: a reduction of the signal-to-noise ratio which indicates a decrease in the signal strength, and a reduction of the degree of resolution of the six hyperfine structure lines. After this spectrum had been obtained, the sample was exposed to the moist air of the laboratory for three days and another spectrum was taken at the end of this time. This second spectrum is shown in Figure 28-B. The free radical line remained strong, but the manganese resonance pattern had almost regained its original strength and degree of resolution.

Analysis of the Spectra

Because of the presence of fine structure in these spectra, it was impossible to obtain an accurate value for the hyperfine structure constant, A', in Equation 6. It was possible, however, to obtain a fairly good approximation to A', since the fine structure interaction was not excessively strong. An examination of the spectra of manganese-Dowex-50 IV and manganese-Dowex-50 V revealed that each of the four inner lines of the overall six-line spectrum appeared to be resolving into three. Taking the midpoints of these broad, poorly-resolved triplets as the positions of the simple lines described by Equation 6, it was found that the separation between lines two and five (=3A') was

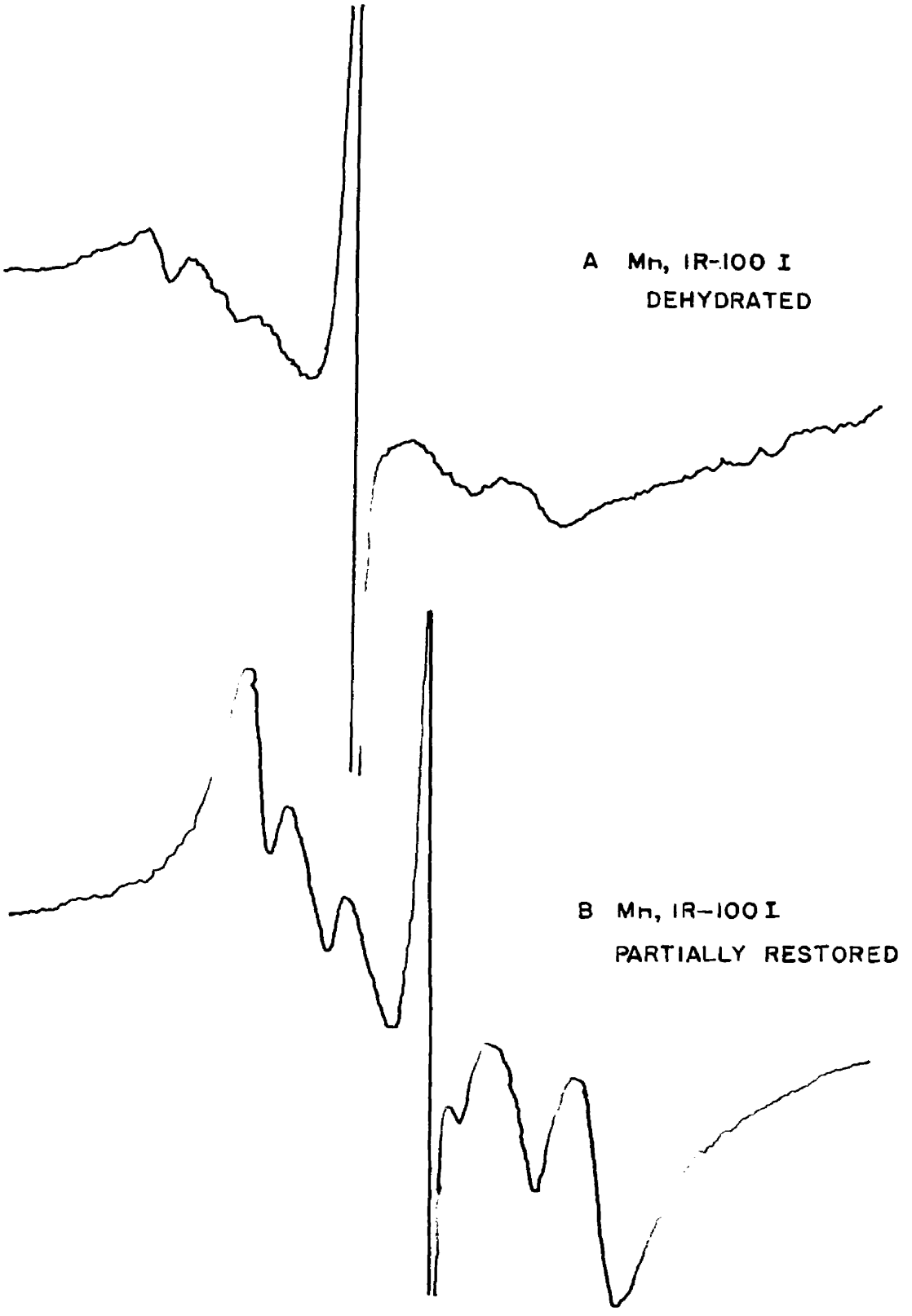

Figure 28. Spectra of manganous ion adsorbed on Amberlite IR-100 and subsequently dehydrated. The concentration of Mn is 0.740 m. moles/g.

288 gauss, and the separation between lines three and four (=A') was 96 gauss. The two outside lines in the spectrum were very narrow and appeared to be unresolved. The separation between them (=5A') was 475 gauss. Thus one obtained values of A' of 95, 96 and 96 gauss respectively, by measuring the separation between the pairs of lines one and six, two and five, and three and four. It was not possible to locate precisely the midpoints of the four inner lines in the less completely resolved spectra, but the outer lines remained rather sharp up to the limit of resolution. The separation between these outer lines was measured for all the spectra of manganese-Dowex-50 and the results were A' = 96, 96, 97, 97, 98 gauss for samples V, IV, III, II, I, in that order. Thus it would appear that the values of A' obtained from the separation of the outer lines are fairly accurate (± 3 gauss) even for poorly resolved spectra. Using this result, values of A' were obtained for all the manganese spectra which showed any resolution. The results are listed in Table III.

TABLE III

APPROXIMATE A' VALUES FOR MANGANESE POWDER SAMPLES

Adsorbent	A' (± 3 gauss)	Samples Used
Dowex-50	96	I, II, III, IV, V
IR-100	95	III, IV, V
Zeolite	96	III
Charcoal	96	I
Silica gel	96	I

Copper

Preparation of Samples

The method of analysis used for cupric ion was the iodometric method as described by Pierce and Haenish (41). An approximately 0.01 N solution of sodium thiosulfate was made up and standardized against metallic copper in the manner also described by Pierce and Haenish (41). Approximately 0.13 gram samples of metallic copper were dissolved in nitric acid and diluted to 250 ml. in a volumetric flask. Fifty ml. aliquots of these solutions were taken for titration by the thiosulfate solution. It was found that 0.1300 grams of copper was equivalent to 5 x (44.64± 0.01) ml. of thiosulfate solution, giving a normality of 0.009164 for the thiosulfate solution.

In order to standardize the approximately 0.1 M cupric sulfate stock solution, 10.00 ml. samples thereof were diluted to 250 ml. in a volumetric flask and 50 ml. aliquots taken for titration. It was found that 10.00 ml. of cupric sulfate solution was equivalent to 5 x (21.67 ± 0.01) ml. of the thiosulfate solution, indicating a concentration in the cupric sulfate solution of 0.09926 moles per liter.

Samples of hydrated cupric ion adsorbed on Dowex-50, Amberlites IR-100, IRC-50H, and IR-4B, zeolite, charcoal, and silica gel were prepared and analyzed according to the general procedure given above. Table IV contains the pertinent analytical data for these samples.

The spectra obtained from the samples of Table IV are reproduced in Figures 29-34. Some spectra are not reproduced here in order to

TABLE IV

ADSORPTION OF CUPRIC ION BY VARIOUS ADSORBENTS

Sample		Wt. in g. of Adsorbent	Ml. $CuSO_4$	Ml. Thiosulfate	Moles Cu^{++} Adsorbed x 10^{+3}	Moles $Cu^{++}/g.$ x 10^{+3}
Cu, IR-100	I	3.2583	50.00	25 x (10.59)	2.537	0.779
	II	3.3885	20.00	22.31	1.781	0.526
	III	3.2952	10.00	1.49	0.979	0.297
	IV	2.9237	5.000	0.11	0.495	0.169
	V	3.0874	1.000	0.0	0.099	0.032
Cu, Dowex-50	I	4.1613	20.00	1.60	1.970	0.474
	II	2.8387	5.000	0.1	0.495	0.174
	III	3.2169	1.000	0.0	0.099	0.031
Cu, Zeolite	I	3.0765	50.00	232.	2.84	0.922
	II	2.6845	20.00	44.99	1.573	0.586
	III	3.6350	10.00	2.87	0.976	0.266
	IV	2.9373	5.000	0.25	0.494	0.168
	V	3.1900	1.000	0.23	0.097	0.031
Cu, IR-4B	I	1.9485	10.00	4.29	0.932	0.478
	II	2.8455	5.000	6.59	0.457	0.161
	III	2.9262	1.000	1.3	0.087	0.030
Cu, Charcoal		2.0209	5.000			
Cu, Silica gel	I	1.9340	5.000	52.89	0.012	0.006
	II	2.6818	1.000	9.00	0.018	0.006
	III	2.9725	0.500	3.67	0.016	0.005
Cu, IRC-50H		No analysis				

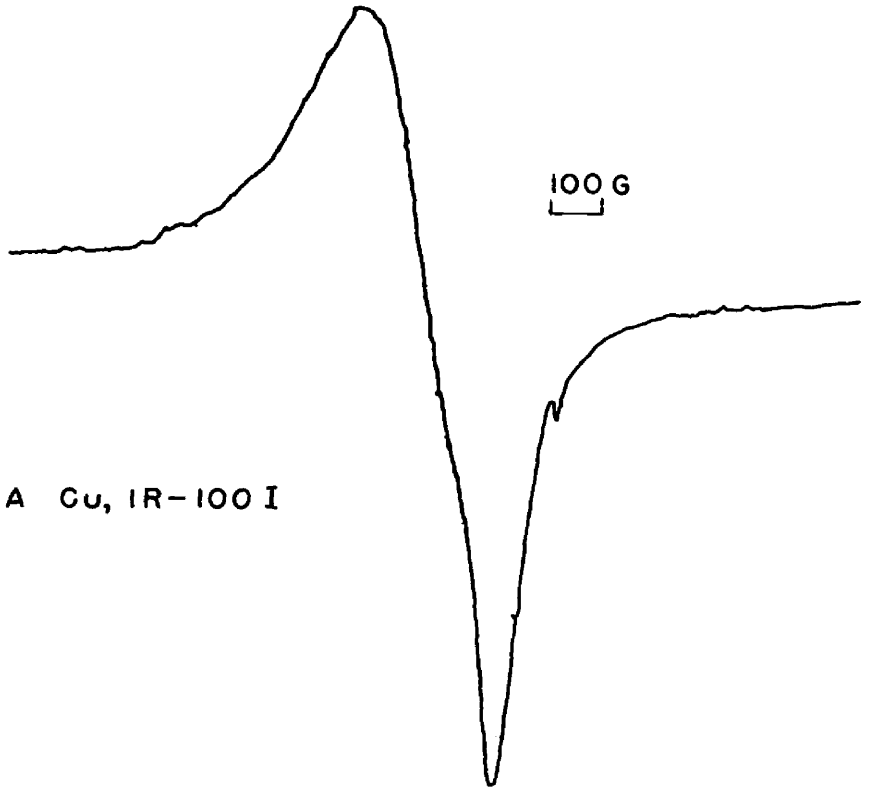

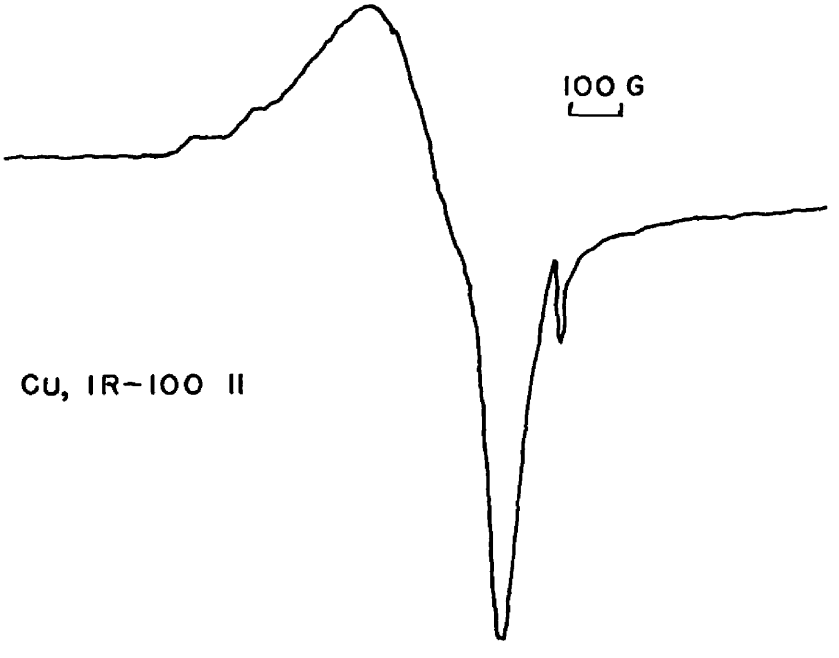

Figure 29. Spectra of cupric ion adsorbed on Amberlite IR-100. The concentration of Cu is: (A) 0.779, (B) 0.526 m. moles/g.

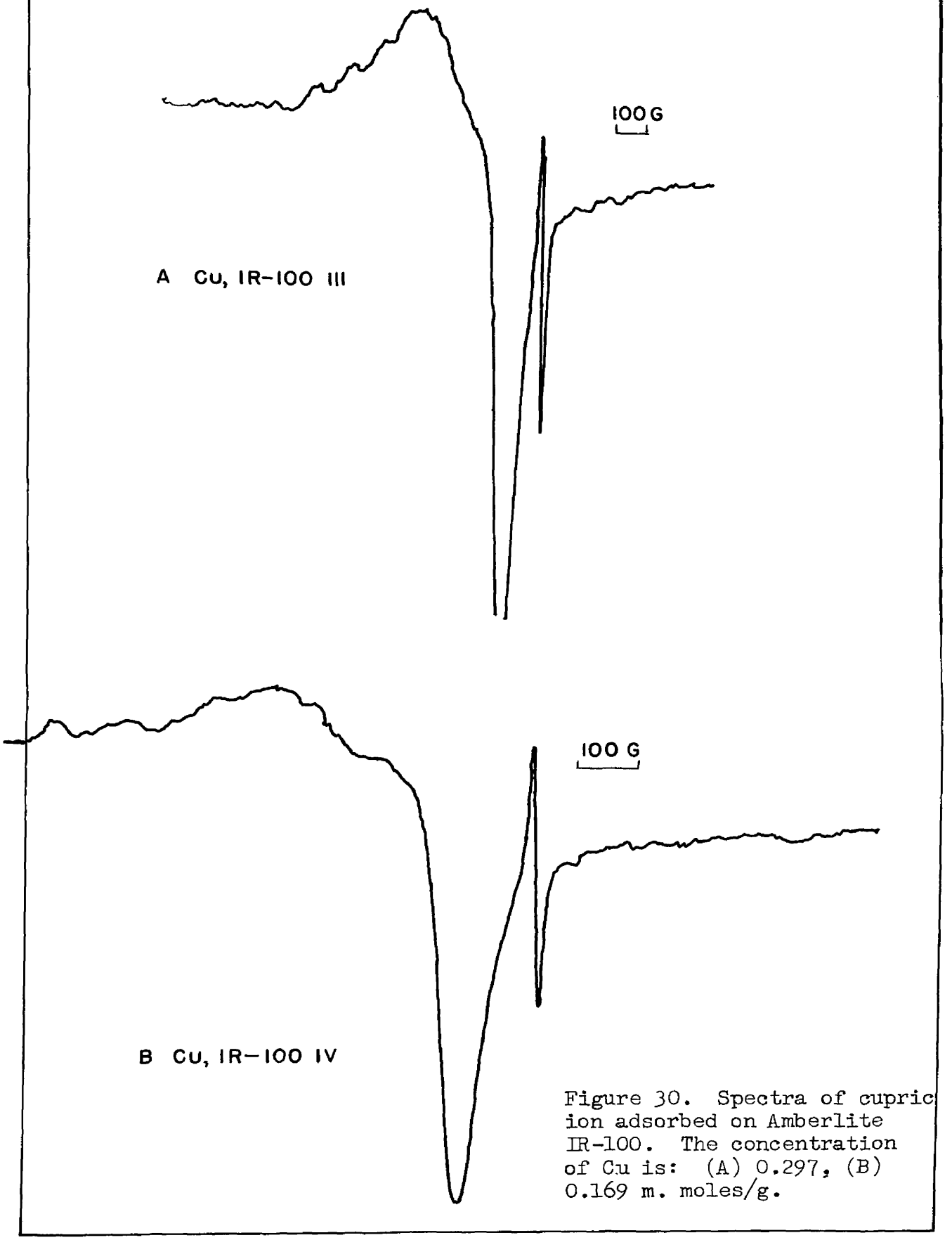

Figure 30. Spectra of cupric ion adsorbed on Amberlite IR-100. The concentration of Cu is: (A) 0.297, (B) 0.169 m. moles/g.

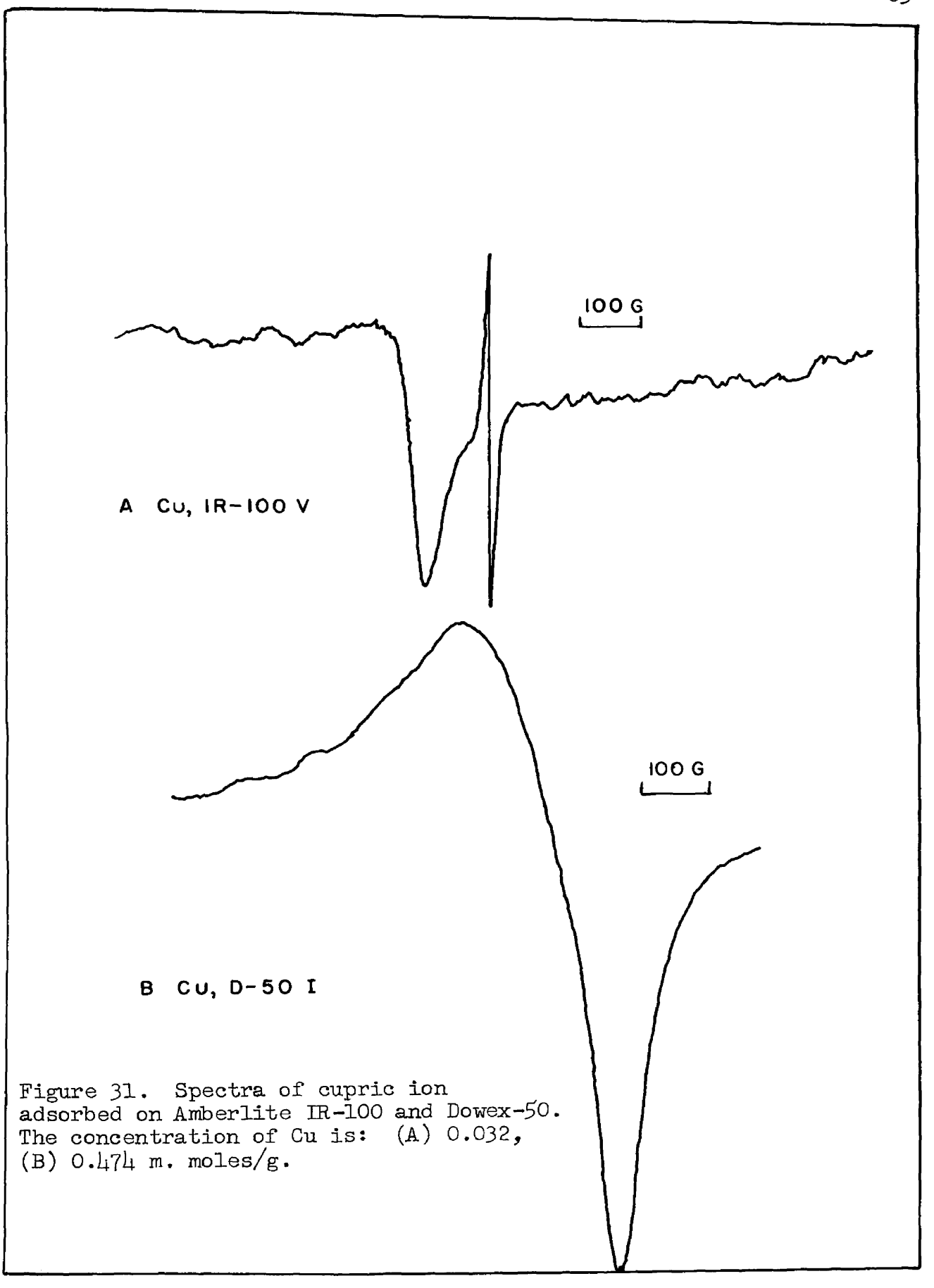

Figure 31. Spectra of cupric ion adsorbed on Amberlite IR-100 and Dowex-50. The concentration of Cu is: (A) 0.032, (B) 0.474 m. moles/g.

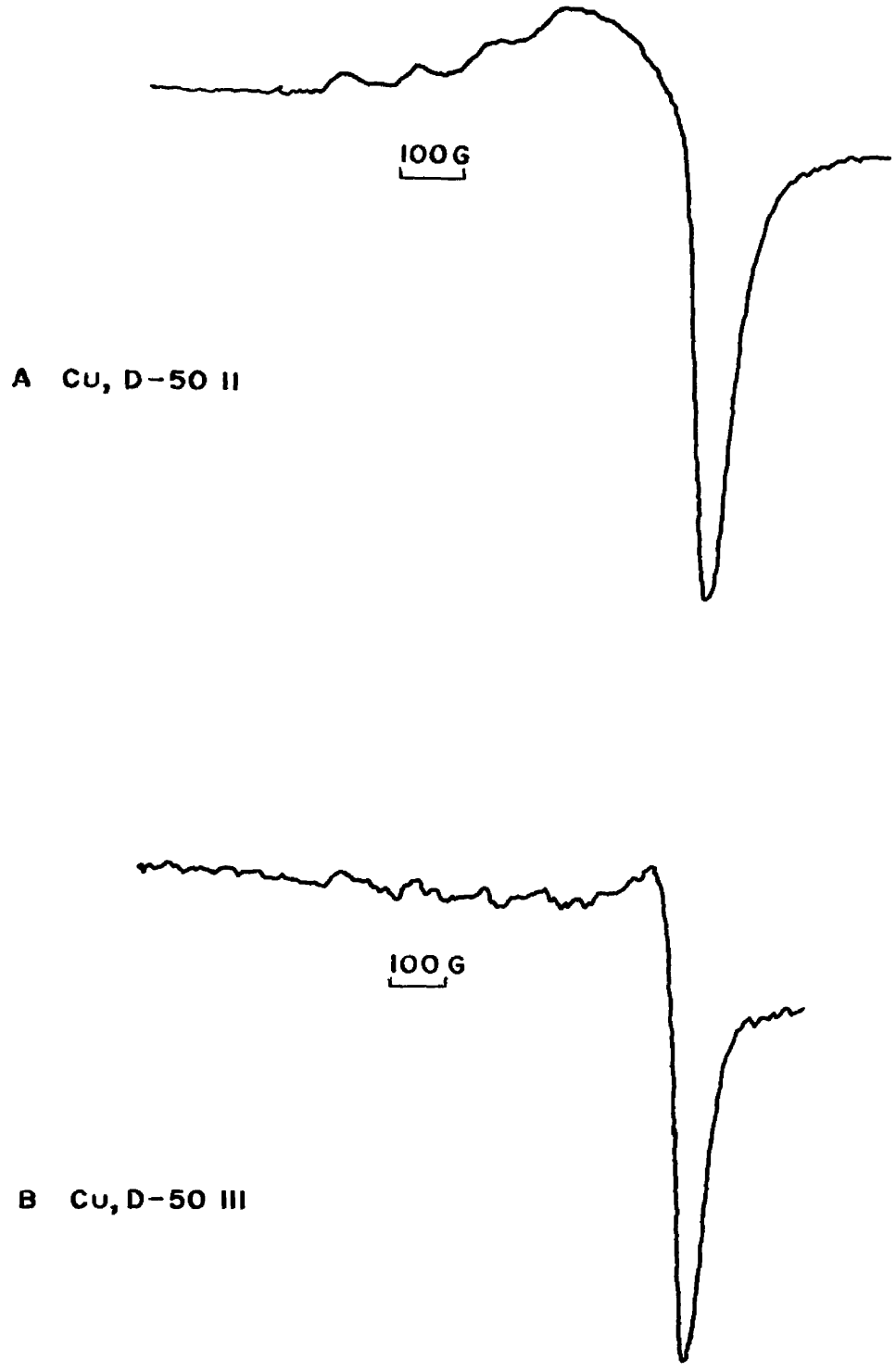

Figure 32. Spectra of cupric ion adsorbed on Dowex-50. The concentration of Cu is: (A) 0.174, (B) 0.031 m. moles/g.

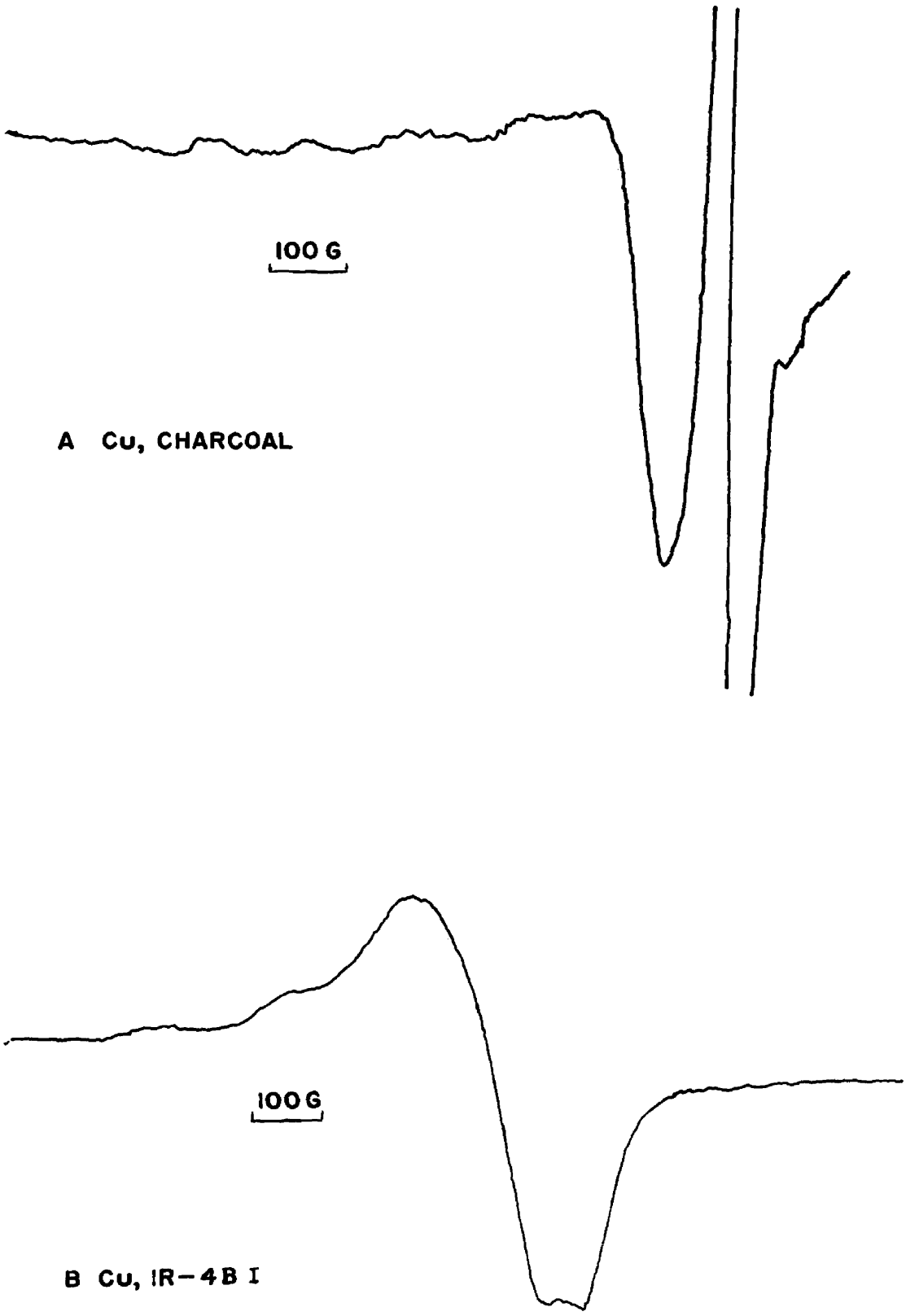

Figure 33. Spectra of cupric ion adsorbed on charcoal and Amberlite IR-4B. The concentration Cu is: (A) 0.040, (B) 0.478 m. moles/g.

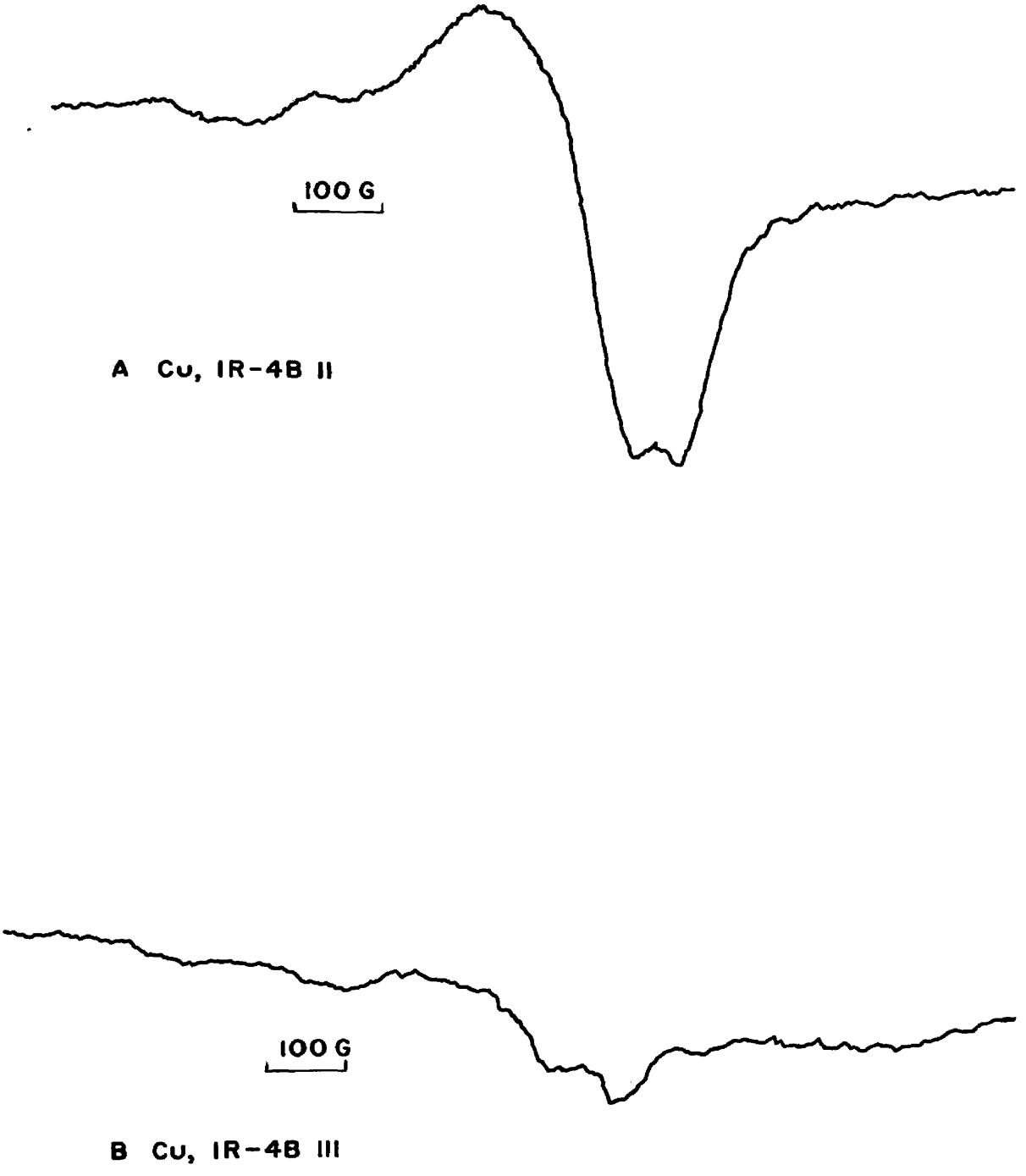

Figure 34. Spectra of cupric ion adsorbed on Amberlite IR-4B. The concentration of Cu is: (A) 0.161, (B) 0.030 m. moles/g.

avoid needless repetition of nearly identical patterns. The complete series of five copper-IR-100 spectra is included as an illustration of the effect of dipolar broadening on the resolution of the pattern. A free radical resonance is noticeable in these spectra and also in the spectrum of copper - charcoal. The three copper-Dowex-50 spectra are also included despite their similarity to the copper-IR-100 spectra, because they are somewhat clearer and better resolved owing to a better signal-to-noise ratio. The five copper-zeolite spectra are not included, being scarcely distinguishable from the copper-Dowex-50 and copper-IR-100 series.

An attempt was made to prepare a series of samples of cupric ion adsorbed on Amberlite IRC-50H, but owing to the fact that the adsorbing power of this resin is low in acidic solution, only a minute quantity of cupric ion was adsorbed. The spectra obtained from the copper-IRC-50H samples were like the spectrum of copper - IR-100 V and are not reproduced here.

Although the analytical data of Table IV indicate a minute amount of adsorption of cupric ion by the silica gel, no paramagnetic resonance absorption signal was found.

Approximately 0.1 M solutions of tetrachloro, tetrabromo , and tetratartrato cuprate (II) complex anions were prepared by adding solid sodium chloride, sodium bromide, and sodium tartrate, respectively, to 100 ml. portions of the 0.09926 molar stock solution of cupric sulfate until the color due to the complex ion did not deepen with further addition. These colors were: tetrachlorocuprate (II) ion, green;

tetrabromocuprate (II) ion, intense brown; tetratartratocuprate (II) ion, deep blue. Then, 10, 5, and 2 ml. samples of these solutions were placed in contact with approximately 3 g. portions of Amberlite IR-4B in stoppered flasks. At the end of four hours the resin was removed on a paper filter and washed several times with distilled water. The clear filtrates obtained from the chloride and bromide complexes were slightly green-blue after adsorption. The intense color of the tartrate complex filtrate was not noticeably diminished by adsorption. The spectra of the first two series of samples were obtained and proved to be indistinguishable from the spectra of copper - IR-4B; hence they are not reproduced here. No paramagnetic resonance absorption signal could be detected in the resin which had been in contact with the solution of the tartrate complex, which fact confirmed the evidence that no adsorption of the tetratartratocuprate (II) ion by IR-4B occurs.

Samples of tetramminocopper (II) complex cation, adsorbed on Dowex-50, Amberlites IR-100 and IRC-50H, zeolite, and charcoal were prepared by taking the existing samples of Table IV and letting them stand in 10 ml. of a 1:4 solution of ammonium hydroxide in distilled water for at least four hours. The zeolite samples turned from a light to a dark blue within a few minutes. Where this color change was not detectable, as in charcoal and IR-100 samples, the adsorbent was allowed to remain in contact with the ammonium hydroxide solution for eight hours. The filtrates obtained upon removal of the adsorbents were colorless, indicating within the nended accuracy that the quantity of cupric ion remained about the same as before the exchange of ammonia

for the water of hydration occurred. The samples were treated in the usual manner and their spectra obtained. An examination of these spectra showed that their parameters were in every case different from those of the spectra of the corresponding hydrated cupric ion samples, although the two sets of spectra were similar in form. However, an anomalous variation in the parameters from sample to sample seemed to indicate that the tetramminocopper (II) ionic complex had partially decomposed. This effect was especially noticeable in the copper - IRC-50H spectra. In fact, the blue color in these samples had reverted to the light blue of the hydrated copper ion after dehydration at 110°C. Only the copper - IR-100 samples seemed unaffected, presumably because the large size of the resin particles hindered the effusion of ammonia. In an attempt to preserve the complex, the samples were again treated with ammonium hydroxide solution as before and washed after filtration, not with distilled water, but with more ammonium hydroxide solution. They were then placed in an ordinary calcium chloride drying tube which was stoppered and fitted with inlet and outlet rubber tubing. This assembly was placed in the drying oven at 100°C and the rubber tubes were passed out through a hole in the top of the oven. The inlet tube was connected to the nozzle of a cylinder of compressed ammonia, and a stream of dry ammonia was passed over the sample throughout the drying process. Visual confirmation of the fact that this new treatment improved matters was afforded by a comparison of the cuprammonium-zeolite samples produced in this way with a portion saved from the previous treatment. The blue color in the normally colorless zeolite

was considerably darkened. The spectra of these samples which were dried in a stream of ammonia gas were obtained immediately upon removal of the samples from the oven in order to minimize the replacing of coordinated ammonia molecules by water molecules from the atmosphere.

Of the spectra obtained in this manner, only 3 are reproduced in Figures 35 and 36. Two samples of the five in the cuprammonium-IR-100 series--samples I and II (the numbering corresponds to the numbering of the hydrated cupric ion series from which they were derived)--are included to indicate both the slight change in the spectra and the trend of the series as the line width decreases with decreasing concentration of paramagnetic species. The cuprammonium-charcoal spectrum, reproduced in Figure 36, presents a problem because the copper resonance overlaps the resonance due to the free radicals in the charcoal. As is indicated in the figure, an attempt was made to separate the two resonances by assuming that the free radical resonance was symmetrical about its center and subtracting the postulated free radical absorption from the total absorption to leave a "corrected" spectrum for the copper absorption.

Analysis of the Spectra

It has been shown (23) that as the line width decreases, the center of the strong very asymmetrical peak in the copper powder spectrum tends toward a value of the field strength given by the equation:

$$H_{\perp} \qquad \Delta E/\beta \; g_{\perp} \qquad (22)$$

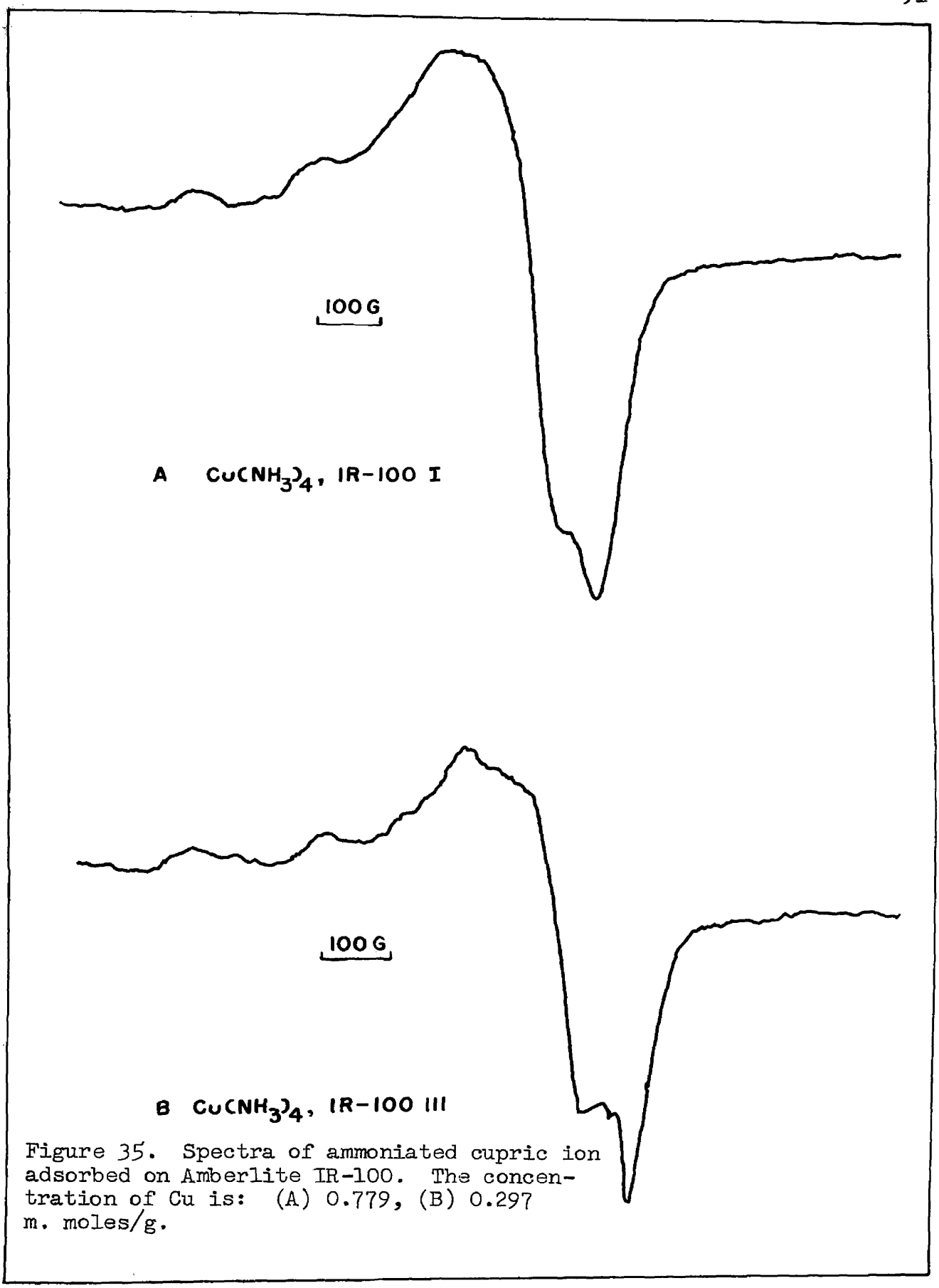

Figure 35. Spectra of ammoniated cupric ion adsorbed on Amberlite IR-100. The concentration of Cu is: (A) 0.779, (B) 0.297 m. moles/g.

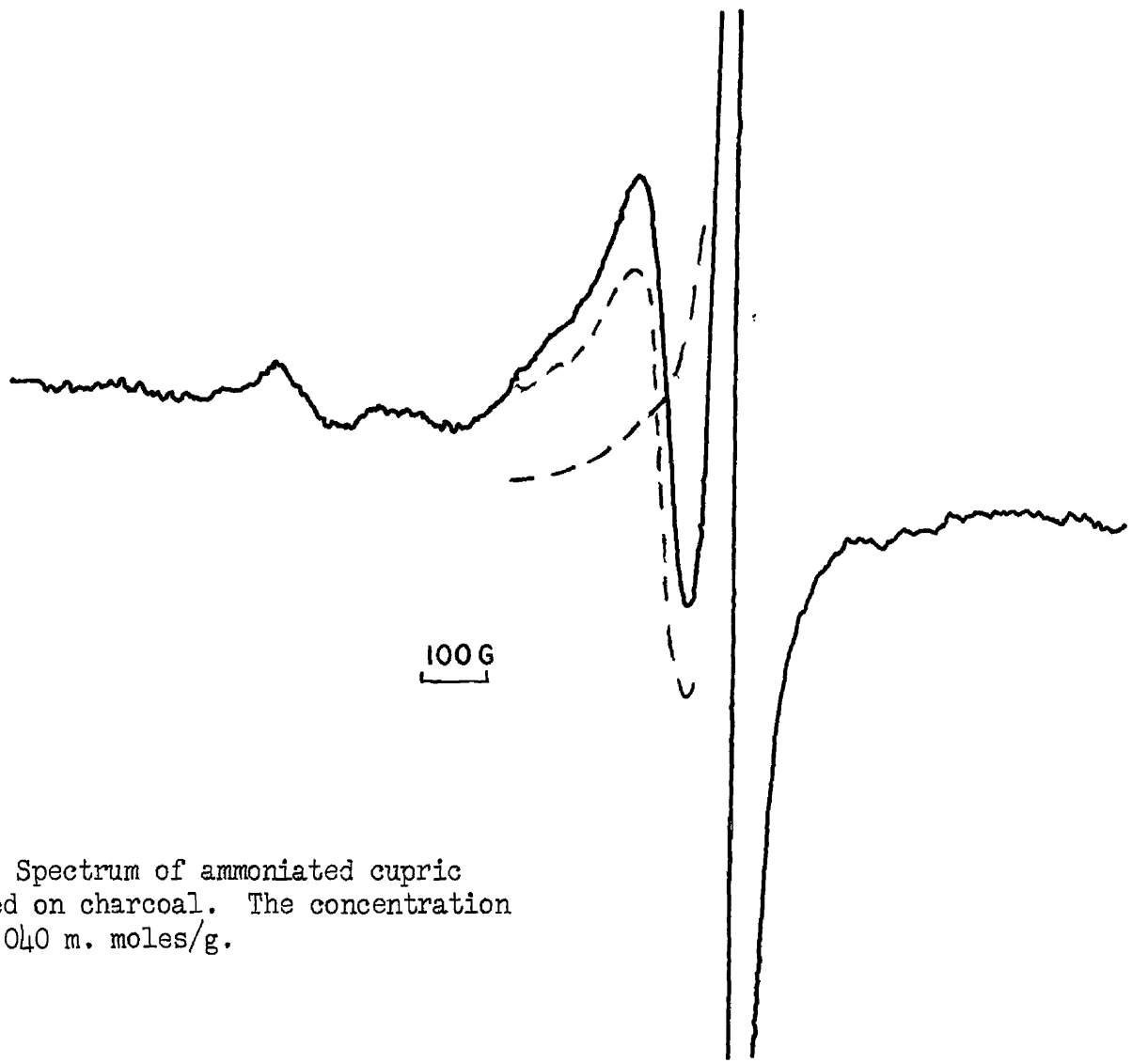

Figure 36. Spectrum of ammoniated cupric ion adsorbed on charcoal. The concentration of Cu is 0.040 m. moles/g.

It has also been shown that the center of the weak, partially obscured four-peak pattern occurs at a field strength of

$$H_{\parallel} = \Delta E/\beta\, g_{\parallel} \qquad (23)$$

and that the separation between these peaks, in gauss, is equal to the hyperfine structure constant, A', in equation 19.

Wherever possible, an effort was made to reduce the error in the determination of $H_{\perp}$, due to the finite line width, by plotting as a function of copper concentration a measurable parameter of the paramagnetic resonance absorption spectrum, which in the limit of zero concentration would approach $H_{\perp}$. A number of quantities might be chosen, including the point of intersection of the first-derivative plot with the base line, or the point of maximum slope in the first-derivative plot. Because of the nature of the spectra at high concentration another closely related parameter was chosen, namely the point of intersection with the base line of a straight line tangent to the first-derivative plot at the point of maximum slope. The use of this parameter, designated H_p, which was identical with the two mentioned above at low concentrations of copper, resulted in a fairly straight line of smaller slope than would have been given by the use of either of the other parameters. This straight line was extrapolated to zero concentration of copper, and the extrapolated value of H_p was taken as $H_{\perp}$ for that series of spectra. The positions of the lines in the weak four-line spectrum were taken to be the points of half-intensity of the peaks appearing in the first derivative plot, on the high-field

side of the peaks. Table V lists the parameters of these spectra, and Figure 37 shows the graphs and extrapolations used to obtain $H_\perp$ for the copper series. Table VI contains a summary of these results.

Values of the quantities $g_{\parallel}$, $g_\perp$, and A for these spectra were computed in the following manner. Where all four of the quantities $H_{3/2}$, $H_{1/2}$ $H_{-1/2}$, $H_{-3/2}$ were known, $H_{\parallel}$ was taken as the average of the two midpoints $1/2(H_{3/2} + H_{-3/2})$ and $1/2(H_{-1/2} + H_{1/2})$. Values $g_{\parallel}$ and $g_\perp$ were then computed from Equation 19. A' was taken as the average of the two quantities $1/3(H_{-3/2} - H_{3/2})$ and $(H_{-1/2} - H_{1/2})$. Where the positions of only two or three of these four lines were known, the positions of the remaining obscured lines were postulated on the basis of the observed lines and the above procedure was then followed. The hyperfine structure interaction constant, A, was computed by means of the relationship,

$$A = \beta\, g_{\parallel}\, A' \qquad (7)$$

The observed values of H_p for the ammoniated copper samples are also plotted in Figure 37 and the lines (not shown in the figure) with slopes equal to the slope of the plot for the copper-zeolite samples were drawn through the points obtained from the most concentrated samples, where the contribution of dipolar broadening to the line width is probably greatest; the intercepts of these postulated plots yield values of $H_\perp$ and $g_\perp$ for the ammoniated samples as listed in Table VII.

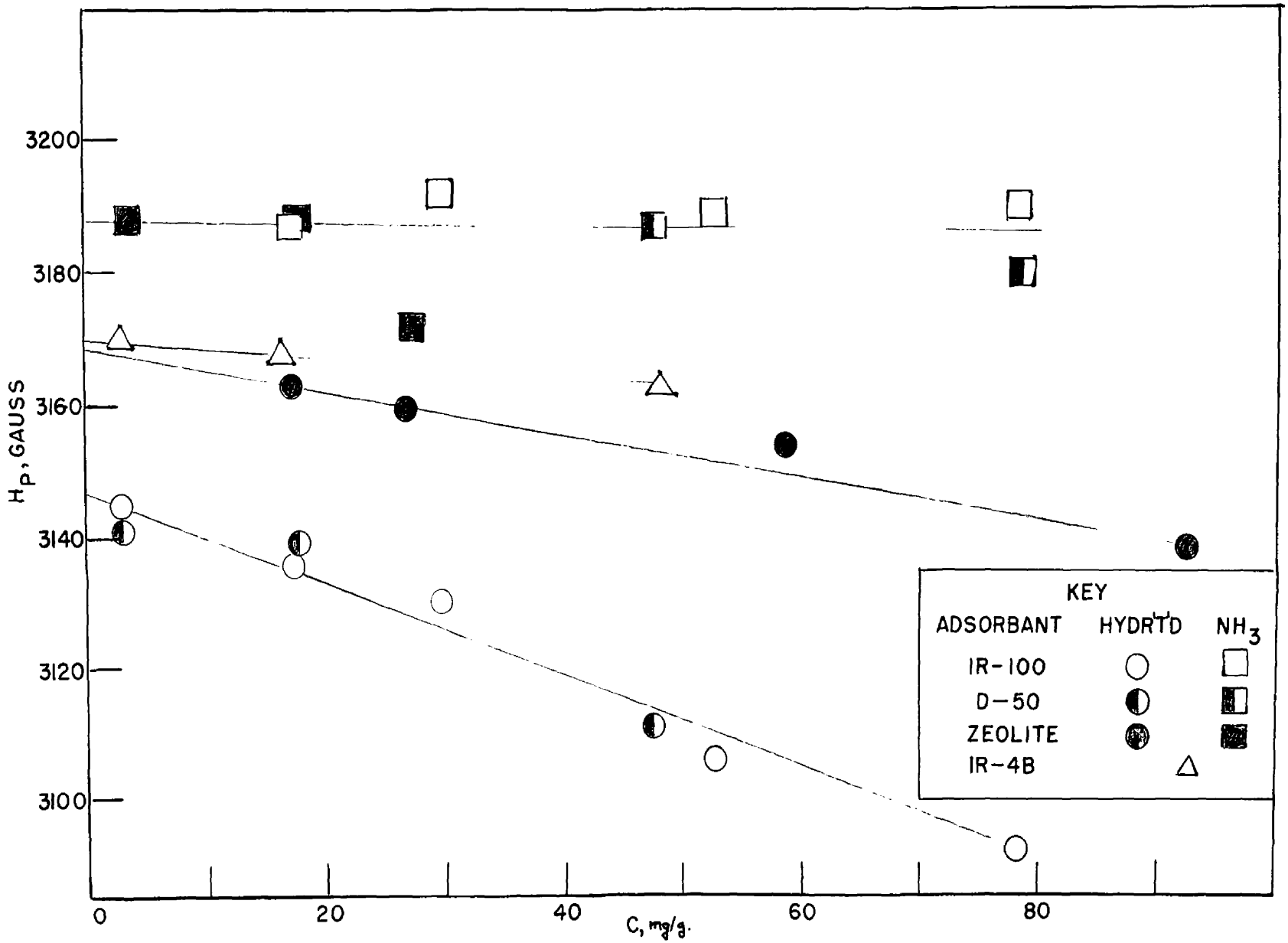

Figure 37. H_P VERSUS CONCENTRATION FOR COPPER SAMPLES

TABLE V

ANALYSIS OF COPPER SPECTRA

Sample		H_p	$H_{3/2}$	$H_{1/2}$	$H_{-1/2}$	$H_{-3/2}$
		Hydrated Copper Samples				
Cu-IR-100	I	3092	-	-	-	
	II	3106	-	-	-	-
	III	3130	2592	2704	2808	-
	IV	3136	-	-	-	-
	V	3145	-	-	-	-
Cu-Dowex-50	I	3111	2583	2692	2818	-
	II	3139	-	-	-	-
	III	3141	-	-	-	-
Cu-Zeolite	I	3138	2606	2735	-	-
	II	3154	-	-	-	-
	III	3159	-	-	-	-
	IV	3163	-	-		-
Cu-Charcoal		3162	2614	2796	2928	3053
Cu-IRC-50H		3169	-	-	-	-
Cu-IR-4B	I	3163	2748	2923	3102	3278
	II	3168	-	-	-	-
	III	3170	-	-	-	-
		Ammoniated Copper Samples				
Cu-IR-100	I	3190	2705	2888	3078	3270
	II	3189	2720	2894	3087	3267
	III	3192	-	-	-	-
	IV	3187	-	-	-	-
Cu-Dowex-50	I	3180	-	-	-	
	II	3187	2711	2878	3055	
	III	-	-	-	-	
Cu-Zeolite	III	3170	-	-	-	
	IV	3185	2701	2877	3050	
	V	3188	-	-	-	
Cu-Charcoal		3187	2702	2863	3053	

TABLE VI

SUMMARY OF RESULTS FOR COPPER POWDER SAMPLES

Sample	$g_\perp$	$g_\parallel$	A', gauss	A, cm^{-1}
Cu-IR-100	2.096	2.39	110	0.0122
Cu-Dowex-50	2.099	2.40	115	0.0128
Cu-Charcoal	2.086	2.32	140	0.0152
Cu-Zeolite	2.083	2.35	130	0.0142
Cu-IR6-50H	2.080	-	-	-
Cu-IR-4B	2.079	2.19	180	0.0184
$Cu(NH_3)_4$-IR-100	2.068	2.21	188	0.0194
$Cu(NH_3)_4$-Dowex-50	2.078	2.22	172	0.0178
$Cu(NH_3)_4$-Charcoal	2.07	2.22	177	0.0184
$Cu(NH_3)_4$-Zeolite	2.072	2.22	175	0.0182
$Cu(NH_3)_4$-IRC-50H	not stable			
$Cu(NH_3)_4$, CuCl, CuBr, IR-4B	same as Cu-IR-4B			

TABLE VII

REVISED ESTIMATES OF $H_\perp$ AND $g_\perp$ FOR AMMONIATED COPPER SAMPLES

Sample	$H_\perp$, gauss	$g_\perp$
$Cu(NH_3)_4$-IR-100	3216	2.052
$Cu(NH_3)_4$-Dowex-50	3208	2.057
$Cu(NH_3)_4$-Zeolite	3208	2.057

Optical Reflectance Spectra

The colorless zeolite allows the determination of the optical absorption spectrum of the cupric ions contained on it. Since the sample was in the form of an opaque powder, it was necessary to obtain the spectrum of the light reflected from it. An amount of colorless zeolite crystals roughly equal to the amount of available copper-containing sample was spread in a thin layer on the horizontal bed of an opaque projector. The powder was illuminated by a 1000 watt tungsten-filament electric lamp and the reflected light was focused and projected by the mirror and lens system of the projector. The beam of light emitted by the projector was focused by a condensing lens on the entrance slit of a Beckman Model DU Spectrophotometer, from which the lamp housing had been removed.[1] A reference curve was then obtained with the colorless zeolite by noting the slit opening required to give a 100% transmittance reading at twenty-mμ intervals throughout the range of 400 to 1000 millimicrons. Then the colorless reference sample was replaced by the copper-containing sample and, using the slit widths indicated by the reference sample, percent transmittance was read from the spectrophotometer scale. The actual quantity being measured was, of course, not transmittance but reflectance. The results of this experiment for hydrated copper-zeolite samples and for an ammoniated copper-zeolite sample are shown in Figure 38.

---

[1]This method of obtaining the reflectance spectrum was suggested by Professor J. C. Sternberg.

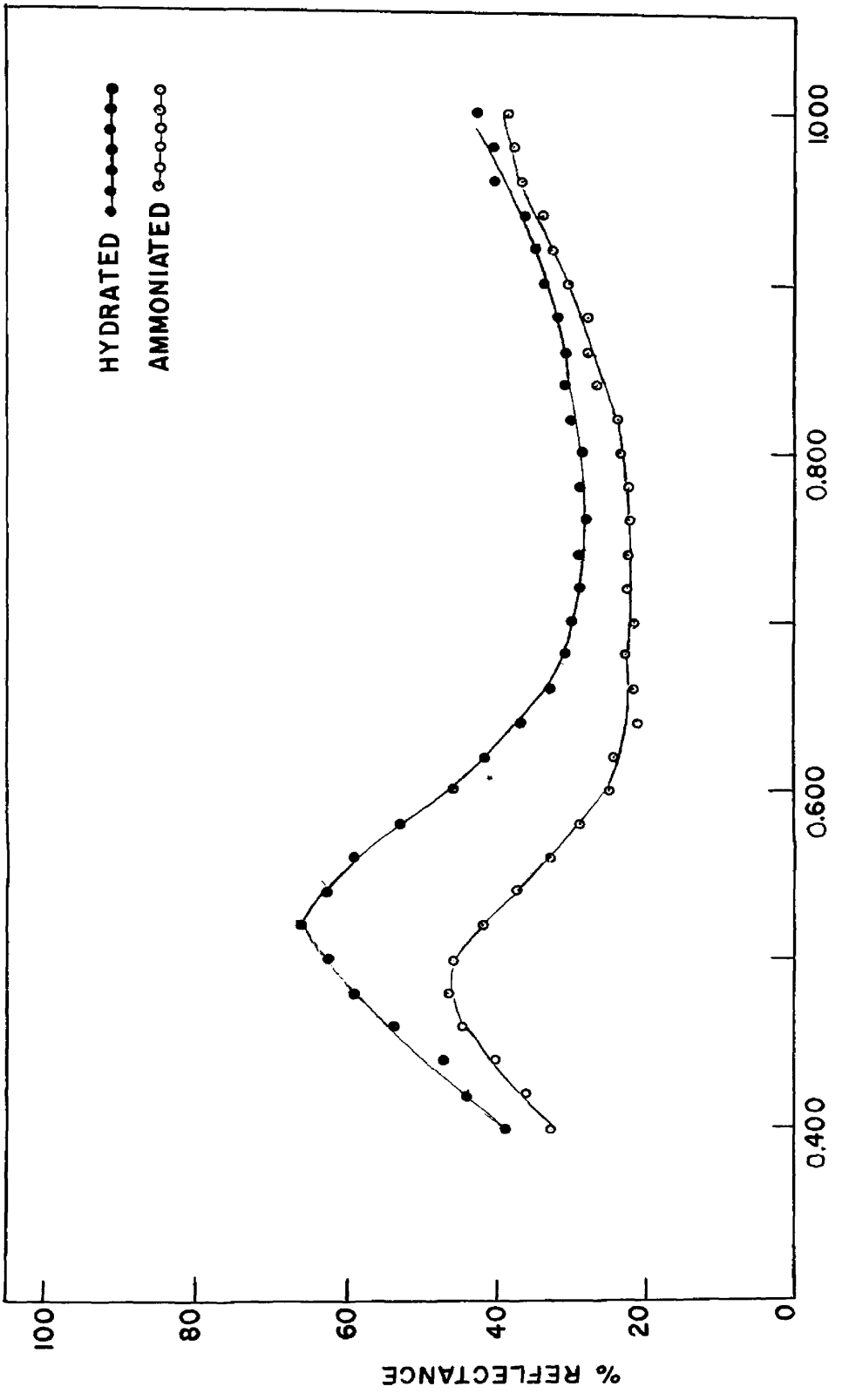

Figure 38. REFLECTANCE SPECTRA OF COPPER-ZEOLITE SAMPLES

Vanadium

Preparation of Samples

An approximately 0.1 M solution of vanadyl sulfate was prepared by dissolving twenty grams of vanadyl sulfate dihydrate in 100 ml. of distilled water and boiling the mixture. A dark blue murky solution was formed. This solution was cooled to room temperature and filtered and the clear blue filtrate was diluted to 1000 ml. with distilled water. The brown colored precipitate was collected on the filter paper and discarded.

The 0.01 N potassium permanganate solution was restandardized against arsenious oxide as described above. It was found that 1.000 ml. of permanganate solution was equivalent to 0.00796 ± 0.00002 g. of arsenious oxide. Thus, the normality of the permanganate solution was N = 0.01288 ± 0.00003.

The concentration of the vanadyl sulfate solution was determined by adding to 5.000 ml. samples of the solution 25 ml. of distilled water and 5 ml. of concentrated sulfuric acid. The solution was heated to boiling at the beginning of the titration with potassium permanganate solution, and again at the end point. A sharp end point was obtained, and it was found that 5.000 ml. of vanadyl sulfate solution was equivalent to 41.00 ± 0.01 ml. of permanganate solution. Hence, the concentration of the vanadyl sulfate was 0.1056 moles per liter.

Samples of vanadyl ion adsorbed on Amberlites IR-100 and IR-4B, Dowex-50, silica gel, and charcoal were prepared and analyzed in the usual manner. The analyses were not successful. With the exception

of the silica gel sample, no sharp end points could be obtained and with the IR-4B samples, no end point whatsoever was detected. These erratic results were probably caused by small quantities of organic matter leached out of the resins by the water. However, since an examination of the spectra obtained from these samples revealed no dependence upon concentration, no attempt was made to improve the doubtful analytical data. These data are collected in Table VIII.

TABLE VIII

ADSORPTION OF $VOSO_4$ BY VARIOUS ADSORBENTS

Sample		Wt. of Adsorbent g.	Ml. $VOSO_4$	Ml. Permanganate
VO-IR-100	I	3.7774	5.000	28.3
	II	2.9258	1.000	17.2
VO-Dowex-50	I	4.6113	1.000	2.3
	II	3.8923	0.500	2.1
	III	3.3015	5.000	-
VO-Zeolite	I	2.9663	10.00	12.3
	II	2.7167	5.000	-
VO-Charcoal		0.5769	5.000	
VO-Silica gel		3.2482	10.00	80.37
VO-IR-4B	I	2.4900	5.000	-
	II	3.3183	1.000	-

Analysis of the Spectra

The typical spectra obtained from these samples are reproduced in Figures 39, 40 and 41. Figure 39 shows the strong pattern of eight

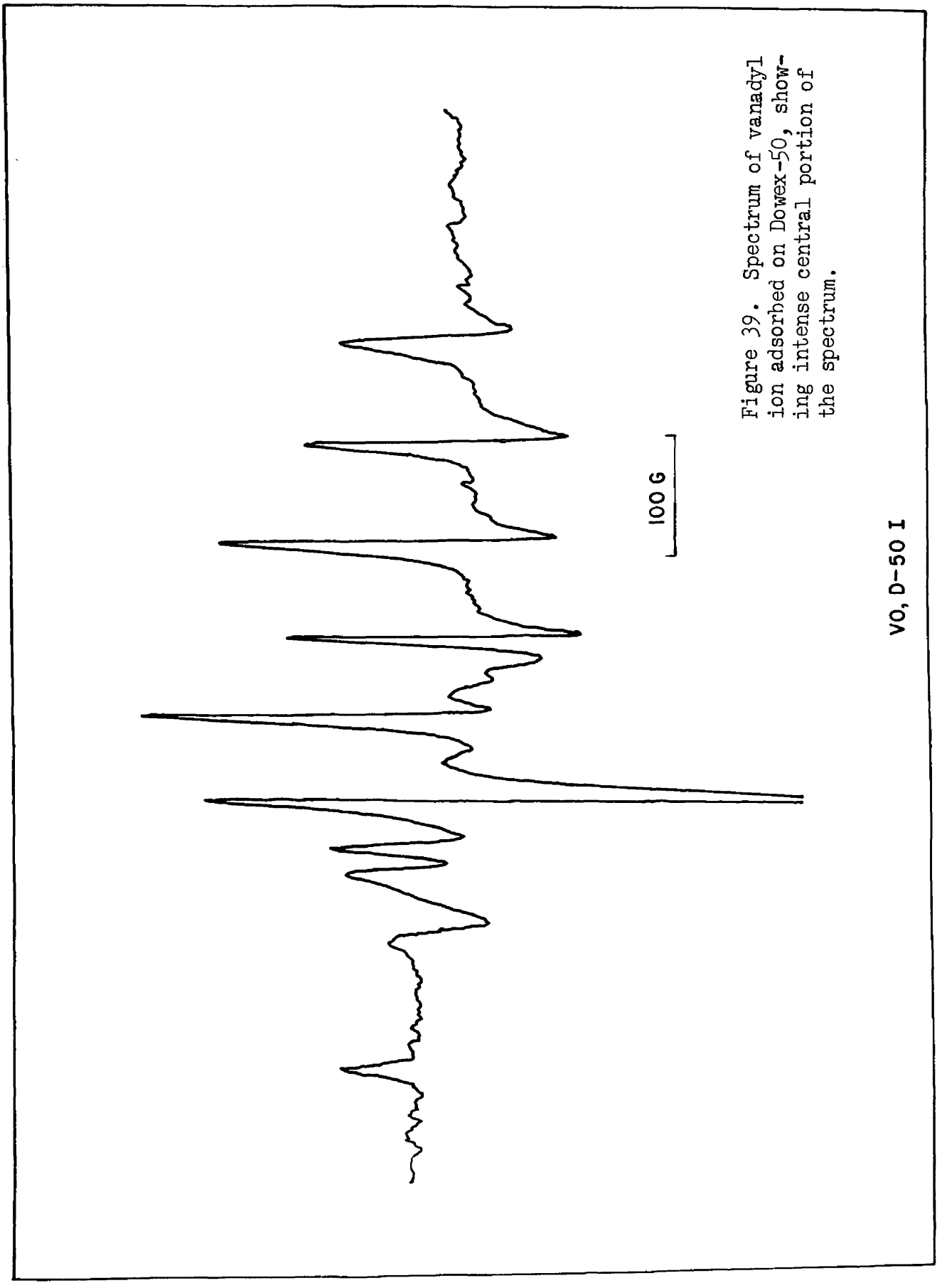

Figure 39. Spectrum of vanadyl ion adsorbed on Dowex-50, showing intense central portion of the spectrum.

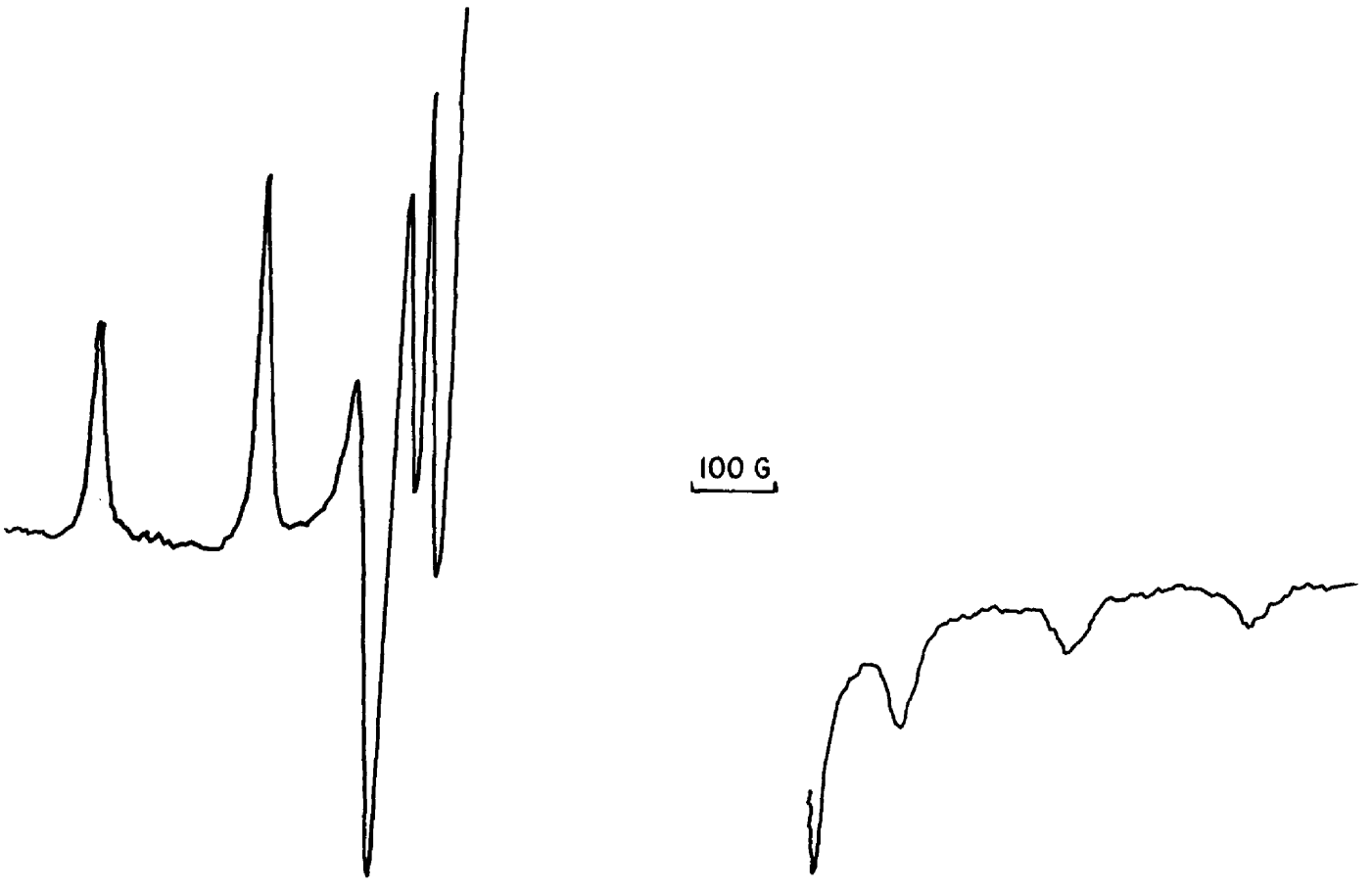

Figure 40. Spectrum of vanadyl ion adsorbed on Dowex-50, showing the weak outer portions of the spectrum.

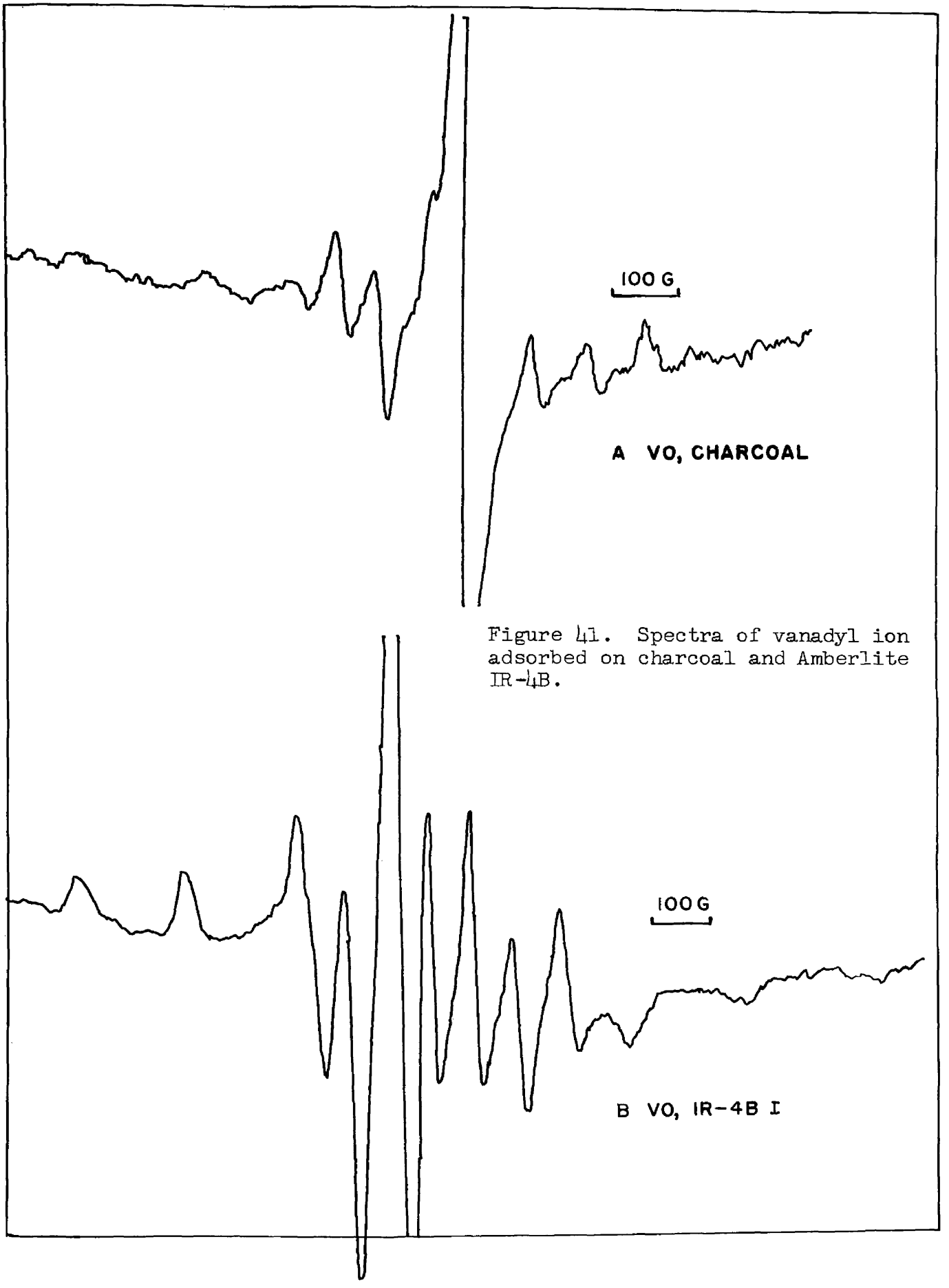

Figure 41. Spectra of vanadyl ion adsorbed on charcoal and Amberlite IR-4B.

more closely spaced lines of the spectrum of VO-Dowex-50 I and Figure 40 shows the weak pattern of eight more widely spaced lines in the spectrum of VO-Dowex-50 III. Here, three of the lines are obscured by the strong central pattern. Since these are also random powder samples, the first group of eight are centered upon $g_{\perp}$, with their separation equal to the constant A' in equation 19. The second, weaker group are centered on $g_{\parallel}$ and are separated by intervals equal to B' in Equation 18. The spectra obtained from the VO-IR-100 samples are nearly identical to the Dowex-50 samples and are not reproduced. The spectra obtained from VO-charcoal and VO-IR-4B are sufficiently different to be included. The signal strength of the VO-charcoal adsorption was too weak to allow the determination of the positions of the broad spectrum corresponding to the parallel orientation. No paramagnetic resonance absorption was observed in the silica gel samples. Table IX contains the measured positions of the lines in these spectra. Attempts to prepare samples of vanadyl ion adsorbed on zeolite failed. When the stock solution of vanadyl sulfate was added to the dried zeolite, the blue color of the solution disappeared and a yellow colored solution was left. The zeolite particles became yellow and black. The addition of sodium sulfite and subsequent acidification resulted in a restoration of the blue color, but left no color or detectable paramagnetic resonance absorption spectrum in the zeolite.

The spectra obtained from the vanadyl samples were satisfactorily described by Equations 18 and 19. The values of the parameters in these equations found for each adsorbent are tabulated in Table X. These parameters were computed in the manner described for the copper samples.

TABLE IX

ANALYSIS OF VO^{++} POWDER SPECTRA

Sample	m	$H_{(\parallel \text{ case})}$	$H_{(\perp \text{ case})}$
VO-Dowex-50	7/2	2713	3044
	5/2	2916	3102
	3/2	3122	3166
	1/2	obscured	3247
	-1/2	obscured	3320
	-3/2	3708	3412
	-5/2	3963	3507
	-7/2	4258	3600
VO-IR-100	7/2	2720	3028
	5/2	2916	3103
	3/2	obscured	3159
	1/2	obscured	3241
	-1/2	obscured	3322
	-3/2	3690	3406
	-5/2	3896	3502
	-7/2	4109	3602
VO-Charcoal	7/2	-	3054
	5/2	-	3113
	3/2	-	3173
	1/2	-	obscured by
	-1/2	-	free radical
	-3/2	-	3404
	-5/2	-	3490
	-7/2	-	3579
VO-IR-4B	7/2	2772	(3082)
	5/2	2945	3139
	3/2	3114	3197
	1/2	3275	3275
	-1/2	-	3327
	-3/2	3630	3396
	-5/2	3817	3469
	-7/2	4038	3550

TABLE X

SUMMARY OF RESULTS FOR VO^{++} SAMPLES

Sample	$g_{\perp}$	$g_{\parallel}$	B', gauss	B, cm^{-1}	A', gauss	A, cm^{-1}
VO-IR-100	1.983	1.93	81	0.00750	200	0.0180
VO-Dowex-50	1.979	1.88	80	0.00740	210	0.0184
VO-Charcoal	1.983	-	76	0.00704	190	-
VO-IR-4B	1.989	1.93	66	0.00612	175	0.0158

DISCUSSION

Manganese

Because the experimentally obtained values of the hyperfine structure interval were identical, within experimental error, for all the samples containing manganese adsorbed by cation exchangers, no conclusion about the amount of covalent bonding to the adsorbents can be made. Van Wieringen (14) reported the magnitude of A' as 98 gauss in phosphor crystals when the manganese ion is surrounded by water molecules or fluoride ions. The bonding was assumed to be ionic. In aqueous solution, Guessic and Williams (43) and Tinkham, Weistein and Kip (44) reported A' = 96 gauss; Kozyrev (35) found A' = 96.5 gauss. The results for the cation exchangers as obtained in this research were A' = 96 gauss. In aqueous solution the manganese ion is surrounded, on the average, by an octahedron of six water molecules. When adsorption from aqueous solution occurs, it seems probable that one of these water molecules is replaced by an oxygen atom which is part of the active group on the adsorbent. Hence, probably only one of the six possible bonds about the central ion is changed when adsorption occurs. The hyperfine structure interval is evidently not very sensitive to small changes in the amount of covalent character of only one of these bonds.

Although the ions in the adsorbed phase are not subject to a periodic crystalline field, the paramagnetic resonance absorption spectra are adequately described by the Hamiltonian expressions satisfied

by ions located in essentially infinite lattices. This result indicates that only the local point-group symmetry of the immediate surroundings of the paramagnetic ion influences the spectrum. The effect of adsorption upon the electrostatic field symmetry is quite apparent in the spectra obtained from the cation exchangers. In aqueous solution and in cubic crystals a simple six-line spectrum is obtained but in crystals of lower symmetry a fine structure appears, which is often of greater magnitude than the hyperfine structure. Consequently, the presence of a weak fine structure in the spectra of manganese on cation exchangers indicates a small departure from cubic symmetry produced by the presence of the negatively charged active group of the adsorbent. The symmetry thus produced is probably tetragonal.

The contribution of water of hydration to the local field symmetry is indicated by the results obtained by dehydrating the sample manganese-IR-100 IV. The spectrum of the original sample was well resolved and showed a pronounced fine structure. Removal of some or all of the coordinated water molecules by dehydration resulted in both a loss in signal strength and a loss in resolution of the spectrum (Figure 28). Some of the manganous ions probably retained a fairly symmetrical arrangement of water molecules; others probably experienced a field of very low symmetry. The former group account for the presence of an observable spectrum; the spectrum of the latter group would be too broad to detect. The original intensity and resolution of the spectrum were restored by exposing the dehydrated sample to the atmosphere,

thereby allowing the coordinated water molecules to be replaced reversibly by moisture from the atmosphere.

All of the samples involving organic ion exchangers which were dehydrated showed a strong free radical resonance in their spectra. The resonance probably arises from broken bonds produced by charring the adsorbent. This fact suggests that the lack of change in some of the spectra of the paramagnetic ions after dehydration was caused by preferential dehydration of the adsorbent which left the complex of water molecules about the ion intact.

The manganese spectra obtained from powdered zeolite showed only a hint of resolution into six components (Figure 26). This lack of resolution even in dilute samples indicates an electrostatic field of lower symmetry than was present in the other cation exchangers.

No resolution was observed in the samples of manganese adsorbed on the anion exchange resin Amberlite IR-4B. There was a single broad resonance peak whose width varied from 230 gauss in the most concentrated sample to 277 gauss in the most dilute one. The decrease in line width with increasing concentration is to be attributed to exchange interaction. The lack of resolution is probably due, not to dipolar broadening, but to an electrostatic field of low symmetry about the ion. Because of the very low concentration of manganese in the fourth sample, it seems unlikely that either spin-lattice or exchange interactions would be present. Consequently, the narrow width of the resonance band observed in this sample probably indicates a reduced hyperfine structure

interval. That the effect of covalent bonding of the ion to the adsorbent should be observed in these spectra seems reasonable when one considers the results of Nachod (45) with cupric ion adsorbed on an anion exchange resin. He postulates the formation of bonds between the central ion and two nitrogen atoms which are part of the active groups of the resin. If the adsorbed manganous ion is in a similar environment, the two bonds to the nitrogens might have a high degree of covalent character and their influence on the spectrum might be considerable.

According to Garstens and Liebson (15), when dipolar broadening first causes the six-line spectrum of manganese in aqueous solutions to be smeared into a single line, the width of the resulting resonance peak is 600 gauss. At higher concentrations the line width is reduced by exchange interaction. The single broad resonance spectra observed by Hershberger and Leifer (13) in powdered crystals of low symmetry had widths ranging from 750 to 1000 gauss. By analogy with these results, it would seem that the hyperfine structure interval of manganese adsorbed on Amberlite IR-4B is, accordingly, about fifty or sixty gauss. This very approximate value for A' indicates, following the proposal of Van Wieringen (14), about forty or fifty percent covalent bonding between the manganese and the resin. The greatest amount of covalent bonding found by Van Wieringen was forty percent, in crystals of zinc telluride containing small amounts of manganese, where the hyperfine structure interval was sixty gauss.

The spectrum of the single crystal of analcite containing manganese was due mostly to manganous ions in a very thin layer at the surface of the crystal. The ions evidently did not penetrate very far into the crystal and their concentration at the surface was probably rather high. Hence, the failure to obtain an appreciable resolution of the hyperfine structure may be explained by dipolar broadening.

Copper

All of the spectra obtained from samples containing cupric ions conformed to the equation developed by Sands (23) for random orientation of tetragonal symmetry axes. From the spectra it was possible to obtain values for the spectral parameters $g_{\parallel}$, $g_{\perp}$ and A in Equations 18 and 19. The line width in all the samples was too great to allow the determination of B.

The various copper samples may be classified into four groups on the basis of the measured parameters. Within each group the g values and hyperfine structure constants were equal within the limits of experimental error.

(1) The copper-IR-100 and copper-Dowex-50 samples possessed the highest g factors and the smallest hyperfine structure intervals of all the samples. The active group in both adsorbents is a sulfonic acid. Since this is a strong acid, the bond between the cupric ion and the adsorbent is probably largely ionic.

(2) Somewhat smaller g factors and larger hyperfine structure intervals were shown by the samples copper-charcoal, copper-zeolite,

and copper-IRC-50H. Only $g_{\perp}$ was measurable for the IRC-50H sample. The active group in the resin is a carboxylic acid; in the zeolite it is a silicate group; in the charcoal the active group is probably similar to a carboxylic acid.

(3) Still smaller g factors and larger hyperfine structure intervals were found in the spectra from the samples containing ammoniated cupric ions. No differences between the various adsorbents were evident.

(4) All the samples involving Amberlite IR-4B as the adsorbent had identical g factors and hyperfine structure intervals within the limits of experimental error. The value of $g_{\parallel}$ obtained from these spectra was the same as that obtained from the spectra of group 3 (above), but $g_{\perp}$ was larger.

On the basis of this classification a few generalizations may be made. The progression of the g values follows Stevens' (24) and Owen's (25,26) molecular orbital theory prediction that covalent bonding should reduce the magnitude of the g factor. In the hydrated samples, the spectrum is sensitive to changes in covalent character of the bond between the ion and the adsorbent. In the ammoniated samples this effect is not evident, partly because the greater line width in these samples leads to more uncertainty in the measured quantities.

The molecular orbital theory also predicts that because the electron cloud is shifted toward the ligands, a decrease in hyperfine structure interaction with the nucleus should occur. Since no change in electron configuration is required by covalent bonding, the configurational interaction postulate of Abragam and Pryce (21) is applicable.

According to this postulate, not the total hyperfine splitting, A and B, but only the isotropic term kP of Equations 13 and 14, is indicative of the degree of interaction with the nucleus, since an overall increase of hyperfine splitting with decreasing g factors is to be expected. Calculation of k for the various samples produced the results collected in Table XI. In the calculations P was assigned a value of 0.032 $cm.^{-1}$ which is an average computed from published results for the spectrum of cupric ion in various crystals.

TABLE XI

HYPERFINE STRUCTURE CONSTANTS AND CONFIGURATIONAL INTERACTION CONSTANTS FOR THE COPPER SAMPLES

Sample	A	k
Cu-IR-100	0.0122 cm^{-1}	0.24
Cu-Dowex-50	0.0128	0.27
Cu-Charcoal	0.0152	0.26
Cu-Zeolite	0.0142	0.26
$Cu(NH_3)_4$-IR-100	0.0194	0.27
$Cu(NH_3)_4$-Dowex-50	0.0178	0.23
$Cu(NH_3)_4$-Charcoal	0.0184	0.25
$Cu(NH_3)_4$-Zeolite	0.0182	0.24
Cu-IR-4B samples	0.0184	0.23

The values for k in Table XI are comparable to the values 0.25 computed by Abragam and Pryce for the copper Tutton salts (21), and 0.26 calculated by Sands (23) for cupric ions in glass. The results of Ingram and Bennett for cupric phthalocyanine (33) lead to a value for k of 0.23. The hyperfine structure interval of cupric acetylacetonate in dioxane (32) indicates a value for k of 0.22.

A slight indication of a trend is discernable in these results. In compounds in which the cupric ion is predominantly surrounded by water dipoles, k is found in the range 0.25 to 0.27, whereas in the more covalent complexes, k is found in the range 0.22 to 0.25. Specifically with regard to the results with the cation exchangers, k is lower in the ammoniated samples than in the corresponding hydrated samples, except for the samples involving Amberlite IR-100. Because these small differences are about of the same magnitude as the uncertainty in k, these observations merely suggest that differences in covalent bonding are reflected by differences in the magnitude of k. More precise g values, such as might be obtained at lower temperatures, might be required to establish this surmise.

The covalent bonding theory of Stevens and Owen cannot be applied quantitatively to the results of this investigation without approximate values for the orbital energy level separations, Δ_3 and Δ_4. The theory states that for the case where both σ and π bonding occur,

$$g_{\parallel} = 2.00 - a^2 b^2 8 \lambda'/\Delta_3 \qquad (25)$$

$$g_{\perp} = 2.00 - a^2(1 + b^2) \lambda'/\Delta_4 \qquad (26)$$

In these equations, the parameters a^2 and b^2 both lie between zero and one. When no covalent σ bonding occurs, $a^2 = 1$; when no covalent π bonding occurs, b^2 equals 1. For the purpose of testing the predictions of the molecular orbital theory, the quantities Δ_3 and Δ_4 for hydrated and for ammoniated cupric ions on zeolite may be approximated on the basis of the reflectance spectra of Figure 38. For the hydrated ion, $\Delta_3 = 12{,}000\ cm^{-1}$, $\Delta_4 = 14{,}000\ cm^{-1}$; for the ammoniated ion,

$\triangle_3$ = 13,000 cm^{-1}; $\triangle_4$ = 15,000 cm^{-1}. Using these approximations and assigning λ' a value of -825 cm^{-1}, one obtains the results shown in Table XII.

TABLE XII

COVALENT BONDING PARAMETERS IN MOLECULAR ORBITAL THEORY

Sample	$g_{\parallel}$	$g_{\perp}$	$\triangle_3$	$\triangle_4$	a^2	b^2
Cu-Zeolite	2.35	2.083	12,000 cm^{-1}	14,000 cm^{-1}	0.74	0.84
$Cu(NH_3)_4$-Zeolite	2.22	2.057	13,000	15,000	0.57	0.74

Because of the numerous approximations involved in the calculations, the results of Table XII are not quantitatively significant. Qualitatively however, the results are quite reasonable, for they state that covalent bonding does indeed occur appreciably in the ammoniated complex and that the contribution of covalent σ bonding is more important than that of covalent π bonding. For the hydrated cupric ion, Owen (26) found a^2 = 0.84 assuming b^2 = 1. McGarvey (32) reported a^2 = 1, b^2 = 0.5 for cupric acetylacetonate, where the presence of a π -electron system in the ligand favors the formation of covalent π bonds with the central ion. He also states that the results of Ingram and Bennett with cupric phthalocyanine (33) suggest that for bonds to nitrogen the σ bonds are also appreciably covalent. That prediction is substantiated by the results of this investigation. In tetramminocopper (II) sulfate pentahydrate, Spence and Carlson (31) found the ratio between λ in the

crystal and λ for the free ion to be 0.55. This ratio is equivalent to the quantity $a^2 b^2$ in Equation 15.

Another indication of the presence of covalent bonding is a hyperfine structure due to interaction with nuclei in the ligands. A large interaction of this sort was reported by Ingram et al. (34). Ingram and Bennett (33) have proposed that an unresolved hyperfine structure interaction with nitrogen nuclei may account for the line width in copper phthalocyanine. If such an interaction is present, they suggest, a constant line width with increasing dilution should be observed. The plots of H_p versus concentration for the various copper samples in Figure 37 are very similar to plots of line width versus concentration, since the difference between H_p and $H_\perp$ is a function of the line width. It will be noted that the slopes of these plots for the ammoniated copper samples and the samples involving Amberlite IR-4B are virtually zero, whereas a considerable variation of H_p with concentration was observed for the hydrated samples. Hence, it seems probable that an unresolved hyperfine structure is responsible for the greater line widths observed in the ammoniated-copper spectra and the spectra obtained from the IR-4B samples. This hyperfine structure would be produced by covalent bonding between the copper ion and the surrounding nitrogen nuclei.

No hyperfine structure was observed centered upon the sharp upper end, H_u, of the copper powder spectra. Consequently, no measurement of the quantity B' in Equation 18 could be made. In the hydrated samples, where the line width at maximum dilution is presumably due to

spin-lattice interaction, the lack of resolution indicates that B' is less than one-third of the observed line width. Since these are powder spectra, no true value for the line width can be obtained. Instead, the separation between the points of maximum positive and negative slope about H_u in the spectrum of copper-Dowex-50 III must be taken. This approximation to the line width gives W = 75 gauss. Consequently, B' is less than twenty-five gauss, and B is less than 0.0026 cm^{-1}. This result is comparable to Sands' (23) observed value of 0.0024 cm^{-1}. Calculation of B by means of Equation 11 leads to the result B = 0.0030 cm^{-1}, in fairly good agreement with the approximate upper limit set by the line width.

The situation is somewhat more complicated in the copper-IR-4B and the ammoniated copper samples, since the line width may be due to unresolved hyperfine structure involving interaction with nitrogen nuclei. A calculation using Equation 11 and based on the average observed g factors and hyperfine structure intervals leads to B = 0.0032 cm^{-1} for copper-IR-4B and B = 0.0019 cm^{-1} for the ammoniated samples. These quantities are both too small to account for the width of the line centered at H_u in these samples. This fact also suggests that an unresolved hyperfine structure is the principal contribution to the line width.

Sussman and Nachod (45) reported preliminary and somewhat inconclusive results on the adsorption of copper by an anion exchange resin. Copper was removed from a copper sulfate solution upon passage through a bed of a salt of an anion exchange resin, and also was removed from

ammoniacal copper sulfate solution upon passage through a bed of alkali-regenerated anion exchange resin. The suggested overall stoichiometry is:

$$Cu^{++} + 2(RNH)Cl = (Cu(RN)_2)Cl_2 + 2H^+ \qquad (27)$$

for the first reaction, and

$$Cu(NH_3)_4^{++} + 4\ RN = (Cu(RN)_4)^{++} + 4\ NH_3 \qquad (28)$$

for the second reaction. In these equations, RN represents the alkali-regenerated anion exchanger base. These authors claimed to have found experimental evidence for the diammine in Equation 27, but were uncertain whether the tetrammine or diammine was found in the reaction represented by Equation 28.

The paramagnetic resonance absorption spectra obtained in this investigation from the copper—IR-4B samples prepared from copper sulfate solution and from ammoniacal copper sulfate solution were indistinguishable. Hence, it seems probable that the copper complexes formed in the two reactions represented by Equations 27 and 28, are the same. Furthermore, since the observed spectra indicate tetragonal symmetry, with g factors and hyperfine structure constants very nearly equal to those of the ammoniated copper spectra on cation exchangers, the tetrammine structure of Equation 28 seems to be a more probable product in both reactions.

The spectra of the samples prepared from the tetrachloro and tetrabromocuprate (II) anions and Amberlite IR-4B are also indistinguishable from the spectrum of copper-IR-4B (Figure 35). The copper was probably adsorbed not in the form of a complex anion, but rather

as the same complex as that formed from aqueous solution of cupric ion. This mechanism appears the more probable because of the loss of color of the complex anion in the solution in contact with the resin. No color change was observed when a solution of tetratartratocuprate (II) anion was placed in contact with the resin, and no copper spectrum appeared in the subsequently dried sample of resin. Apparently the tartrate complex was too stable to release free copper ions to the resin.

Kozyrev (35) reported that the spectrum of cupric ion supercooled in organic solvents at 90°K consisted of an "exchange peak" at g = 2.091 and also four hyperfine-structure peaks separated by an interval of 130 gauss and centered at g = 2.369. It now seems probable that this spectrum was actually a random powder spectrum of the sort observed in this investigation, produced by the reduction of the random molecular motions at low temperature. Interpreted in this manner, the results lead to $g_{\parallel} = 2.369$, $g_{\perp} = 2.091$, and $A = 0.0146\ cm^{-1}$ which are in good agreement with the values obtained by Sands (23) and those obtained in this investigation.

Vanadium

No theoretical investigation of the paramagnetic resonance absorption of quadrivalent vanadium has appeared to date. Two analogous systems have been treated, however. Bleaney (46) considered the case of trivalent titanium, which is isoelectronic with quadrivalent vanadium, in a trigonal field. Polder's (18) treatment of the cupric ion in a

tetragonal field considers the electron configuration to be equivalent to a single positive electron in the d orbitals, that is, an electron "hole". Neither of these analogous systems is completely equivalent to the case of quadrivalent vanadium, however, for Bleaney's treatment is based on trigonal symmetry, and Polder's treatment results in an inversion of the orbital energy levels. Both theories predict g values approaching 2.00 when the energy separation between orbital levels becomes very large, that is, when the symmetry of the axial field departs strongly from cubic symmetry. Since the vanadium in the samples used in this investigation was in the form of the vanadyl ion, VO^{++}, the presence of oxygen would produce a strongly non-cubic, axially symmetrical field. The electrostatic field symmetry accounts, then, both for the proximity of the g factors to the free-spin value, 2.00, and for the very weak spin-lattice interaction as shown by the narrow line width.

All of the spectra of vanadyl ion on various adsorbents conform to the equation developed by Sands (23) for random orientation of symmetry axes. The striking differences in appearance between these spectra and those obtained from the copper samples arise from the fact that the g values of the vanadium spectra are nearly isotropic; the major contribution to the anisotropy comes from a highly anisotropic hyperfine structure. For a given value of the nuclear magnetic quantum number, m, the integrated line shape is given by Equation 17. Since the g factor is nearly isotropic, the upper boundary corresponds sometimes to the parallel orientation and sometimes to the perpendicular orientation of the symmetry axis.

Table IX shows clearly that the separation, in gauss, between the upper and lower boundaries of the broad integrated line corresponding to a given orientation of the nuclear spin, varies with m. The separation is greater for the extreme values of m than for intermediate values, and is a minimum for some intermediate value. The apparent intensity or sharpness of the peaks which mark the upper and lower boundaries is dependent upon the separation between the boundaries, being greatest for the lines whose boundaries are closest together.

The spectrum of vanadyl ion on Amberlite IR-4B, Figure 41-B, provides a striking example of this effect. One line in this spectrum is much more pronounced than the others; in fact, the maximum and minimum values of the slope lie outside the scope of the figure. This line corresponds to the transition for m = 1/2, and the separation between its upper and lower boundaries is probably of approximately the same magnitude as the line width.

From the g factors and hyperfine structure constants collected in Table X, a trend similar to the one observed in the copper samples may be discerned. The g factors remain constant, probably within the limits of experimental error. This fact indicates that the strongly non-cubic electrostatic field produced by the oxygen of the vanadyl radical overshadows any minor changes in spin-orbit interaction produced by the adsorbent. The hyperfine structure intervals, however, do vary from one adsorbent to another. The interval is largest in the two sulfonic acid-type cation exchangers, slightly smaller on charcoal, and much smaller when bonding to nitrogens on the anion exchanger occurs.

The magnitude of the hyperfine structure interaction (about 0.018 cm^{-1} for A) indicates that the promoted s-electron hypothesis of Abragam and Pryce may be required for the vanadyl ion, too. The decrease in splitting with increase of covalent character in the bonding suggests a shift of the magnetic electron toward the ligand in accordance with the molecular orbital theory of Stevens and Owen.

The relative signs of the two hyperfine structure constants, A and B, are predicted by theory but cannot be measured directly, since the hyperfine structure interval is a measure only of their absolute values. Indirect means must be employed to evaluate the relative signs of the constants.[1] When an isotropic contribution to the splitting is present, as predicted for the copper spectrum, an examination of the way the absolute values of A and B change with variation of this isotropic term reveals their relative sign. For the copper spectrum, decreasing k causes the absolute value of A to decrease and the absolute value of B to increase, according to Equation 14, when the constants have opposite sign. The observations by Pake and Sands (37) of an eight line spectrum for vanadyl ion in aqueous solution, where any anisotropic contributions would be averaged out, confirms the presence of such an isotropic contribution also to the vanadyl spectrum. Hence, the fact that the absolute values of A and B both decrease with increasing covalent bonding indicates that A and B probably have the same sign.

---

[1]Bleaney (10) suggested one method of doing so for the case where $S \neq 1/2$.

The thirteen line spectrum observed by Kozyrev (35) for vanadyl salts in non-aqueous solutions at $90^{o}K$ is undoubtedly a random pattern of the sort observed in this investigation. The reduction of molecular motion at the low temperature would produce a random orientation of the symmetry axes such as occurred in the powder spectra reported here. Interpretation of Kozyrev's results in this manner leads to $g_{\parallel} = 1.92$; $g_{\perp} = 1.960$; $A = 0.0178\ cm^{-1}$; $B = 0.0070\ cm^{-1}$; which are in good agreement with the results of this investigation.

SUMMARY

Paramagnetic resonance absorption spectra were obtained for samples containing manganous, cupric, and vanadyl ions adsorbed on various adsorbents. The adsorbents included two forms of commercial sulfonic-acid-type cation exchange resins, a carboxylic-acid-type cation exchange resin, an anion exchange resin, silica gel, commercial zeolite, and sugar charcoal activated at 400° centigrade.

The spectra were obtained by means of a paramagnetic resonance spectrometer employing a transmission cavity which resonated at 9,240 megacycles. The microwave radiation was generated by a klystron, detected by a silicon diode crystal, and the resulting signal was analyzed by a lock-in amplifier and displayed on a strip-chart recorder. Magnetic field strengths were measured by means of the magnetic resonance frequency of the proton. The g values and hyperfine structure intervals were computed on the basis of measured line positions.

A study of the spectra of manganese adsorbed on various resins enables a number of conclusions to be drawn concerning the properties of the adsorbed ions. All the spectra of the manganese samples had g values of 2.00. All but the spectra obtained from the anion exchange resin showed nuclear hyperfine structure with intervals of 96 gauss between the various lines. The presence of a weak fine structure in the charcoal and cation exchange resin spectra indicated electrostatic fields of less than cubic symmetry, probably tetragonal. A lower symmetry, which left the hyperfine structure barely detectable, was

present in the zeolite samples. The electrostatic field symmetry about the manganous ions bound to the anion exchange resin was even lower; no hyperfine structure was resolved. The hyperfine structure interval indicated essentially ionic bonding about the manganous ion in all the spectra where resolution was obtained. The line width of the unresolved spectrum of manganese on an anion exchange resin suggested approximately fifty percent covalent bonding between the manganese and the resin.

The most useful information was obtained from the study of adsorbed cupric ion because variations in the g values and hyperfine structure constants were observed in the copper samples. These quantities depended upon both the nature of the adsorbent and upon the coordinated ligands about the cupric ion. Higher g values and smaller hyperfine structure intervals were present in the spectra of hydrated cupric ions on the sulfonic-acid-type cation exchangers. The g values decreased and the hyperfine structure intervals increased as the amount of covalent character in the bond to the adsorbent increased. For a given adsorbent, the g values were substantially reduced and the hyperfine structure interval increased when the coordinated water molecules attached to the cupric ion were replaced with ammonia molecules. The spectra of the samples containing cupric ions adsorbed on the anion exchanger suggest the formation of bonds to four nitrogen atoms on the adsorbent. Some evidence was found for an unresolved hyperfine structure due to interaction of the electron spin with the nitrogen nuclei in both the anion exchanger and the ammoniated samples. The results with the copper samples seem to support the molecular orbital theory proposed by Stevens and Owen.

Very narrow lines and g values very close to 2.00 indicate a strongly non-cubic, axially symmetrical electrostatic field about the vanadyl ion. Hyperfine structure interaction constants with absolute magnitudes of 0.0182 and 0.00745 cm^{-1} for A and B, respectively, were found for vanadyl ion adsorbed on the sulfonic-acid-type cation exchangers. These constants were reduced by covalent bonding in the case of vanadyl ion adsorbed on the anion exchanger to 0.0158 and 0.00612 cm^{-1}, respectively. Assuming that the decrease was due principally to a decrease in an isotropic contribution to the hyperfine structure, it was shown that the constants A and B must have the same relative sign.

In general, the spectra obtained from the adsorbed ions were similar to the spectra of these ions when in solution or in crystals of known symmetry. Consequently, it was possible to draw a number of conclusions concerning the nature of the bonding between the ions and the adsorbents, and the nature of the adsorbed phase.

REFERENCES

1. E. K. Zavoisky, J. Phys. (U.S.S.R.) 9, 245 (1945); C. A., 40, 1072 (1946).

2. R. L. Cummerow and D. Halliday, Phys. Rev., 70, 433 (1946).

3. D. M. S. Bagguley and J. H. E. Griffiths, Nature, 160, 532 (1947).

4. J. E. Wertz, Chem. Rev., 55, 829 (1955).

5. D. J. E. Ingram, "Spectroscopy at Radio and Microwave Frequencies," Butterworths Scientific Publications, London, England, 1955.

6. W. Gordy, W. V. Smith and R. F. Trambarulo, "Microwave Spectroscopy," John Wiley and Sons, New York, N. Y., 1953.

7. B. Bleaney and K. W. H. Stevens, Repts. Progr. in Phys., 16, 108 (1953).

8. K. D. Bowers and J. Owen, ibid., 18, 304 (1955).

9. A. Abragam and M. H. L. Pryce, Proc. Roy Soc. (London), A205, 135 (1951).

10. B. Bleaney, Phil. Mag., 42, 441 (1951).

11. J. H. Van Vleck, Phys. Rev., 74, 1168 (1948).

12. H. M. McConnell, J. Chem. Phys., 24, 904 (1956).

13. W. D. Hershberger and H. N. Leifer, Phys. Rev., 88, 714 (1952).

14. J. S. Van Wieringen, Discussions Faraday Soc., 19, 118 (1955).

15. M. A. Garstens and S. H. Liebson, J. Chem. Phys., 20, 1647 (1952).

16. M. Cohn and J. Townsend, Nature, 173, 1090 (1954).

17. B. R. McGarvey, J. Phys. Chem., 61, 1232 (1957).

18. D. Polder, Physica, 9, 709 (1942).

19. C. Kikuchi and R. D. Spence, Am. J. Phys., 18, 167 (1950).

20. D. M. S. Bagguley and J. H. E. Griffiths, Proc. Roy. Soc. (London), A201, 366 (1950).

21. A. Abragam and M. H. L. Pryce, ibid., A206, 164 (1951).

22. A. Abragam, Physica, 17, 209 (1951).

23. R. H. Sands, Phys. Rev., 99, 1222 (1955).

24. K. W. H. Stevens, Proc. Roy. Soc. (London), A219, 542 (1953).

25. J. Owen, ibid., A227, 183 (1955).

26. J. Owen, Discussions Faraday Soc., 19, 127 (1955).

27. J. B. Howard, J. Chem. Phys., 3, 813 (1935).

28. M. Kotani, J. Phys. Soc. Japan, 4, 293 (1949).

29. L. E. Orgel, J. Chem. Soc., 4756 (1952).

30. B. Bleaney, K. D. Bowers and D. J. E. Ingram, Proc. Phys. Soc., A64, 758 (1951).

31. R. D. Spence and E. H. Carlson, J. Chem. Phys., 24, 471 (1956).

32. B. R. McGarvey, J. Phys. Chem., 60, 71 (1956).

33. D. J. E. Ingram and J. E. Bennett, Discussions Faraday Soc., 19 140 (1955).

34. D. J. E. Ingram, J. E. Bennett, P. George and J. M. Goldstein, J. Am. Chem. Soc., 78, 3545 (1956).

35. B. M. Kozyrev, Discussions Faraday Soc., 19, 135 (1955).

36. F. W. Lancaster and H. Gordy, J. Chem. Phys., 19, 1181 (1951).

37. G. E. Pake and R. H. Sands, Bull. Am. Phys. Soc., 29, 18 (1954).

38. M. T. Rogers, et al., Final Technical Report, Contract Nonr 02300, NR 358-232, 1952-54.

39. A. G. Ingalls (ed.), "Amateur Telescope Making, Advanced," Scientific American Publishing Co., New York, N. Y., (1952).

40. J. J. Lingane and R. Karplus, Ind. Eng. Chem., Anal. Ed., 18, 191 (1946).

41. W. C. Pierce and E. L. Haenisch, "Quantitative Analysis," John Wiley and Sons, New York, N. Y., (1948).

42. R. E. VanderVennen, Unpublished Ph. D. Thesis, Michigan State University, (1954).

43. J. E. Guessic and D. Williams, Phys. Rev., 99, 612 (1955).

44. M. Tinkham, R. Weinstein and A. F. Kip, Phys. Rev., 84, 848 (1951).

45. F. C. Nachod (ed.), "Ion Exchange: Theory and Application," Academic Press Inc., New York, N. Y., 1949.

46. B. Bleaney, Proc. Phys. Soc., A63, 407 (1950).

47. C. A. Hutchison, Jr., Technical Report No. 1, Contract N6ori-20, Institute for Nuclear Studies, University of Chicago, Spring, 1951.